

LOCKHEED MARTIN ENERGY RESEARCH LIBRARIES



3 4456 0515391 8

CENTRAL RESEARCH LIBRARY
DOCUMENT COLLECTION

ORNL-4764

1

H
S
S
T

HEAVY-SECTION STEEL TECHNOLOGY PROGRAM

*Semiannual Progress Report
Period Ending August 31, 1971*

248

OAK RIDGE NATIONAL LABORATORY
CENTRAL RESEARCH LIBRARY
DOCUMENT COLLECTION

LIBRARY LOAN COPY

DO NOT TRANSFER TO ANOTHER PERSON

If you wish someone else to see this
document, send in name with document
and the library will arrange a loan.

UCN-7969
13 3-67



OAK RIDGE NATIONAL LABORATORY

OPERATED BY UNION CARBIDE CORPORATION • FOR THE U.S. ATOMIC ENERGY COMMISSION

Printed in the United States of America. Available from
National Technical Information Service
U.S. Department of Commerce
5285 Port Royal Road, Springfield, Virginia 22151
Price: Printed Copy \$3.00; Microfiche \$0.95

This report was prepared as an account of work sponsored by the United States Government. Neither the United States nor the United States Atomic Energy Commission, nor any of their employees, nor any of their contractors, subcontractors, or their employees, makes any warranty, express or implied, or assumes any legal liability or responsibility for the accuracy, completeness or usefulness of any information, apparatus, product or process disclosed, or represents that its use would not infringe privately owned rights.

Contract No. W-7405-eng-26

**HEAVY-SECTION STEEL TECHNOLOGY PROGRAM
SEMIANNUAL PROGRESS REPORT
For Period Ending August 31, 1971**

F. J. Witt, Program Director

APRIL 1972

OAK RIDGE NATIONAL LABORATORY
Oak Ridge, Tennessee 37830
operated by
UNION CARBIDE CORPORATION
for the
U.S. ATOMIC ENERGY COMMISSION

LOCKHEED MARTIN ENERGY RESEARCH LIBRARIES



3 4456 0515391 8



Contents

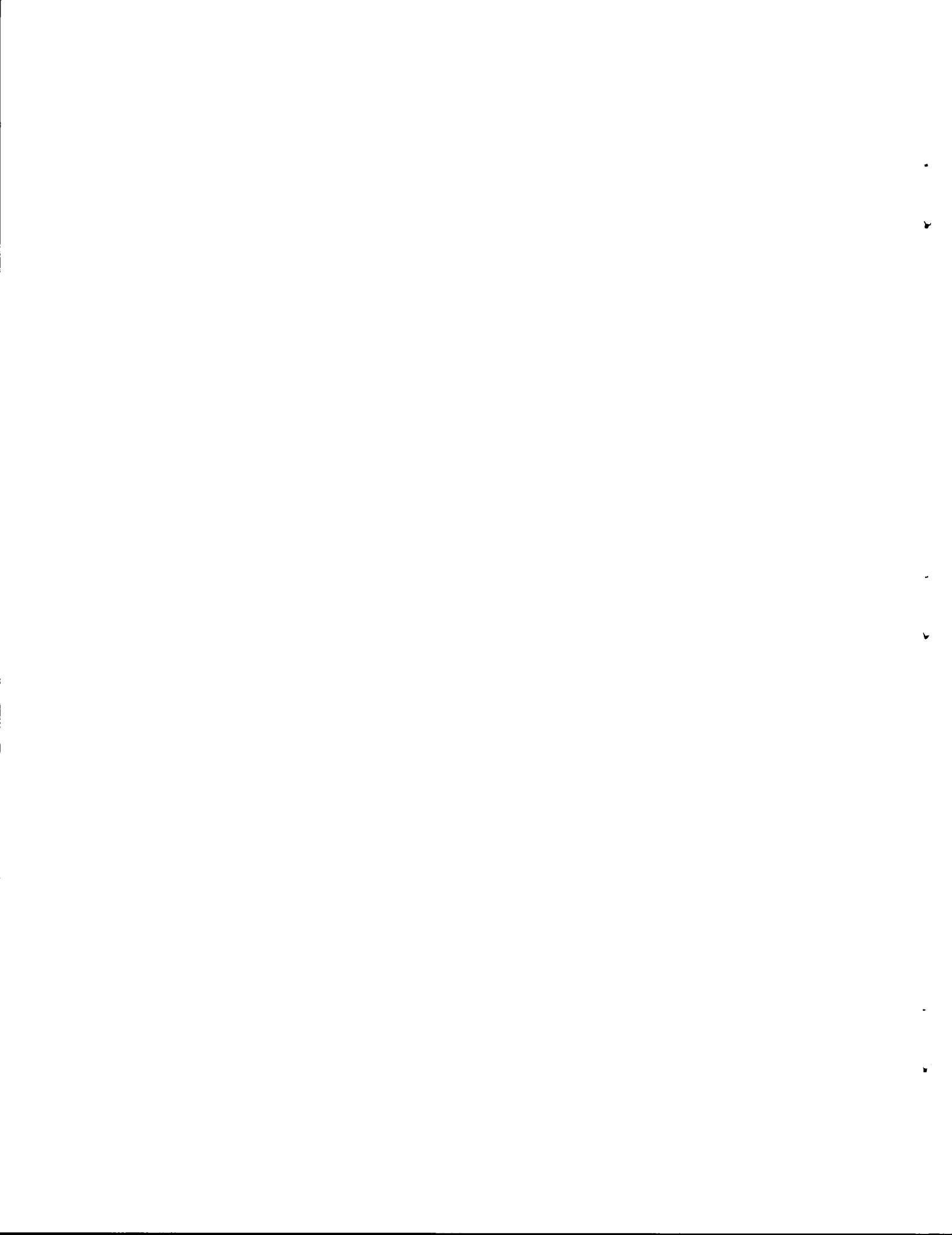
FOREWORD	v
SUMMARY	vii
1. PROGRAM ADMINISTRATION AND PROCUREMENT	1
2. INVESTIGATIONS OF UNIRRADIATED MATERIALS	3
Material Characterization and Variability	3
Fracture Mechanics Investigations	4
Strain Rate and Crack-Arrest Studies	4
Effects of Strain Gradients on the Gross Strain Crack Tolerance of A533 B Steel	6
Test plan	8
Experimental	11
Strain measurement	11
Initial test results	16
Three-Dimensional Elastic-Plastic Stress and Strain Analyses for Fracture Mechanics	17
Fracture Mechanics Characterization of HSST Program Materials	21
Experimental test procedure	21
Results	21
Fatigue and Crack-Propagation Investigations	21
Cooperative research between the HSST program, ORNL, and Japan Atomic Energy Research Institute	22
Fatigue-Crack Growth Characteristics of Nuclear Pressure Vessel Grade Materials	23
3. INVESTIGATIONS OF IRRADIATED MATERIALS	25
Irradiation Effects on the Fracture of Heavy-Section Pressure Vessel Steels	25
Objective	25
Irradiation of 4T Specimens – ETR Dummy Gamma-Heat Test	25
Base Material Studies of ASTM A533 B; Correlation of Changes in Yield Strength and Fracture Toughness Produced by Irradiation	27
Base Material Studies of ASTM A533 B; Comparison of Transverse and Longitudinal Fracture and Tensile Properties	28
ASTM A533-B Submerged-Arc Weldment; Irradiation Effects on Weld Metal Fracture and Tensile Properties	30

Radiation Hardening and Embrittlement in ASTM A533, Grade B, Class 1 Steel	33
Postirradiation Dynamic-Tear and Charpy-V Performance of 12-in.-thick A533-B Steel Plates and Weld Metal	35
Introduction	35
Composition and Heat Treatment	35
Irradiations	36
Results	37
Discussion	41
Conclusions	45
Acknowledgments	46
4. PRESSURE VESSEL INVESTIGATIONS	48
Testing of 6-in.-thick Flawed Tensile Specimens	48
Six-in.-thick Flawed Tensile Specimens with Weldments	48
Specimen description	48
Test results	48
One-in.-thick Flawed Tensile Specimens	49
Specimen description	49
Test results	51
Acoustic Emissions Monitoring	51
Experiments	51
Results	54
Shape Factors for Nozzle Corner Cracks	56
Definitions	58
Results	59
K_{Ic} measurements	59
Shape factor determination	60
Sample Calculation for a Reactor Vessel	60
Nozzle experimental stress analyses	61
Procurement of Intermediate Test Vessels	62

Foreword

The Heavy-Section Steel Technology (HSST) Program is a USAEC-sponsored effort for investigating the effects of flaws, variations of properties, stress raisers, and residual stress on the structural reliability of present and contemplated water-cooled-reactor pressure vessels. The cognizant engineer for USAEC is J. R. Hunter. At ORNL the program is under the Pressure

Vessel Technology Program, of which G. D. Whitman is Director. The HSST program is being carried out in very close cooperation with the nuclear power industry. Prior reports in this series are ORNL-4176, ORNL-4315, ORNL-4377, ORNL-4463, ORNL-4512, ORNL-4590, ORNL-4653, and ORNL-4681.



Summary

The Heavy-Section Steel Technology (HSST) Program is concerned with the primary vessels for water reactors, with the main emphasis being placed on the effects of flaws, material inhomogeneities, and discontinuities on the behavior of the vessels under normal operating and accident conditions. The program is coordinated with efforts by the manufacturing and utility sectors of the nuclear power industry to assess the in-service structural safety of the massive pressure vessels typical of those used in boiling- and pressurized-water reactor systems. In the HSST program particular emphasis is placed on developing a technology that can be used to establish the margin of safety against failure of the vessels, particularly catastrophic failure beyond the control of plant safety features.

Fracture phenomena under the environmental conditions of interest and the effects of section thickness on the fracture behavior of the large reactor vessels are being examined through a systematic progression of specimen sizes up to the equivalent of a full section thickness of 12 in. The program will culminate in a series of simulated service tests in which deliberately flawed vessels of substantial thickness will be tested to fracture. Through the culmination of the HSST effort, as well as that of the nuclear industry, a technology should be developed that will assist the USAEC regulatory bodies, the professional code-writing bodies, and the nuclear power industry in providing the safety standards necessary to maintain a vigorous economical industry with proper regard to public health and welfare.

There are 12 tasks of the HSST program. In this report the activities of these tasks are grouped under administration and procurement, unirradiated materials, irradiated materials, and pressure vessel investigations.

There are eight active research and development subcontracts sponsored by the HSST program. Results from these efforts as well as those performed at ORNL

are extensively reported in technical reports and publications.

Evaluation of the data obtained under the variability study continues. Extensive load and energy parameter studies are being made on data obtained from an instrumented Charpy impact machine. The study includes the testing of sharp-crack Charpy specimens. Complementary slow-bend tests are also being made.

Crack-arrest fracture toughness measurements were made at Materials Research Laboratory on specimens which have an increasing stress intensity field. The preliminary results showed that the crack-arrest toughness was independent of the stress intensity gradient. This strongly implies that crack-arrest fracture toughness K_{Ia} is a material property just as K_{Ic} is. Additional work is in progress.

TRW Systems, Inc., has initiated a study of the effects of strain gradients on gross strain crack tolerance. Experimental techniques have been developed for testing surface-cracked specimens in bending at low temperatures, the principal problems being the strain measurements. Testing is in progress.

Brown University has performed a three-dimensional elastic-plastic analysis on a rectangular tensile specimen containing a semielliptical flaw. Strain hardening was taken into account. The analysis enhanced the feasibility of using the finite-element method for elastic-plastic behavior in the region of a flaw.

Compact-tension specimens 1, 6, and 9 in. thick were fabricated from HSST plate 03 by Westinghouse Electric Corporation. The specimens were tested in the temperature range from approximately 0 to approximately 550°F. Both longitudinal and transverse specimens were tested. The data are being used to establish lower-bound K_{Ic} values as well as pertinent K_{Icd} parameters that may be used in fracture analyses.

Two studies of the fatigue crack propagation characteristics of A533 steel were completed, one by

Westinghouse Electric Corporation, and the other by the Japan Atomic Energy Research Institute as a cooperative effort. For the same conditions of testing the results were quite similar in that a nuclear reactor environment excluding irradiation did not enhance the room-temperature crack growth rate in an air environment. A considerable increase in growth rate was noted for a high strain range of about 0.7%. Low cycling speeds manifested periods of stagnation.

At Hanford Engineering Development Laboratory, the ETR 4T dummy gamma-heat experiment was completed. Thermal gradients through the specimen thickness were less than calculated using low-power gamma-heat flux data. The maximum ΔT at the specimen crack line was 200°F. Also, the shift in transition temperature in plane strain fracture toughness K_{Ic} due to irradiation has been correlated with the effect of irradiations on the yield strength of A533 B pressure vessel steel. The correlation, believed to be valid to fluences of 8×10^{19} neutrons/cm² ($E > 1$ MeV), is preliminary in nature because of the incomplete determination of the irradiated material fracture toughness transition.

Transverse tensile properties for irradiated and unirradiated ASTM A533 B steel were compared with longitudinal plate properties. Yield and ultimate strength properties and their response to irradiation were found to be orientation independent. Unirradiated K_{Ic} fracture toughness for transverse (WR) orientation was also similar to longitudinal (RW) orientation fracture toughness. Fracture toughness K_{Ic} of the A533 submerged-arc weldment was shifted by +390°F for the 50-ksi $\sqrt{\text{in.}}$ level after irradiation to approximately 3×10^{19} neutrons/cm² ($E > 1$ MeV). Weld tensile yield and ultimate strength properties were similar to plate properties for equivalent irradiation levels.

The irradiation investigation of Charpy-V and dynamic-tear specimen results were completed by the U.S. Naval Research Laboratory as part of a cooperative effort. Charpy-V (C_v) and dynamic-tear (DT) test comparisons were developed for the irradiated condition of two 12-in.-thick A533 B steel plates and a submerged-arc weld deposit. Low-temperature (<300°F, 149°C) and elevated temperature (550°F, 288°C) irradiations were conducted. Fluences for the eight irradiation experiments ranged from 2.5 to 3.3×10^{19} neutrons/cm² ($E > 1$ MeV).

Postirradiation C_v and DT midenergy transition temperature increases were found comparable for both plate and weld deposit (quarter-thickness position evaluations). For the plate, percentage reductions in C_v and DT shelf energy with irradiation also compared

well. As a result, preirradiation DT-to- C_v shelf energy ratios appeared to be retained with irradiation. Shelf observations are in agreement with recent findings for A543, A302 B, and other A533 steel plates, which illustrate a DT-to- C_v shelf energy ratio of 8.0:1 for pre- and postirradiation conditions. It is concluded that postirradiation DT properties of A533 B plate, including midenergy transition and shelf level, can be calculated with reasonable accuracy from postirradiation C_v results for use in fracture safety analyses. Assessments of shelf level toughness before and after irradiation are developed by ratio analysis diagram (RAD) procedures.

Unlike observations for plate, a significant reduction in the DT-to- C_v shelf energy ratio by irradiation was found for the weld deposit. Weld metal fracture appearances suggest preferred paths for fracture within the duplex (layered) microstructure.

Studies of load and energy parameters obtained from testing irradiated Charpy specimens on an instrumented Charpy machine were made. All the energy parameters decreased with irradiation. A much greater effect was noted for the weld investigation.

Southwest Research Institute continues to test large 6-in.-thick tensile specimens containing sharp flaws. A total of 13 such specimens have now been tested. The last three specimens tested contained flaws in a submerged-arc weld. These specimens exhibited tougher behavior at lower temperatures than the plate specimen. Strains based on a 24-in. gage length spanning the flaw exceed 1%, even for the specimens tested at 0°F. A series of 1-in.-thick models of the larger specimens are also being tested. A total of 7 specimens were tested, with 19 additional specimens scheduled for testing.

Acoustic emission measurements were also made on the specimens tested at Southwest Research Institute. Plots of emission vs stress intensity were made, and three modes of behavior were noted. The acoustic emissions increase rapidly before yield, exhibit a small plateau near the yield point, and increase again under gross plastic deformation. Both sizes of specimens behaved in quite the same fashion, with the larger specimen exhibiting a higher rate of emission than the smaller ones.

Shape factors (C) for nozzle corners as a function of flaw sizes were obtained experimentally from two sizes of epoxy pressure vessels. Such factors may be used in brittle fracture calculations. The values ranged between 2 and 2.8 for small flaw sizes but decreased as a function of flaw size to about 1.5 for very large flaws. When applied to a reactor vessel assumed to be undergoing pressure tests where K_{Ic} has been measured

(140,000 psi $\sqrt{\text{in.}}$ at 50°F), flaws as small as 2 in. deep would be expected to produce fracture at design pressure.

The six 6-in.-thick pressure vessels are still being fabricated. Difficulty in obtaining welds that pass the

inspection requirements are being experienced, and vessel delivery has been delayed by another four to six months.



1. Program Administration and Procurement

The Heavy-Section Steel Technology (HSST) Program is one of the larger USAEC safety engineering research programs. The major concern of the program is the primary vessels for water reactors, with the main emphasis being placed on the effects of flaws, material inhomogeneities, and discontinuities on the behavior of the vessels under normal operating and accident conditions. Particular emphasis is placed on developing a technology that can be used to establish the margin of safety against failure of the vessels, particularly catastrophic vessel failure beyond the control of plant safety features.

Fracture phenomena under the environmental conditions of interest and the effects of section thickness on the fracture behavior of the large reactor vessels are being examined through a systematic progression of specimen sizes up to the equivalent of a full section thickness of 12 in. The program will culminate in a series of simulated service tests in which deliberately flawed vessels of substantial thickness will be tested to fracture.

The program is coordinated with efforts by other government agencies and the manufacturing and utility sectors of the nuclear power industry both in the United States and abroad. These total efforts were recently summarized in issues of *Nuclear Engineering and Design*^{1,2} and should result in the quantification of safety assessments which are needed by the USAEC regulatory bodies, the professional code-writing bodies, and the nuclear power industry.

The activities of the HSST program are carried out under 12 separate tasks. About three-fourths of the task activities are performed under subcontract by research facilities throughout the United States. Currently there are 8 research and development subcontracts in force. In addition, a panel of 28 scientists and engineers with expertise in material technology has been organized to serve in an advisory capacity to the program.

Dissemination of results from research in progress and completed is carried out through several channels. Detailed discussions of HSST program investigations may be found in HSST semiannual progress reports,³ technical and documentary reports,⁴⁻²¹ and technical manuscripts.²²⁻³⁴ The most current technical publications (a collection of 13 papers) may be found in a recent issue of *Nuclear Engineering and Design*.³⁵⁻⁴⁷ Information meetings are held on an annual basis; the abstracts of the papers presented at the 1971 meeting are given in Ref. 2. The information meeting for 1972 is scheduled for April 25 and 26, 1972, at Oak Ridge National Laboratory.

Administratively the HSST program is carried out under 12 tasks. However, for reporting purposes here, the research areas are discussed under investigations of unirradiated materials, investigations of irradiated materials, and pressure vessel investigations. The major procurement items are the intermediate test vessels. The status of the procurement of the vessels is summarized in Chapter 4.

1. "Information," Abstracts of papers presented at the Fourth Semiannual Information Meeting of the Heavy-Section Steel Technology Program, *Nucl. Eng. Des.* 14(2), 352-61 (December 1970).

2. "Information," Abstracts of papers presented at the Fifth Annual Information Meeting of the Heavy-Section Steel Technology Program, *Nucl. Eng. Des.* 17(1), 170-78 (August 1971).

3. F. J. Witt, *HSST Program Semiannual Progr. Repts.* Aug. 31, 1967, ORNL-4176; Feb. 29, 1968, ORNL-4315; Aug. 31, 1968, ORNL-4377; Feb. 28, 1969, ORNL-4463; Aug. 31, 1969, ORNL-4512; Feb. 28, 1970, ORNL-4590; Aug. 31, 1970, ORNL-4653; Feb. 28, 1971, ORNL-4681.

4. S. Yukawa, *Evaluation of Periodic Proof Testing and Warm Prestressing Procedures for Nuclear Reactor Vessels*, HSSTP-TR-1, General Electric Company (July 1, 1969).

5. L. W. Loechel, *The Effect of Section Size on the Transition Temperature in Steel*, MCA-69-189, Martin Marietta Company (1969).

6. P. N. Randall, *Gross Strain Measure of Fracture Toughness of Steels*, HSSTP-TR-3, TRW Systems Groups (Nov. 1, 1969).
7. C. Visser, S. E. Gabrielse, and W. Van Buren, *A Two-Dimensional Elastic-Plastic Analysis of Fracture Test Specimens*, WCAP-7368, Westinghouse Electric Corporation (1969).
8. T. R. Mager, F. O. Thomas, and W. S. Hazelton, *Evaluation by Linear Elastic Fracture Mechanics of Radiation Damage to Pressure Vessel Steels*, WCAP-7328 (Rev.), Westinghouse Electric Corporation (October 1969).
9. W. O. Shabbits, W. H. Pryle, and E. T. Wessel, *Heavy Section Fracture Toughness Properties of A 533 Grade B, Class 1 Steel Plate and Submerged Arc Weldment*, WCAP-7414, Westinghouse Electric Corporation (December 1969).
10. F. J. Loss, *Dynamic Tear Test Investigations of the Fracture Toughness of Thick-Section Steel*, NRL-7056 (also HSST-TR-7), U.S. Naval Research Laboratory.
11. P. B. Crosley and E. J. Ripling, *Crack Arrest Fracture Toughness of A 533 Grade B Class 1 Pressure Vessel Steel*, HSSTP-TR-8, Materials Research Laboratory (March 1970).
12. T. R. Mager, *Post Irradiation Testing of 2 T Compact Tension Specimens*, WCAP-7561, Westinghouse Electric Corporation (August 1970).
13. T. R. Mager, *Fracture Toughness Characterization Study of A 533 Class 1 Steel*, WCAP-7558, Westinghouse Electric Corporation (September 1970).
14. T. R. Mager, *Notch Preparation in Compact Tension Specimens*, WCAP-7579, Westinghouse Electric Corporation (November 1970).
15. N. Levy and P. V. Marcal, *Three-Dimensional Elastic-Plastic Stress and Strain Analysis for Fracture Mechanics, Phase 1: Simple Flawed Specimens*, HSSTP-TR-12, Brown University (December 1970).
16. W. O. Shabbits, *Dynamic Fracture Toughness Properties of Heavy Section A 533 Grade B Class 1 Steel Plate*, WCAP-6723, Westinghouse Electric Corporation (December 1970).
17. P. N. Randall, *Gross Strain Crack Tolerance of A 533-B Steel*, HSSTP-TR-14, TRW Systems Group (May 1, 1971).
18. H. T. Corten and R. H. Sailors, *Relationship between Material Fracture Toughness Using Fracture Mechanics and Transition Temperature Tests*, T.&A.M. Report No. 346, University of Illinois (Aug. 1, 1971).
19. C. E. Childress, *Fabrication History of the First Two 12-in.-Thick ASTM A 533, Grade B, Class 1 Steel Plates of the Heavy Section Steel Technology Program, Documentary Report 1*, ORNL-4313 (February 1969).
20. C. E. Childress, *Fabrication History of the Third and Fourth 12-in.-Thick ASTM A 533, Grade B, Class 1 Steel Plates of the Heavy Section Steel Technology Program, Documentary Report 2*, ORNL-4313 (Pt. 2) (February 1970).
21. C. E. Childress, *Fabrication Procedures and Acceptance Data for ASTM A 533 Welds and a 10-in.-Thick ASTM A 543 Plate of the Heavy Section Steel Technology Program, Documentary Report 3*, ORNL-4313 (Pt. 3) (January 1971).
22. *HSST Intermediate Vessel Closure Analysis*, Technical Report E-1253(b), Teledyne Materials Research Company (Mar. 25, 1970).
23. C. L. Segaser, *Conceptual System Design Description of the Intermediate Vessel Tests for the Heavy Section Steel Technology Program*, ORNL-TM-2849 (June 1970).
24. F. J. Witt and R. G. Berggren, *Size Effects and Energy Disposition in Impact Specimen Testing of ASTM A 533, Grade B Steel*, ORNL-TM-3030 (August 1970).
25. D. A. Canonico, *Transition Temperature Considerations for Thick-Wall Nuclear Pressure Vessels*, ORNL-TM-3114 (October 1970).
26. G. D. Whitman and F. J. Witt, *Heavy Section Steel Technology Program*, ORNL-TM-3055 (October 1970).
27. D. A. Canonico and R. G. Berggren, *Tensile and Impact Properties of Thick Section Plate and Weldments*, ORNL-TM-3211 (January 1971).
28. C. E. Childress, *Manual for ASTM A 533 Grade B Class 1 Steel (HSST Plate 03) Provided to the International Atomic Energy Agency*, ORNL-TM-3193 (March 1971).
29. C. L. Segaser, *Feasibility Study - Irradiation of Heavy Section Steel Specimens in the South Test Facility of the Oak Ridge Research Reactor*, ORNL-TM-3234 (May 1971).
30. R. W. Derby and C. L. Segaser, *Quality Assurance Program Plan, Intermediate Vessel Test Facility*, ORNL-TM-3373 (May 1971).
31. G. C. Robinson, *Discussion of SwRI Model Parametric Tests*, ORNL-TM-3313 (June 1971).
32. C. W. Hunter and J. A. Williams, *Fracture and Tensile Behavior of Neutron-Irradiated A 533-B Pressure Vessel Steel*, HEDL-TME 71-76, Hanford Engineering Development Laboratory (Feb. 5, 1971).
33. J. G. Merkle, L. F. Kooistra, and R. W. Derby, *Interpretation of the Drop-Weight Test in Terms of Strain Tolerance (Gross Strain) and Fracture Mechanics*, ORNL-TM-3247 (June 1971).
34. N. Krishnamurthy, *Three-Dimensional Finite Element Analysis of Thick-Walled Vessel-Nozzle Junctions with Curved Transition*, ORNL-TM-3315 (July 1971).
35. F. J. Witt, "Introduction: HSST Program Investigations," *Nucl. Eng. Des.* 17(1), 1-3 (August 1971).
36. D. A. Canonico and R. G. Berggren, "Tensile and Impact Properties of Thick-Section Plate and Weldments," *Nucl. Eng. Des.* 17(1), 4-15 (August 1971).
37. F. J. Loss, "Effect of Mechanical Constraint on the Fracture Characteristics of Thick-Section Steel," *Nucl. Eng. Des.* 17(1), 16-31 (August 1971).
38. P. B. Crosley and E. J. Ripling, "Crack Arrest Toughness of Pressure Vessel Steels," *Nucl. Eng. Des.* 17(1), 32-45 (August 1971).
39. P. N. Randall and J. G. Merkle, "Gross Strain Crack Tolerance of Steels," *Nucl. Eng. Des.* 17(1), 46-63 (August 1971).
40. N. Levy, P. V. Marcal, and J. R. Rice, "Progress in Three-Dimensional Elastic-Plastic Analysis for Fracture Mechanics," *Nucl. Eng. Des.* 17(1), 64-75 (August 1971).
41. T. R. Mager, "Fracture Toughness Properties of Heavy Section A 533, Grade B, Class 1 Steel Plate and Submerged-Arc Weldment," *Nucl. Eng. Des.* 17(1), 76-90 (August 1971).
42. F. J. Witt and T. R. Mager, "Fracture Toughness K_{Icd} Values at Temperatures up to 550°F for ASTM A 533 Grade B, Class 1 Steel," *Nucl. Eng. Des.* 17(1), 91-102 (August 1971).
43. R. G. Berggren and W. J. Stelzman, "Radiation Strengthening and Embrittlement in Heavy Section Plate and Welds," *Nucl. Eng. Des.* 17(1), 103-15 (August 1971).
44. J. R. Hawthorne, "Postirradiation Dynamic Tear and Charpy-V Performance of 12-in.-Thick A 533-B Steel Plates and Weld Metal," *Nucl. Eng. Des.* 17(1), 116-30 (August 1971).
45. C. W. Hunter and J. A. Williams, "Fracture and Tensile Behavior of Neutron-Irradiated A 533-B Pressure Vessel Steel," *Nucl. Eng. Des.* 17(1), 131-48 (August 1971).
46. D. A. Canonico, "Transition Temperature Considerations for Thick-Wall Steel Nuclear Pressure Vessels," *Nucl. Eng. Des.* 17(1), 149-60 (August 1971).
47. S. C. Grigory, *Testing the Six-Inch Thick Flawed Tensile Specimen for the Heavy Section Steel Technology Program*, *Nucl. Eng. Des.* 17(1), 161-69 (August 1971).

2. Investigations of Unirradiated Materials

The materials investigations under the Heavy-Section Steel Technology Program are divided, in general, into studies of unirradiated materials and studies of irradiation effects. The studies of unirradiated materials include inspection, characterization, variability determinations, transition temperature investigations, fracture mechanics studies, and fatigue-crack propagation tests. The current work in these areas is discussed in this section. No work specifically under the transition temperature task is in progress. Additional results for unirradiated materials are presented in Chapter 3; inspection activities are reported in Chapter 4.

MATERIAL CHARACTERIZATION AND VARIABILITY

W. J. Stelzman

Material is being studied from HSST plates 02 and 03 at locations shown in Fig. 2.1 together with previously studied regions.¹ Plate sections 02AH, 02F, 03CA, 03CB, and 03GA are being investigated at the top surface and $\frac{1}{4}$ -T locations only. Materials from plate section 02HC at the top surface, $\frac{1}{4}$ -T, $\frac{1}{2}$ -T, $\frac{3}{4}$ -T, and back surface locations are being tested. Testing of standard Charpy V-notch and 0.178-in.-gage-diam tensile specimens is in progress.

Additional fracture load and fracture energy parameter data are being generated from the load-time records obtained during previous impact testing. Attempts are being made to determine methods of correlation and applicability to data from other types of test specimens. Load-time records from the submerged-arc weldment impact tests on WL-oriented specimens¹ from the $\frac{1}{12}$ -T location were also studied. The fracture load parameters

and the fracture energy parameters are shown in Figs. 2.2 and 2.3. The Charpy energy curve for the same thickness location is shown in Fig. 2.4. These same parameters for submerged-arc weldment material irradiated at 565°F are described in Chapter 3. The properties of the submerged-arc weldment have been described in a previous report.²

Load-time (deflection) records are also being utilized in a study to determine the ability of the Charpy V-notch specimen to produce data from which quantitative fracture toughness parameters may be obtained. Testing of compact-tension, Charpy V-notch impact

2. D. A. Canonico, "Characterization of Heavy-Section Steel Weldments," *ibid.*, pp. 29-35.

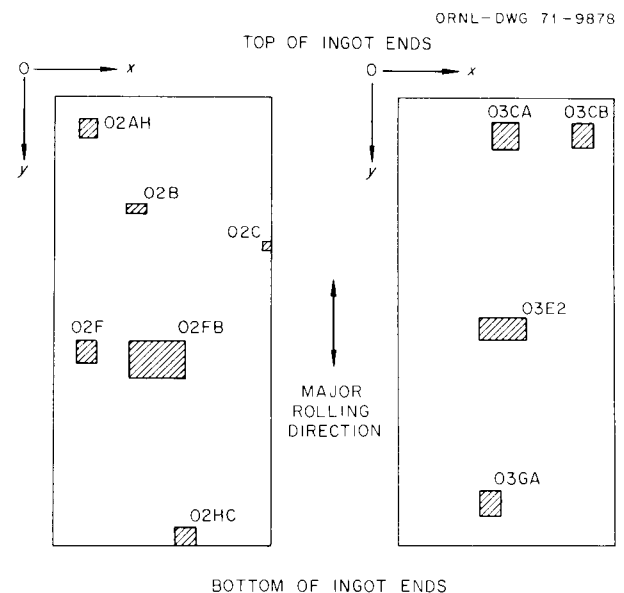


Fig. 2.1. Test locations in HSST plates 02 and 03.

1. R. G. Berggren, "Material Characterization and Variability," *HSST Program Semiannu. Progr. Rep. Feb. 28, 1969*, ORNL-4463, pp. 20-29.

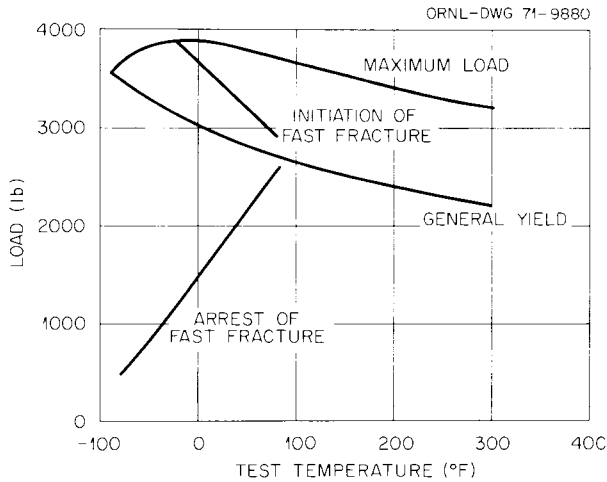


Fig. 2.2. Effect of temperature on load parameters determined in instrumented Charpy tests on HSST submerged-arc weldment 51B; WL-oriented specimens.

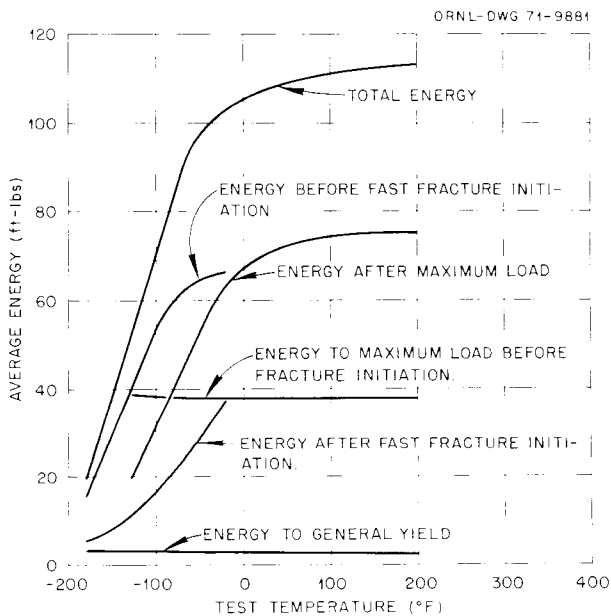


Fig. 2.3. Effect of temperature on energy parameters determined in instrumented Charpy tests on HSST submerged-arc weldment 51B; WL-oriented specimens.

and slow-bend, and tensile specimens with standard machined, fatigue-cracked, and electron-beam-weld crack starter notch configurations will be performed at fixed test temperatures (-50 , 0 , 50 , and 200°F). The machined Charpy V-notch impact and slow-bend tests have been completed.

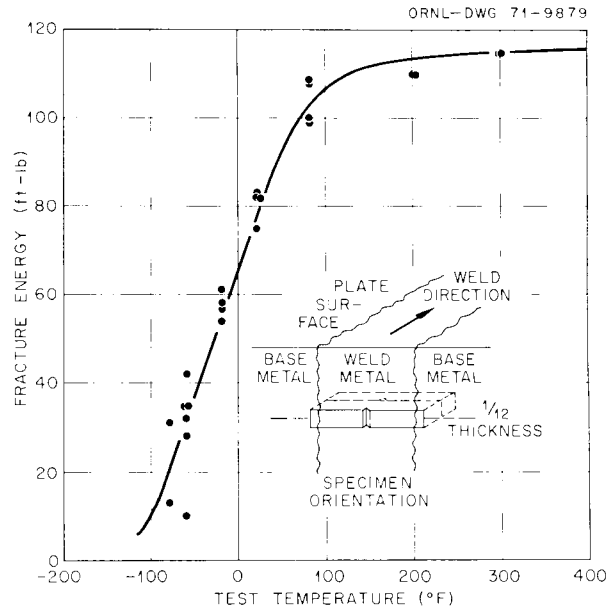


Fig. 2.4. Charpy V-notch test results for HSST submerged-arc weldment 51B at $1/12$ -T location.

FRACTURE MECHANICS INVESTIGATIONS

J. G. Merkle

The objectives of the fracture mechanics investigations are (1) to establish the applicability of fracture mechanics methods as currently understood to the low-alloy steels being used in reactor pressure vessels, (2) to extend the applicability of this body of knowledge to cover the tougher behavior at higher temperatures, and (3) to develop new methods specifically applicable for predicting the fracture behavior of steels that undergo gross plastic strains before fracture. These objectives are being pursued through a series of subcontracts, with related tasks (described elsewhere) contributing significantly to the developments. The activities under the subcontracts are discussed here.

Strain Rate and Crack-Arrest Studies³

P. B. Crosley E. J. Ripling
Materials Research Laboratory

This report summarizes our most recent test series, the purpose of which was to measure the arrest fracture

3. Work being performed under UCCND Subcontract No. 3152 between Union Carbide Corporation and Materials Research Laboratory.

toughness K_{Ia} in an increasing K field. We previously presented a curve of arrest fracture toughness vs testing temperature.⁴ All of these arrest data were collected on TDCB (tapered double-cantilever beam) specimens. This type of specimen has a zero K gradient (with crack length a), and, consequently, there was still a question as to whether or not a crack would arrest at these same values in an increasing K field. This question is of interest for two reasons: (1) to demonstrate that K_{Ia} is an invariant, it must be shown to be independent of the way in which it is measured; and (2) in most structures K increases with a , so that if K_{Ia} is to be a useful property, it must be applicable to such structures.

To determine whether or not K_{Ia} was invariant, and independent of K gradient, a series of six tests were run using single-edge notched (SEN) specimens. A schematic drawing of the specimens is shown in Fig. 2.5. The specimens were side grooved, as were the TDCB specimens, in order to prevent the formation of shear lips that would have interfered with the measurement

4. F. J. Witt, *HSSST Program Semiannu. Progr. Rep. Feb. 28, 1971* ORNL-4681.

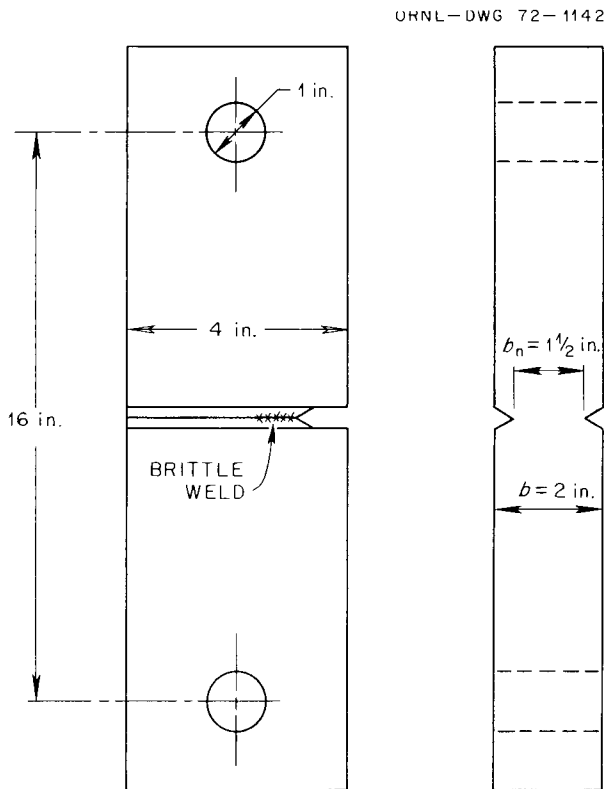


Fig. 2.5. Schematic drawing of test specimen.

of K_{Ia} . As shown previously at room temperature and above, it was necessary to use a thermal gradient (in the 2-in.-thick specimens) in order to obtain the data. However, in these tests, a metallurgical gradient was used. The metallurgical gradient was produced by putting an electron beam weld at the base of the machined notch. (The welding was done by ORNL.⁴) No metal was added to the specimen in the course of welding; instead the base metal was essentially melted and redeposited. Because of the rapid quench, the hardness of the weld metal was a great deal higher than that of the base plate.

The K_{Ia} of the base plate for the SEN specimens is measured by bracketing values of applied K (i.e., K_I) for which the crack will either arrest or propagate in the base plate. The approximate crack depth for these specimens was known prior to testing, since a is equal to the sum of the machined notch and brittle weld (and possibly the heat-affected zone as well) once the crack is initiated. Hence, if a load P were applied to the specimen so that the combination of P and a exceeded K_{Ia} , the crack should propagate through the base plate; if it were less than K_{Ia} , the crack should arrest at the end of the weld. The problem in running such a test is one of having the crack propagate through the brittle weld at the desired value of P . For example, if the brittle weld were fatigue precracked, the depth of the fatigue crack would have to be closely controlled so that the K_{Ic} of the weld would occur at the proper value of P . This difficulty was avoided by precracking at a chosen load by use of a hydrogen charge as suggested by ORNL personnel. By this method, the unprecracked specimen is loaded to the desired value of P , after which the weld at the exposed tip of the machined crack is hydrogen charged. This charge then initiates the running crack, which can extend under the desired value of load through the brittle weld. The test setup for conducting such tests is shown in Fig. 2.6.

Six tests of this type were conducted. One specimen was loaded to the capacity of the testing machine without charging and did not crack. The other five were hydrogen charged under load, and the crack propagated through the brittle weld. In three of these specimens the crack was arrested by the base plate, while in the other two the crack propagated through the complete specimen. Those specimens that did not completely fracture were cooled and broken in bending to examine the fracture surface so that a , the actual crack length, could be measured. There was found to be some uncertainty in selecting a value of a by fracture appearance since the weld does not terminate in a sharp line, but in a series of spikes, as shown in Fig. 2.7a. This

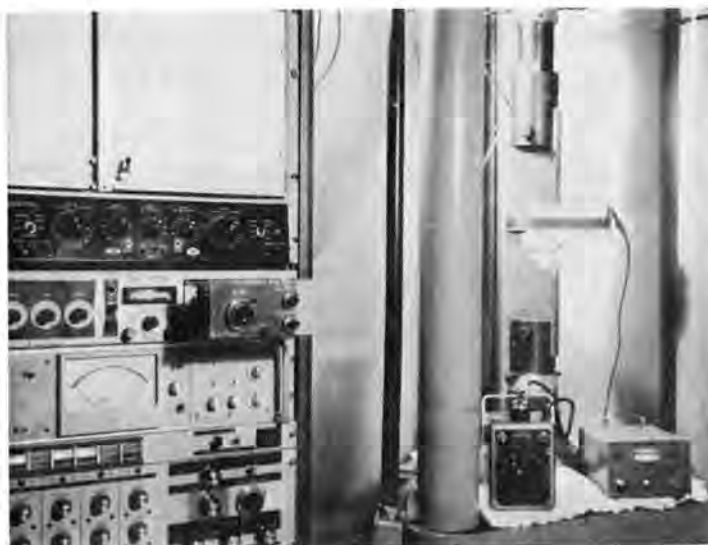


Fig. 2.6. Photograph of test setup showing hydrogen charging arrangement.

“spiked” appearance is more apparent in Fig. 2.7*b*, which shows the other half of this same specimen after grinding and etching. (The electron beam weld is so narrow that the deepest part of the weld is removed on grinding off the surface roughness. Hence the crack length will be somewhat less if measured on Fig. 2.7*b* than on 2.7*a*.) The last of the tested specimens that arrested was heat tinted prior to final fracture. As shown in Fig. 2.7*c*, this procedure marks the crack quite well, eliminating the uncertainty in selecting a ; this procedure will be used in all subsequent tests. The appearance of the heat-tinted specimen suggests that the effective crack length for the brittle weld is near the end of the deepest spike. Using this definition of crack length, a could be estimated to about 0.1 in., which represents an error of about 10% in K .

The values of K for each of the five tests in which the weld cracked are plotted in Fig. 2.8 along with the scatter band previously obtained. Note that the overlapping band in which the crack may or may not arrest identifies the same value of K_{Ia} as given by the bottom of the scatter band at room temperature. Hence, for these tests at least, K_{Ia} as measured by a TDCB specimen (with zero K gradient) and by an SEN specimen (with a positive K gradient) is the same.

In addition to demonstrating that K_{Ia} is an invariant, the use of SEN specimens with a brittle weld appears to make it possible to measure K_{Ia} at temperatures above those over which data are now available. In fact, the

upper temperature limit for measuring K_{Ia} appears to be the highest temperature at which a brittle crack can be propagated in the weld. If the brittle weld and charging procedure were used with TDCB specimens, or any specimen in which the K gradient were not positive, it would not be necessary to bracket the K_{Ia} values; instead, each test should yield a distinct value of K_{Ia} so long as the crack arrests at some distance beyond the weld.

Effects of Strain Gradients on the Gross Strain Crack Tolerance of A533 B Steel⁵

P. N. Randall

TRW Systems Group of TRW, Inc.

The reasons for studying the effects of strain gradients on gross strain crack tolerance are twofold. First, previous test data have been obtained in axial tension, but in the typical service application most regions of high strain are local, with gross strain gradients in the direction of crack advance and also along the normal to the crack plane. The thick-walled pressure vessel also has a strain gradient through the membrane wall. Thus an understanding of strain-gradient effects is needed to guide the application of test data to design.

⁵ Work performed under UCCND Subcontract No. 3134 between Union Carbide Corporation and TRW, Inc.

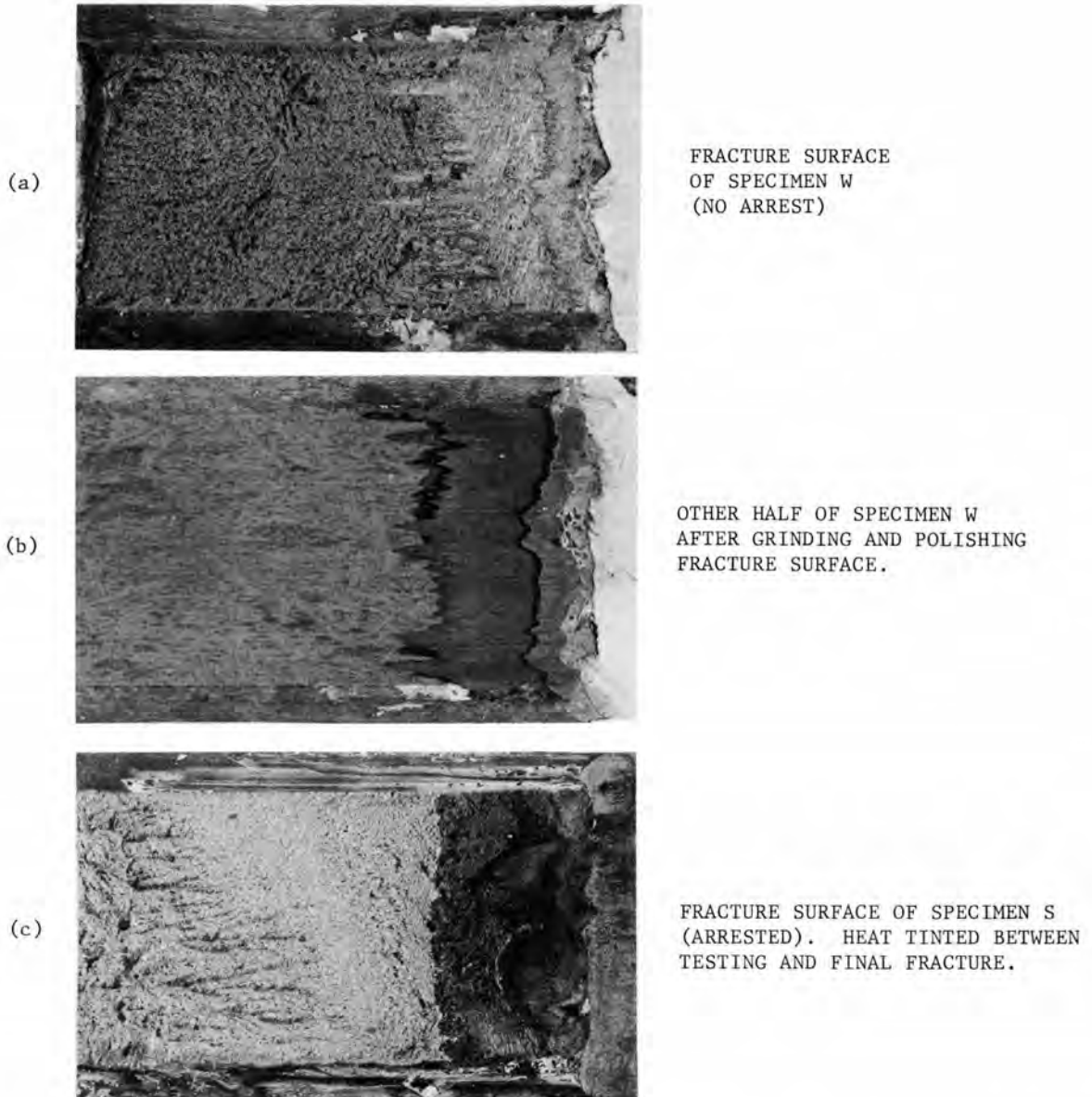


Fig. 2.7. Fracture appearance of several SEN specimens. Cracks in all cases extending from right to left, that is, brittle weld on right.

The second reason for this study is to broaden our investigation of the gross strain concept. For example, we still have questions about where, on the specimen, gross strain should be measured. The reasons were previously discussed⁶ in the light of the concept of a local, crack-tip strain criterion for fracture, the critical magnitude of which depended on constraint and hence

on the extent of the plastic zone. Being unable to measure the local crack-tip strain, we measure gross strains at a distance from the crack. Experience has taught that both the net-section gross strains and those in the gross sections above and below the crack are important.

Thus we expect to find in this study that the worst specimen configuration is one that focuses a high gross strain level in the cracked region to produce a high value of local crack-tip strain, ϵ_f , and that also produces

6. P. N. Randall, *Gross Strain Crack Tolerance of A533-B Steel*, HSSTP-TR-14, TRW Systems Group (May 1, 1971).

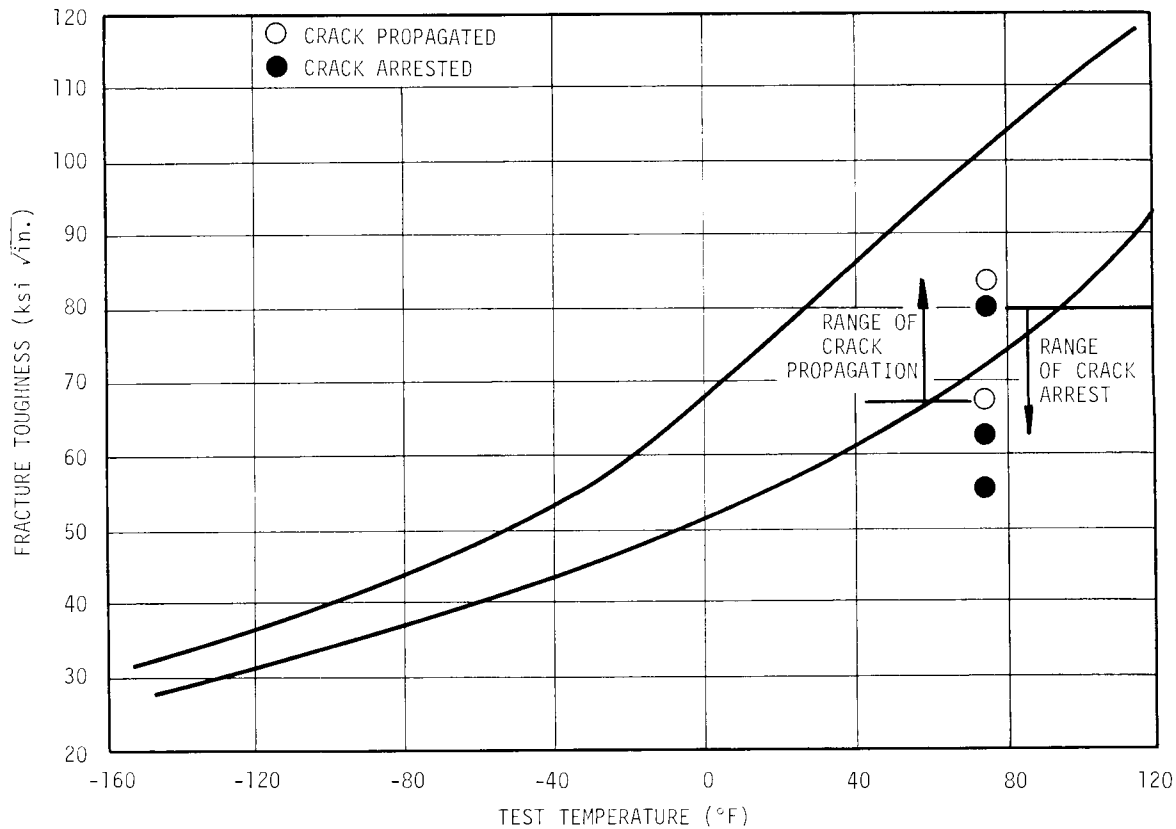


Fig. 2.8. Crack arrest and propagation values obtained on SEN specimen compared with scatter band obtained on tapered double-cantilever beam specimens.

a relatively low gross strain level just beyond the vicinity of the crack. This will limit the extent of the plastic zone, thereby producing maximum constraint at the crack tip and a low value of ϵ_{lc} , the critical local strain. A tensile or bend specimen with a crack in a groove or fillet represents the configuration described. Some tests of this kind are planned. We also plan to test the effects of transverse strain gradients alone, using beams of various depths. Finally, a tensile specimen with shallow grooves on both the cracked face and the back face will be tested to measure the effect of an axial gradient alone, or nearly so.

Test plan

Transverse strain gradients are to be studied with beam specimens loaded in four-point bending. The specimen proper is 0.60 in. thick, 2.64 in. wide, and 22 in. long, with a semielliptical crack 0.68 in. long at midspan on one face of the specimen. These were grown in bending fatigue, with a stress cycle of +4 to

+39 ksi, once the crack appeared at the end of the ground slot used for a crack starter. Based on last year's experience, these cracks should be 0.22 in. deep, because the specimen geometry is identical to the intermediate size tested then.

Three degrees of severity of transverse strain gradient are to be tested, as shown in Fig. 2.9. The measure of severity indicated beside each sketch is the ratio of strain at the crack-tip depth to that at the surface. Beam depth is to be varied by welding on a backup bar or slave beam, as indicated schematically in Fig. 2.10. The welds do not extend into the gage length because there is no shear to transmit between the specimen and backup bar in the midspan region between the loading points.

In the first three test series, shown in Fig. 2.9, strain decreases in the direction of crack advance. In series 4 (Fig. 2.10) strain is made to increase in the direction of crack advance by welding the backup bar to the cracked face. This configuration simulates a crack on the inside diameter of a heavy-walled vessel.

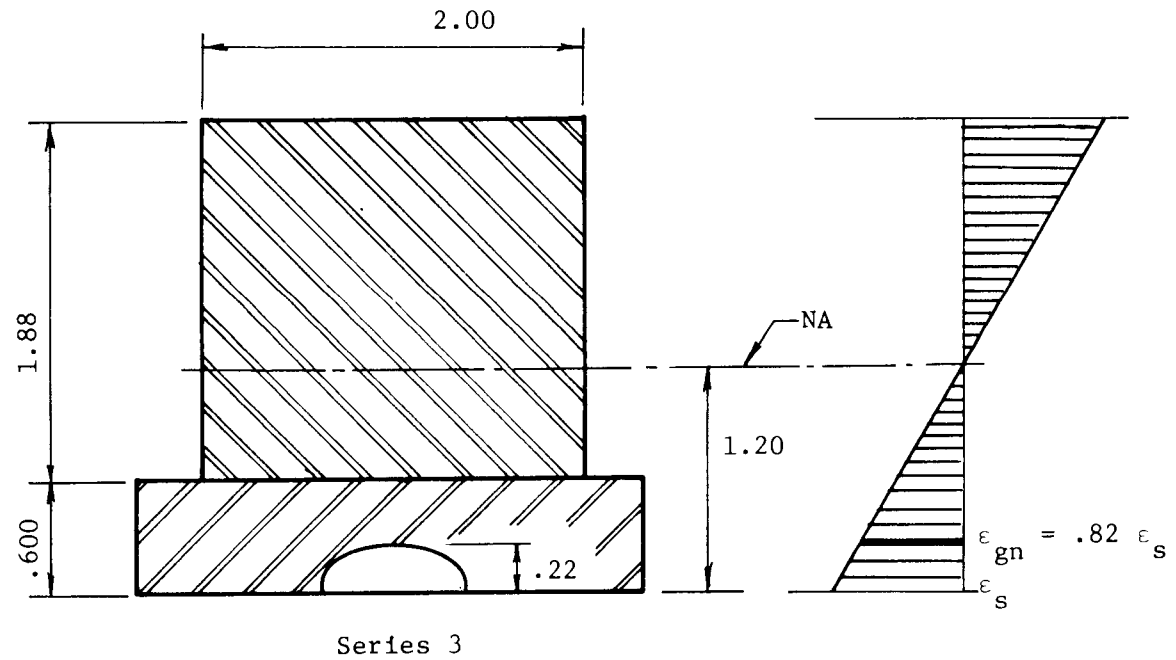
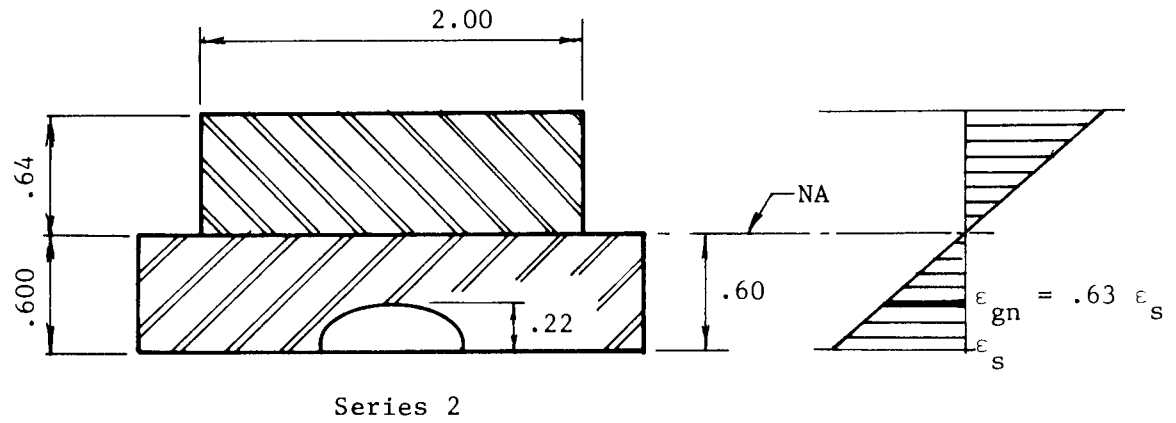
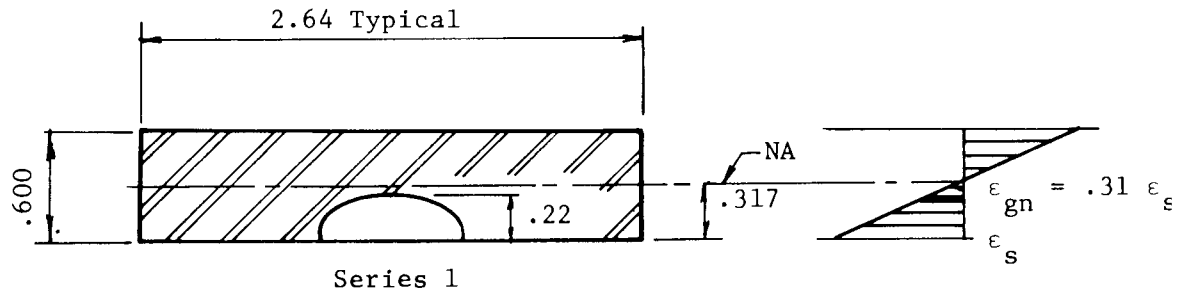


Fig. 2.9. Beam cross sections to be used to produce transverse strain gradients.

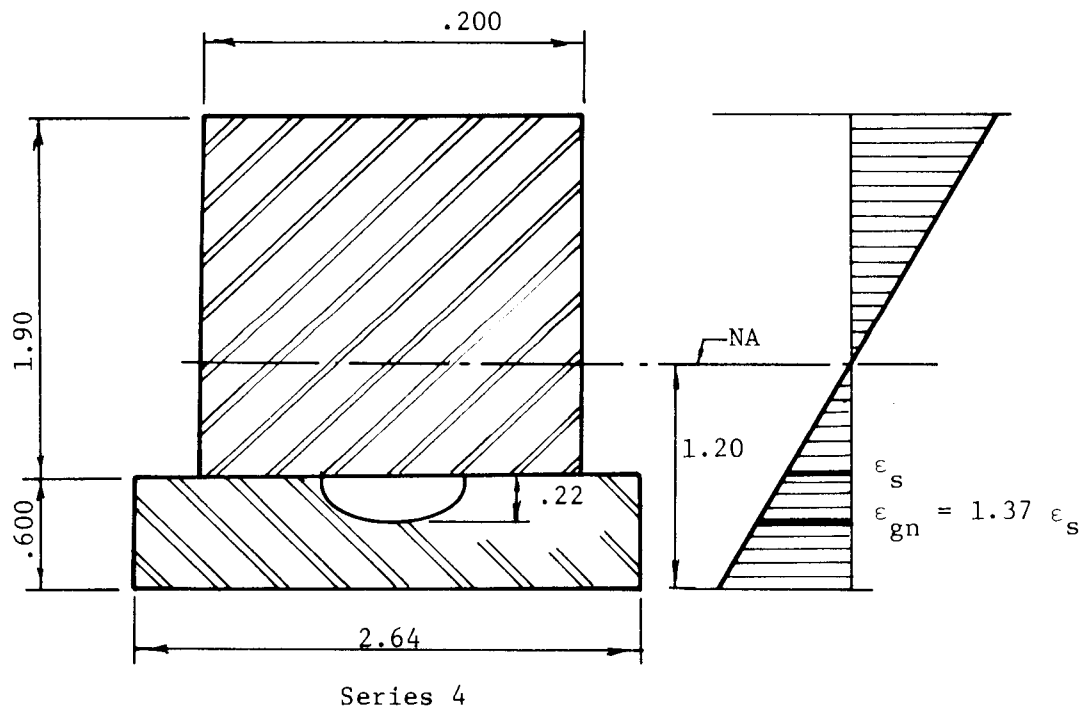
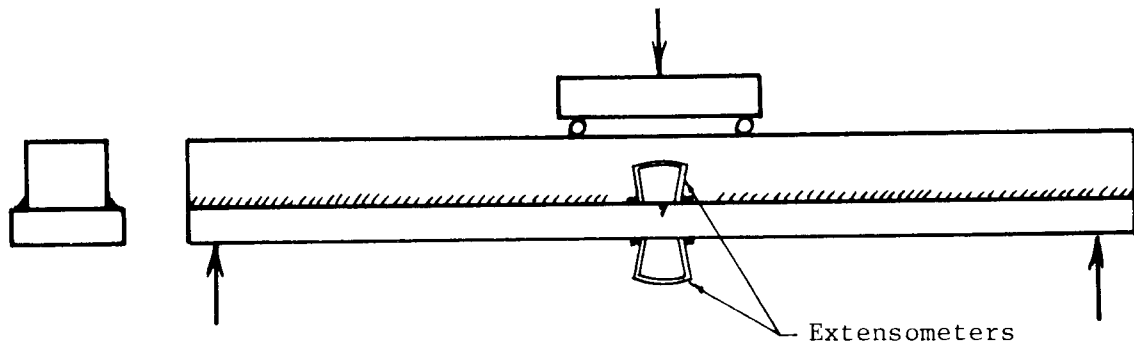


Fig. 2.10. Built-up beam to be used to produce a strain gradient that increases in the direction of crack advance.

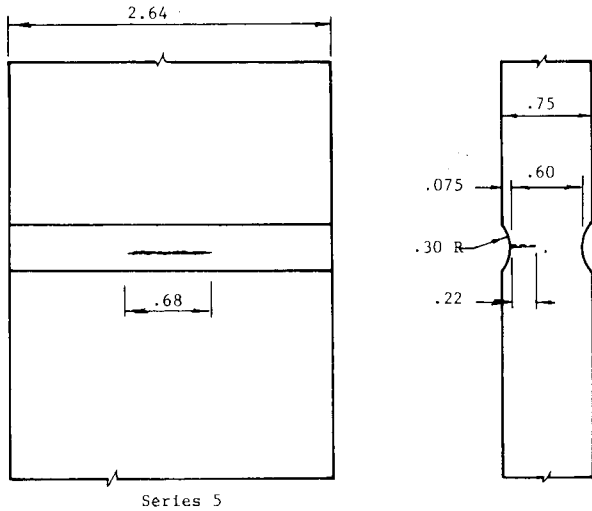


Fig. 2.11. Double-face-notched bar for tests of the effects of axial gradients.

Series 5, Fig. 2.11, represents an attempt to produce an axial strain gradient without introducing much transverse gradient also. It is an attempt to enhance the net-section effects found earlier to see how important axial gradients are in a crack-in-a-notch configuration. In those tests, when the specimen width was reduced, the transition temperature rose, which was the opposite effect from that predicated on constraint effects. The cause was believed to be an increase in constraint produced by yielding in the net section, with no yielding above or below the crack because of the low gross stress there. The mild notches in the series 5 specimen cause the gross stress to be only 80% of the average stress on the notched section.

Series 6 and 7, Fig. 2.12, represent the crack-in-a-notch configuration, which has all the effects of axial and transverse strain gradients combined. Series 6 will be tested in axial tension and series 7 in bending. Later results may indicate that a backup bar should be used in series 7 to produce a smaller transverse gradient.

Experimental

Material. All the test specimens and backup bars were cut from plate 02. The locations are shown in Fig. 2.13. The material for backup bars had been set aside previously because there were quite a few slag inclusions indicated. As before, the specimens were sawed from the block and Blanchard ground to finished dimensions. Those used in tension had a reduced section formed by a milling operation.

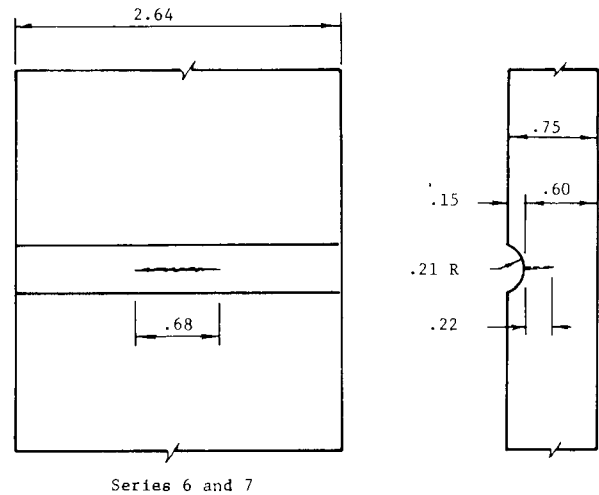


Fig. 2.12. Single-face-notched bar for tests of the effects of axial plus transverse gradients.

Test fixtures. A new bend fixture, shown in Fig. 2.14, had to be designed and built to accommodate the large loads expected in some tests. Four-point loading is used. The span between the loading pins was made 6.00 in. to clear the gage region, which totals 5.20 in. For thin specimens, a span of 14 in. is used to get large strains without excessive deflections; for the remainder, a span of 19 in. is provided. The pins are free to turn in lubricated seats. They do not roll, because they must carry the transverse forces that develop when the beam deflects a considerable distance.

The load cell used in tension, a 2-in.-diam threaded rod with strain gages mounted on it, is also used here, but in compression. It serves to connect the center loading pins to the crosshead of the testing machine.

Cooling of the bend specimens is accomplished in the box shown in Fig. 2.14. Liquid nitrogen is admitted to the ends and the center section separately, where it immediately vaporizes to cool the specimen.

Strain measurement

The choice of displacements to be measured was based on the requirement that the test results provide evidence on the effects of strain gradients without introducing other differences between the tensile and the bend tests. Thus, gross strain in the net section ϵ_{gn} was again defined as the average strain in a gage length of 3.2 in. spanning the plane of the crack. Gross strain in the gross section ϵ_{gg} was measured on 1-in. gage lengths in uncracked sections of the beam as described

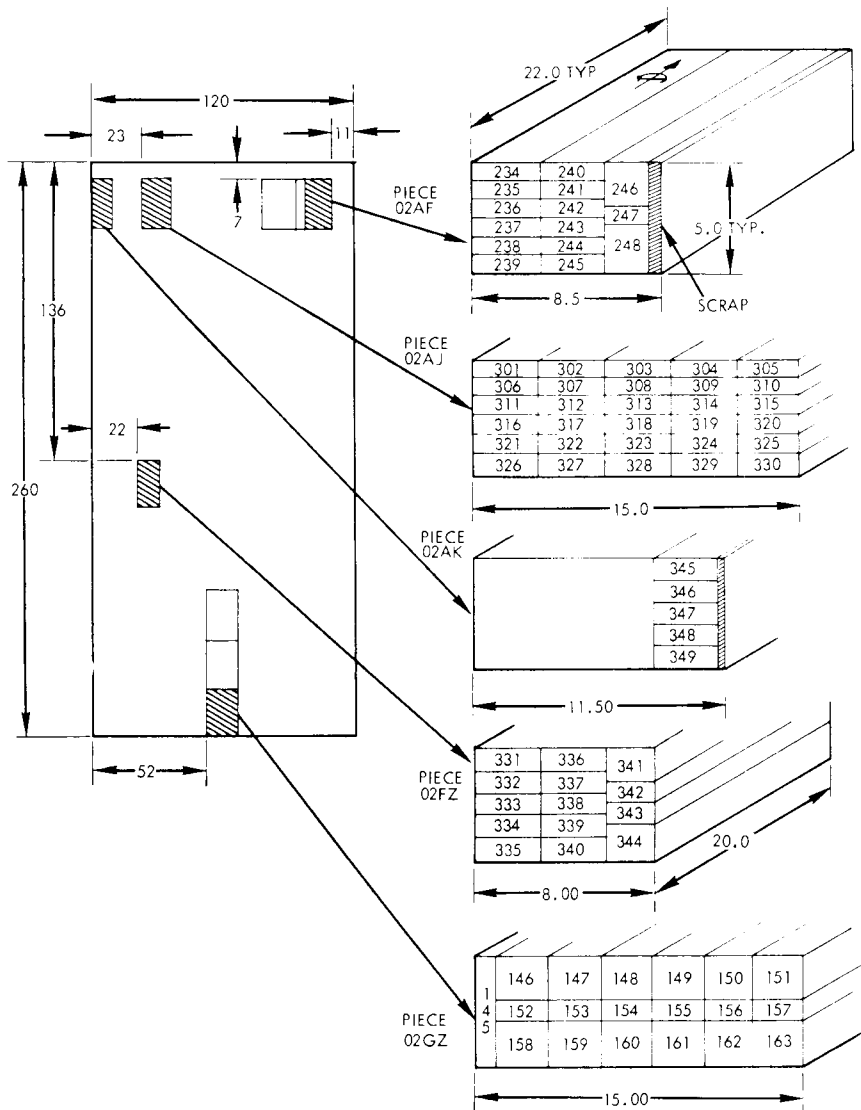


Fig. 2.13. Layout of specimens in plate 02. All blocks were cut with the 5-in. thickness centered on the plate midplane. Those not detailed were reported in HSSTP-TR-14, Ref. 2.

below. Crack opening displacement, COD, was measured in the same way as before.⁶

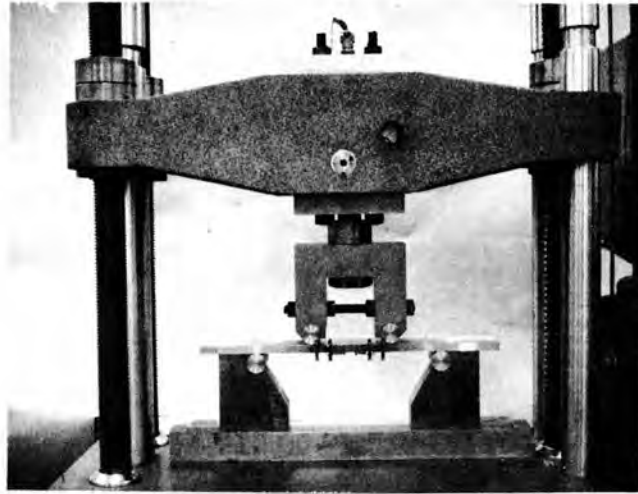
The angle changes produced by the bending caused some changes in the extensometer design and in the method of attachment to the specimen.

The gage points are the fillet welds that connect the gage blocks to the specimen as illustrated in Fig. 2.15. The extensometer system, shown in Fig. 2.16, makes use of the same strain-gaged flexures as before, but the arms have been rebuilt to provide a V-groove that bears on the pin of each adapter while allowing free rotation of the pin. The pins for the ϵ_{gg} measurements are

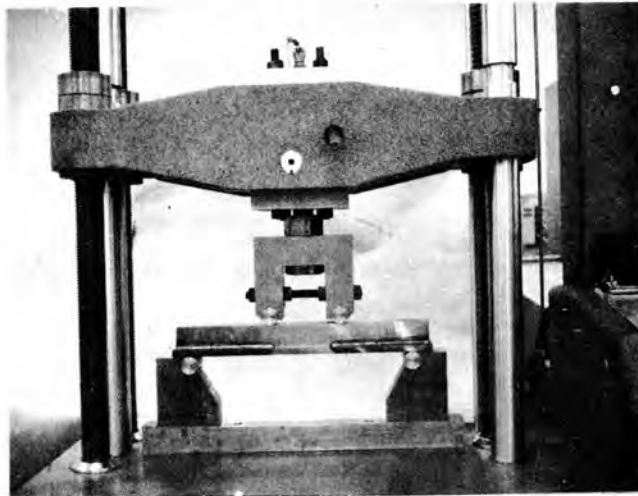
positioned above and below the specimen to magnify their motion and to improve sensitivity.

To avoid multiple extensometer geometries, some of which would be quite large, adapters were provided for the ϵ_{gn} measurement as shown. Their span is larger for the compression face (top) than for the tension (bottom) face, because the two will travel toward null from opposite directions. As shown in Fig. 2.16, the extensometer arms are reversed so they will fall free when the specimen breaks.

Five records are obtained from the seven extensometers. Load is recorded as the abscissa on three X - Y



14-IN. SPAN



19-IN. SPAN

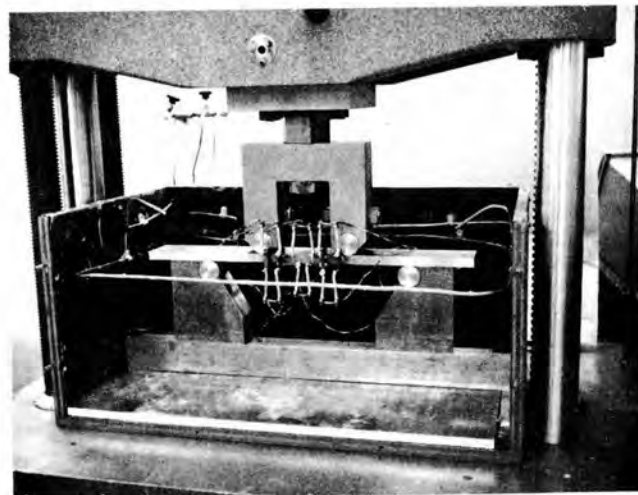


Fig. 2.14. Bend fixture and cooling box.

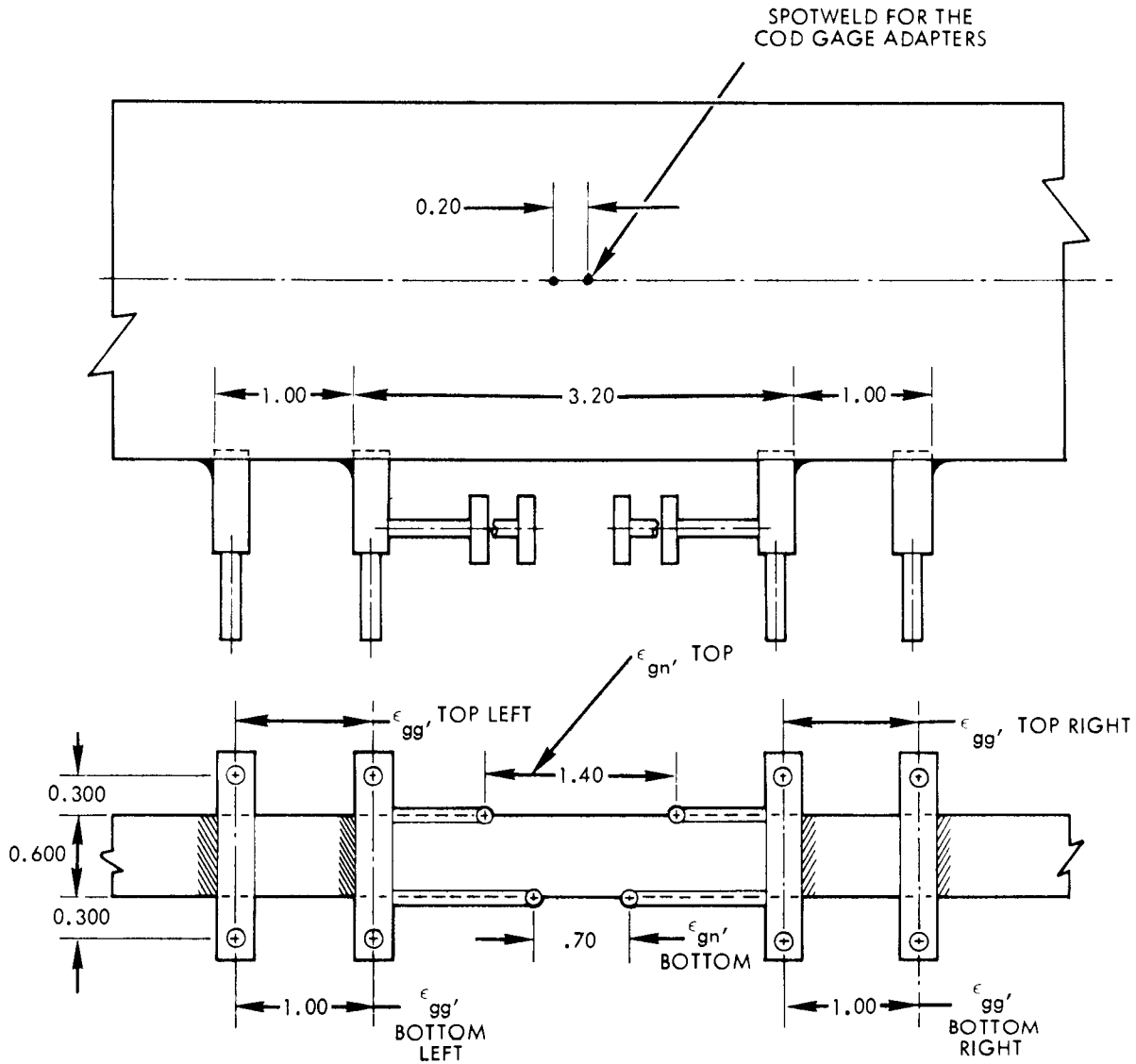


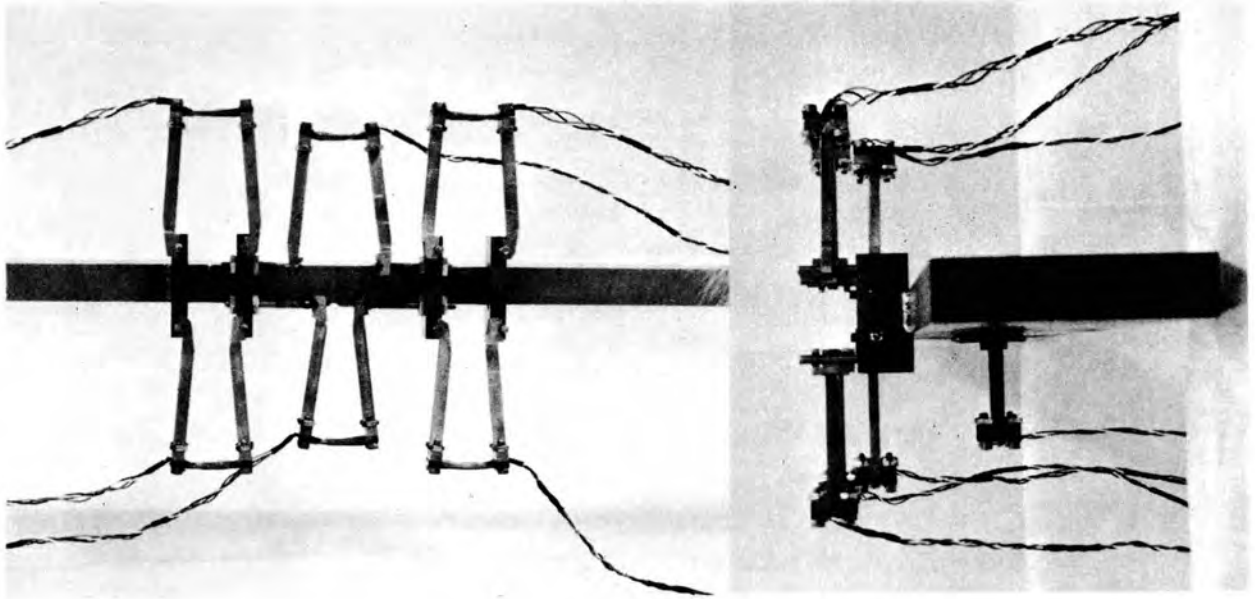
Fig. 2.15. Gage block layout and adapters for the extensometers.

plotters. Displacements ϵ_{gn} , top, and ϵ_{gn} , bottom, are recorded on one plotter. On another plotter are recorded ϵ_{gg} , top (average of left and right) and ϵ_{gg} , bottom (average).

A third, single-pen plotter is used for recording COD vs load. No averaging of measurements on opposite edges of the specimen was attempted. We believe the differences would be small, because the rigid bend fixture constrains both edges to deflect the same amount.

Reduction of the displacement data requires some analysis, because a ductile specimen produces a large

amount of relative rotation of the gage blocks, as shown in Fig. 2.17. Derivations of the expressions used to obtain surface strains ϵ_{gn} from the recorded displacements are given in Fig. 2.18. A derivation of similar form was made for ϵ_{gg} , but it was found to be unnecessary for the tests in this series. A simple linear interpolation will be used to compute the displacements at the specimen surfaces. Most of the complications arise from the fact that the pins that bear in the V-grooves of the extensometer arms do not lie in the plane of the cross section that contains the gage points (the fillet welds). Assumptions basic to this derivation



(COD gage removed)

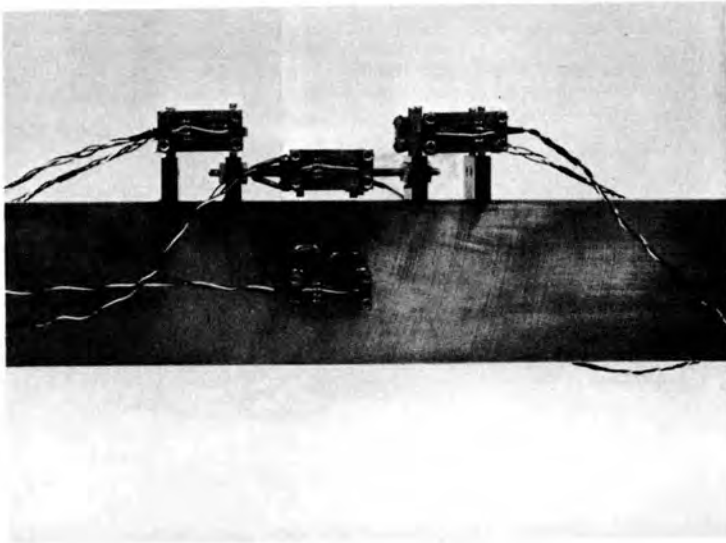


Fig. 2.16. Three views of the extensometer system.

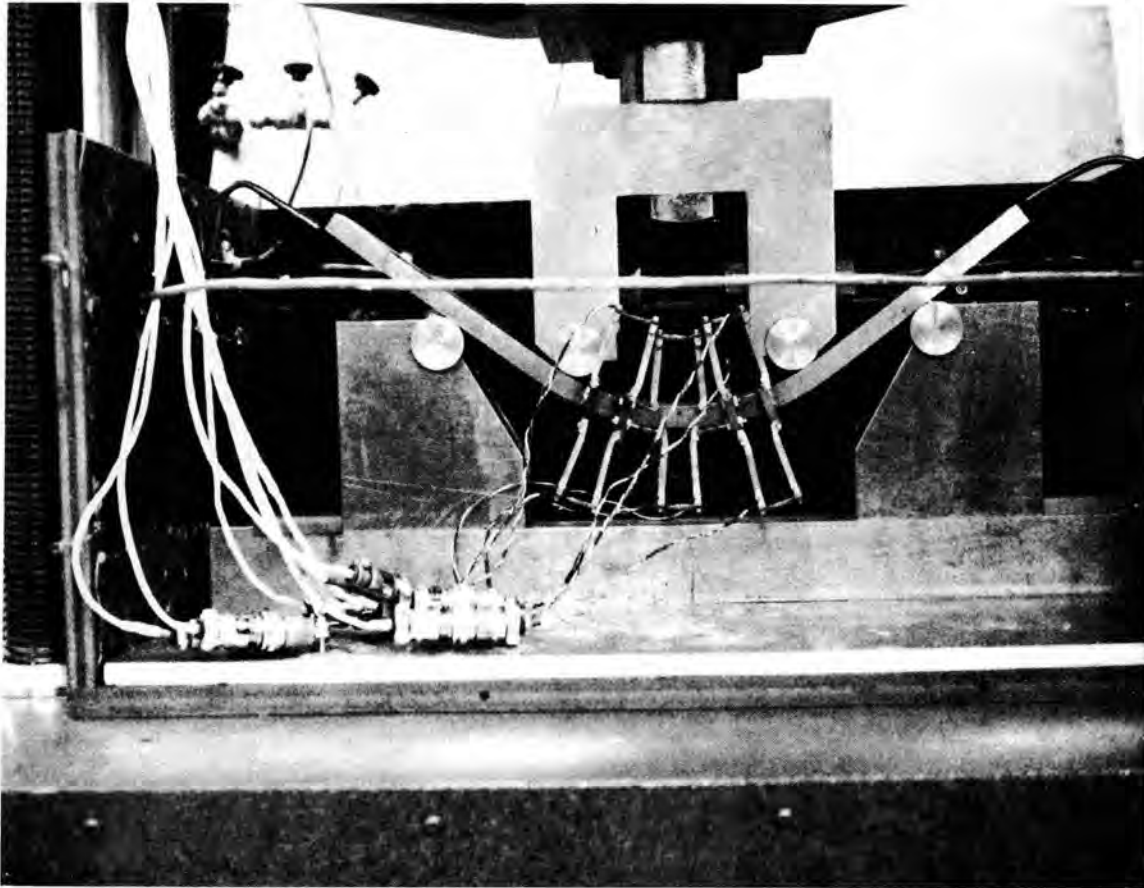


Fig. 2.17. Specimen 235 (0.600 in. thick) before the load was removed at completion of test at room temperature.

are: (1) plane sections remain plane; (2) the specimen axis deforms in a circular arc within the span between the upper rollers — the region of uniform bending moment; and (3) the specimen cross section remains rectangular; that is, no significant anticlastic curvature.

Initial test results

The first trial of the extensometer system was obtained at room temperature with 0.6-in.-thick specimen 235, shown in Fig. 2.17. The load had passed through a maximum shortly before as a result of changes in direction of the reaction forces instead of from crack growth, and the test was stopped. Theoretically, the compressive strain on the top surface of the specimen should have been equal to the tensile strain on the bottom, and in the elastic range this was true. The tensile strain at ϵ_{gn} bottom was 1.5%; ϵ_{gn} top was slightly over 1%. The values of ϵ_{gg} top and bottom were somewhat closer at that time. As loading continued, the

disparity grew steadily greater until at the end of the test the strain distribution was as given below.

	ϵ_{gnc}	ϵ_{ggc}
Top	-3.8%	-2.6%
Bottom	+6.9%	+6.2%
Upward shift in neutral axis	88 mils	127 mils

One probable reason for the shift in neutral axis was the development of axial tension from friction in the loading fixtures at large deflections. Another was the development of anticlastic curvature, which was quite noticeable. The edges of the specimen dropped down about 0.05 in. below the center. The gage blocks tilted also, but they were removed before we thought to measure the amount. This will be done in future tests above the transition temperature, and a correction will be made in the reduction of data (Fig. 2.18).

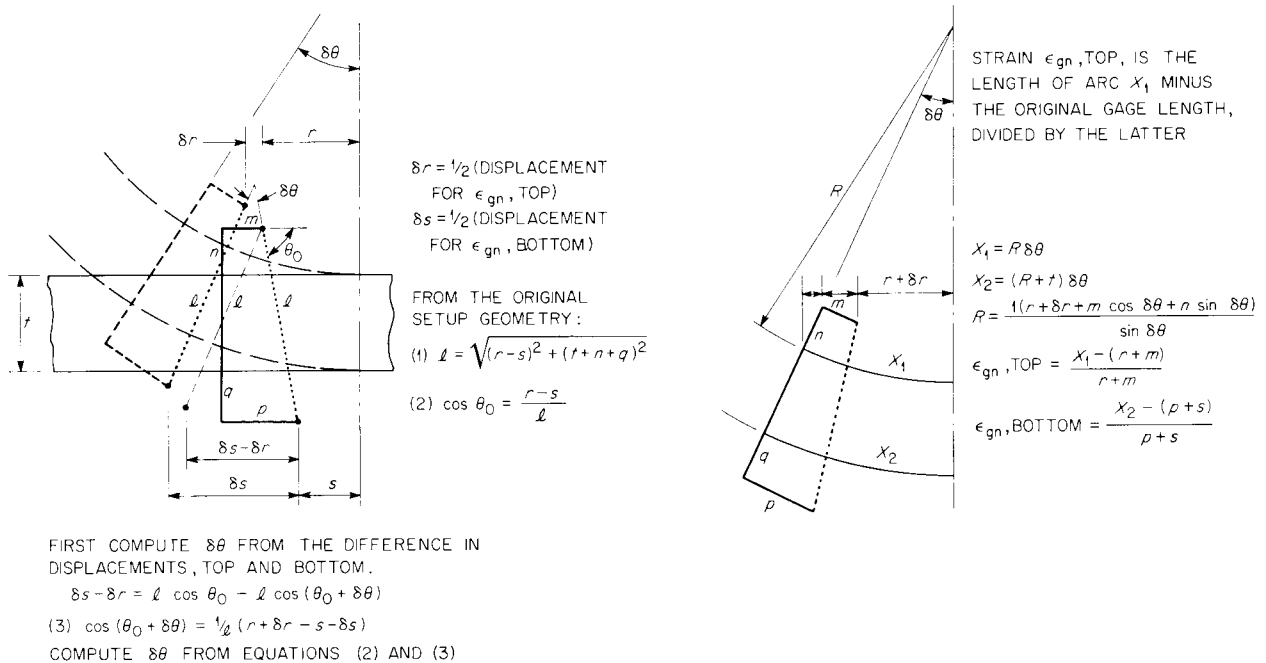


Fig. 2.18. Derivation of expressions for surface strains obtained from recorded displacements.

The second test result was obtained from a specimen of series 3, with the neutral axis positioned 0.60 in. above the top of the specimen proper to produce an elastic strain gradient having a ratio of 1:2 between ϵ (top) and ϵ (bottom). The specimen was tested at -30°F , with results that were comparable with those for tension tests of specimens with 0.22-in.-deep cracks reported earlier. No yielding occurred in the gross section. In the net section, ϵ_{gnc} bottom was 0.51% and ϵ_{gnc} top was 0.20%. Their ratio had been about 0.44 until yielding began. Yielding on the bottom surface only shifts the neutral axis upward.

After these initial results, testing will start with series 1 and go through the test plan in sequence. A prime purpose in doing each series is to locate and define the shape of the transition in critical gross strain values with temperature and to compare the results with those obtained earlier in tension.

Three-Dimensional Elastic-Plastic Stress and Strain Analyses for Fracture Mechanics⁷

P. V. Marcal N. Levy J. R. Rice
Brown University

The long-term objective of this program is to develop an elastic-plastic analysis of a complex three-dimen-

sional cracked structure. This analysis can be applied to a variety of safety problems, for example, a crack at the junction of two cylindrical intersections. However, it is important to proceed toward this goal by a series of well-ordered steps. The advance at each stage can then be consolidated by comparisons with experimental results. We have previously reported⁸ the elastic, perfectly plastic analysis of a part-through surface cracked tensile specimen being tested for the HSST program by Southwest Research Institute. We have recently repeated this same analysis, as planned, using the finite-element layout shown in Fig. 2.19, and assuming the material to be an elastic, isotropically strain-hardening Mises material. Figure 2.20 shows a portion of the effective stress vs equivalent plastic strain curve of the material (A533, grade B, class 1 steel) as determined by a uniaxial tensile test. Although the average true stress vs plastic strain curve beyond the maximum load in the tensile test was given, we confine ourselves to that portion of the curve below the

7. Work being performed under UCCND Subcontract No. 3153 between Union Carbide Corporation and Brown University.

8. N. Levy and P. V. Marcal, *Three-Dimensional Elastic-Plastic Stress and Strain Analysis for Fracture Mechanics. Phase I: Simple Flawed Specimens*, HSST Technical Report No. 12.

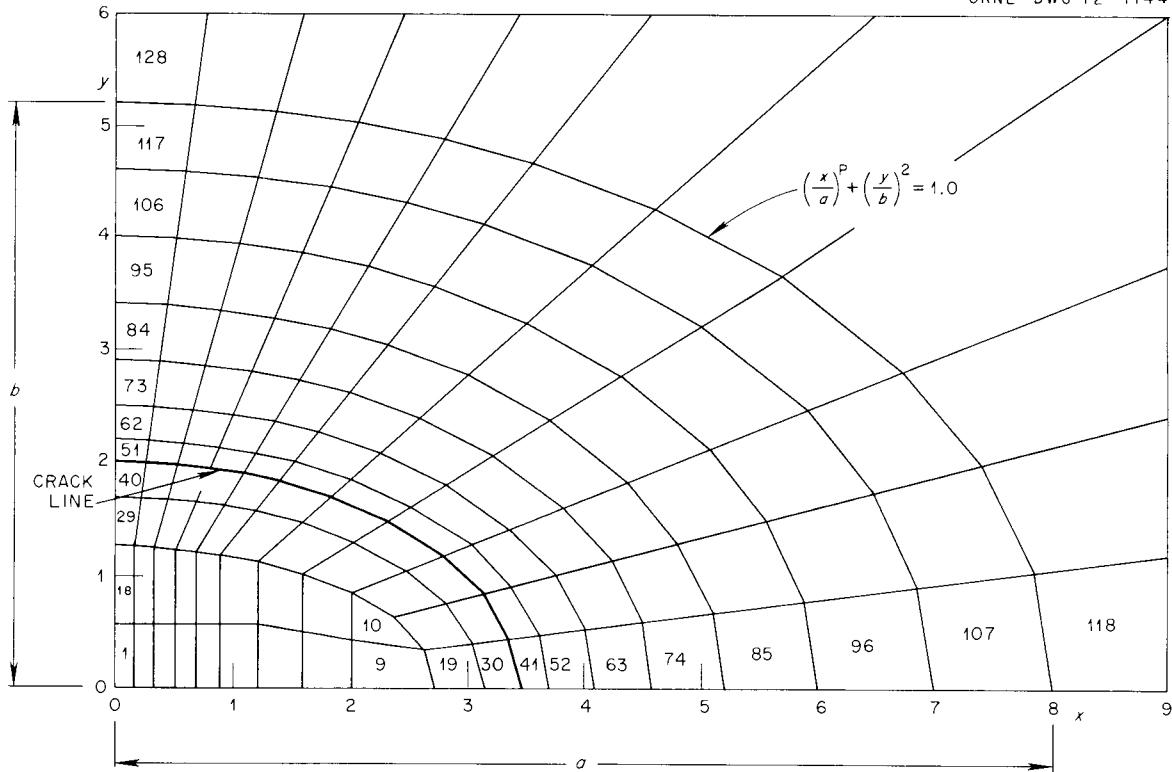


Fig. 2.19. Mesh distribution in the crack plane.

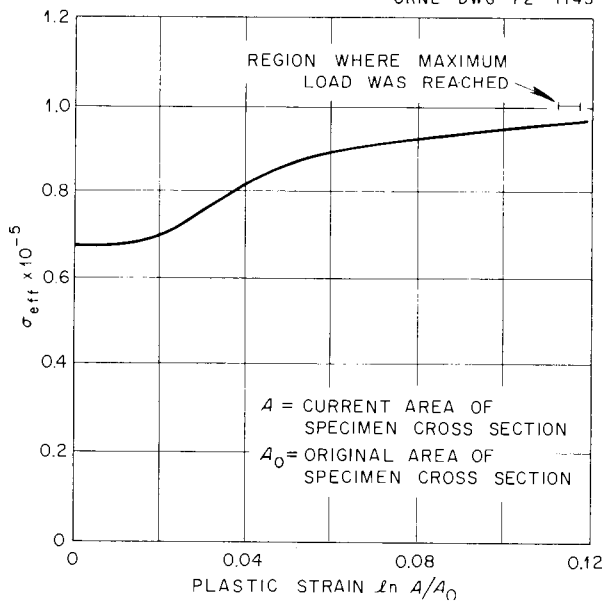


Fig. 2.20. Dimensionless stress-plastic strain curve.

maximum load. At the maximum load, necking occurs, the stress ceases to be homogeneous, and the average true stress vs plastic strain clearly depends on the geometry of the neck. It is therefore doubtful that this portion of the curve will be applicable to the yielding elements in a flawed specimen where the geometrical constraints are different. Thus, to study the behavior in the plastic range with strain hardening, load increments were added to the elastic load, and the solution was terminated as soon as the effective stress in one or more elements reached the value corresponding to the maximum load in the tensile test. This occurred in the elements at the crack line in the plane of the crack when the loading stress σ_{∞} attained the value of 1.2 of the yield stress. The tangent modulus approach as formulated by Marcal and King⁹ was followed. As for the perfectly plastic case, loading of the specimen was

9. P. V. Marcal and I. P. King, "Elastic-Plastic Analysis of Two-Dimensional Stress Systems by the Finite Element Method," *Int. J. Mech. Sci.* 9(3), 143-55 (1967).

made by imposing uniform displacement in a direction perpendicular to the plane of the crack.

As the load increments were added to the elastic load, it was found that initially the plastic strains in the yielding elements were of the same order as the elastic strains due to the constraints on deformation imposed by the elements still below the initial yielding stress σ_0 . Thus the strain-hardening effects were negligible up to the load that corresponded to the limit load in the perfectly plastic material. In fact, the shape and the extent of the plastic zones at various load increments for the strain-hardening material were essentially the same as for the perfectly plastic material (see Figs. 2.21 and 2.22) as long as the average imposed stress was below the initial yield stress. As the imposed stress was increased further, the plastic zone spread rapidly, and at $\sigma_w = 1.05\sigma_0$, all the elements had yielded with the exception of the elements 1 to 30 adjacent to the crack free surface (see Fig. 2.19).

Fig. 2.23 shows the variations of σ_{zz}/σ_0 in the elements along the crack line with the angle measured

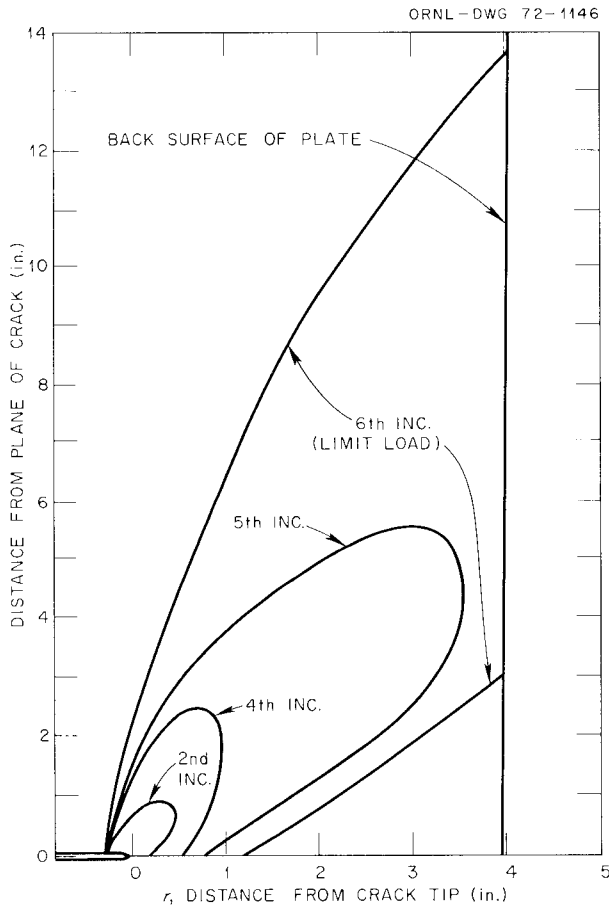


Fig. 2.21. Elastic-plastic boundaries in the midplane.

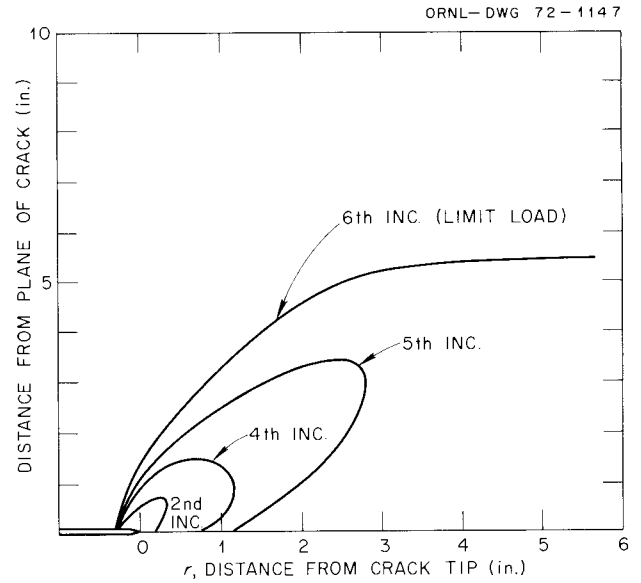


Fig. 2.22. Elastic-plastic boundaries on the free surface.

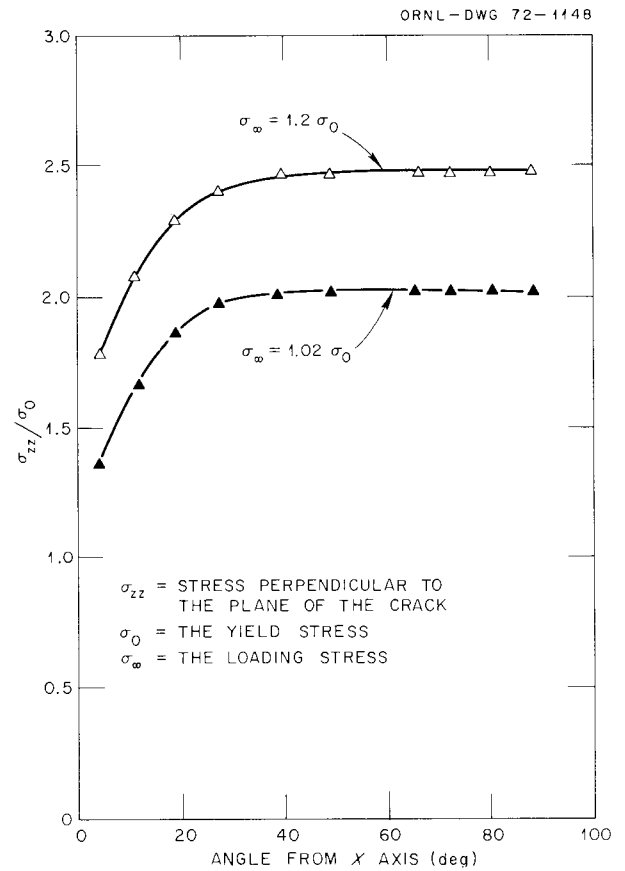


Fig. 2.23. Normal stress distribution along crack tip.

from the x axis (Fig. 2.19) for two loading stress σ_∞ levels. It is obvious that σ_{zz}/σ_0 varied little in the elements along the crack except in those nearest to the free surface of the specimen. This fact permits us to consider element 51 (Fig. 2.19) as representative of all the elements along the crack line.

Figures 2.24 and 2.25 show the variation of the equivalent plastic strain and the σ_{zz} stress in element 51. As shown in Fig. 2.23, the equivalent plastic strain increased very rapidly when the loading stress σ_∞ approached the value corresponding to the yield load in a perfectly plastic material with a yield stress equal to the initial yield stress of the strain-hardening material. In Fig. 2.25, a similar behavior may be observed for the variation of the stress σ_{zz} with the loading stress. The numerical results indicate the same behavior for the hydrostatic tension. It is noted that the ratio σ_{zz}/σ_{eff} , where σ_{eff} is the current yield stress, tends toward the value of approximately 2.1, which is comparable with the ratio of σ_{zz} to the yield stress in the perfectly plastic material. This suggests that the degree of constraint is essentially maintained even though higher stress values have been induced through the work hardening.

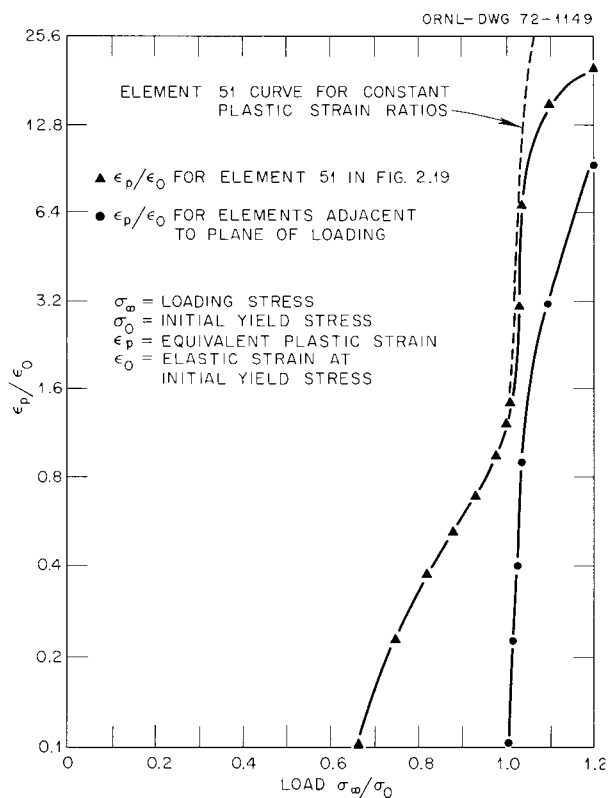


Fig. 2.24. Plastic strain history.

In the work performed to date, we have obtained the numerical solution for a semielliptic crack in a plate. Several useful conclusions can be drawn from this work concerning parameters considered significant in fracture mechanics. The stress intensity factor along the minor axis of the crack has been calculated, and the significance of the moment induced by the uncracked region of the plate was assessed. In the plastic range, the magnitude of the triaxiality, obtained at the crack tip along the minor axis has been shown to be two-thirds of the value obtained in the plane strain. Furthermore, although the finite element used for analysis did not give the crack opening at the crack tip, a measure of this has been obtained from the value of the crack surface separation near the crack tip. This separation is proportional to the square of the imposed load.

In conclusion, we have demonstrated the feasibility of using the finite-element method to extract useful and important information on the stress state near the tip of a semielliptic crack in a plate of a given configuration. Because of the improvements made in the efficiency of the computer program, it is now feasible to obtain numerical solutions for various crack configurations (i.e., various crack depth/plate thickness and crack

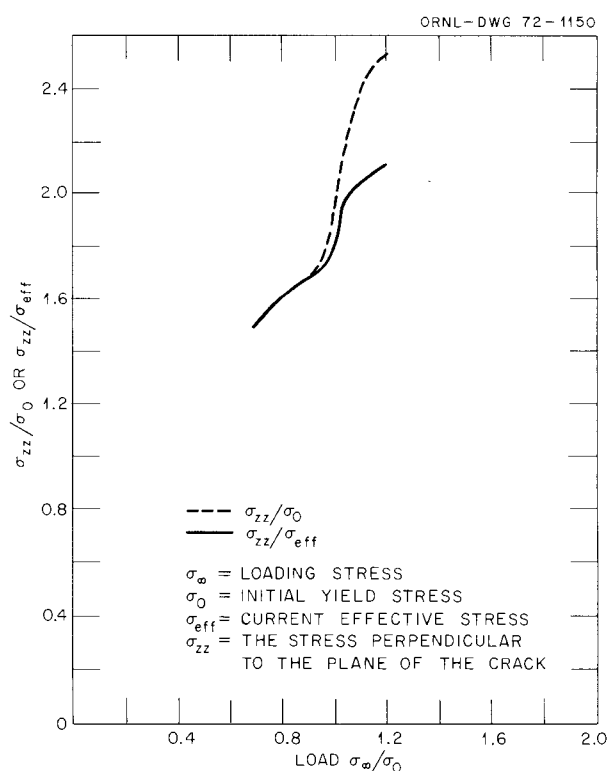


Fig. 2.25. Normal stress history for element 51.

length/plate thickness ratios). Future work should be concerned with parametric studies of the flawed tensile specimen and comparisons with available experimental results.

Fracture Mechanics Characterization of HSST Program Materials¹⁰

T. R. Mager
Westinghouse Electric Corporation

As previously reported, Witt¹¹ proposed an equivalent-energy method for relating crack size, temperature, and stress levels at maximum load to fracture and outlined a procedure for obtaining the fracture toughness value K_{Icd} . Using the equivalent-energy method as set forth by Witt,¹¹ data developed this report period were used for determining upper and lower bounds¹² on the fracture toughness of A533, grade B, class 1 steel.

Experimental test procedure

Ten 1-in.-thick, seven 6-in.-thick, and two 9-in.-thick compact-tension specimens were evaluated this report period. All the specimens were machined from HSST plate 03. Six of the ten 1T compact-tension specimens were pre-fatigue cracked according to the ASTM recommended procedure.¹³

The ten 1T compact-tension specimens were machined with the crack front oriented transverse to the rolling direction and the load applied with the rolling direction. Thus the specimens were oriented in the rolling direction (RW). Ten 1T compact-tension specimens fabricated from HSST plate 03 and oriented in

the transverse (WR) direction were evaluated the previous report period.¹⁴ Four of the seven 6T specimens were oriented in the RW direction, while the remaining three specimens were oriented in the WR direction. The two 9T specimens were oriented in the RW direction.

Results

The 1T compact-tension specimens were tested at temperatures from 0 to 550°F. Using the method previously outlined,¹¹ K_{Icd} values were calculated at each test temperature. The K_{Icd} data are summarized in Table 2.1. Four of the ten specimens were not precracked prior to testing. The data in Table 2.1 indicate that sharp notched specimens (fatigue precracked) exhibit a lower K_{Icd} value than unnotched specimens.

Data from the testing of the 6T and 9T specimens are summarized in Table 2.2. Results in Table 2.2 indicate that orientation has an effect on the upper shelf K_{Icd} values and that specimens oriented in the transverse direction exhibit lower K_{Icd} values. The K_{Icd} data indicate a very high resistance to fracture at 550°F.

Future work will include evaluating specimens fabricated from an Ni-Cr-Mo-V rotor forging steel for which valid plane strain upper shelf data exist.¹⁵ These tests will be used to validate the equivalent-energy concept.

Fatigue and Crack-Propagation Investigations

L. F. Kooistra

Crack growth rate studies have been conducted in an environment of high-temperature reactor-grade water (without irradiation) at two separate laboratories. The investigation sponsored by the HSST program has been completed, and a paper on this work was presented at the Fifth Annual Information Meeting of the HSST program at the Oak Ridge National Laboratory.¹⁶ A final report is in the last stages of preparation.

Concurrently a similar program is being sponsored by the Japan Atomic Research Institute, and a paper on this work was reported by L. F. Kooistra at the

10. Work performed under UCCND Subcontract No. 3196 between Oak Ridge National Laboratory and Westinghouse Electric Corporation.

11. F. J. Witt, "Equivalent-Energy Procedures for Predicting Gross Plastic Fracture," paper presented at Fourth National Symposium on Fracture Mechanics, Carnegie-Mellon University, Aug. 24-26, 1970 (in publication).

12. F. J. Witt and T. R. Mager, "A Procedure for Determining Bounding Values on Fracture Toughness K_{Ic} at Any Temperature," paper presented at Fifth National Symposium on Fracture Mechanics, University of Illinois, Aug. 28-Sept. 1, 1971 (in publication).

13. ASTM Standard E399-70T, *Tentative Method of Test for Plane-Strain Fracture of Metallic Materials*, ASTM Standards, Part 31, 1970.

14. T. R. Mager, "Fracture Mechanics Characterization and Crack Preparation Studies of HSST Program Materials," *HSST Program Semiannu. Progr. Rep. Feb. 28, 1971*, ORNL-4681, p. 41.

15. J. A. Begley and W. A. Logsdon, *Correlation between K_{Ic} and Charpy V Properties for Rotor Steels*, Westinghouse Research Laboratories Scientific Paper 71-1E7-MSLRF-P1 (June 1971).

16. T. R. Mager, "Fatigue Crack Growth Characteristics of Nuclear Pressure Vessel Grade Materials," paper 1, presented at the Fifth Annual Information Meeting of the HSST Program, Mar. 25-26, 1971.

Table 2.1. Fracture toughness results determined from testing 1T compact-tension specimens oriented in the RW direction at temperatures up to 550°F (plate section 03)

Specimen designation	Test temperature (°F)	Crack length (in.)	Some fracture toughness parameters ^a (ksi $\sqrt{\text{in.}}$)				K_{Icd} (ksi $\sqrt{\text{in.}}$)
			KD	KQ	KU	KF	
3C11	+50	1.105	38.4	50.0	98.3	17.6	122.1
3C12	+100	1.086	47.0	66.1	103.7	17.1	218.0
3C13	+200	1.086	37.3	49.0	103.5	17.1	248.0
3C14	+200	1.070	36.3	58.0	104.5	17.0	261.0
3C15	+550	1.085	34.1	51.6	96.2	17.0	232.4
3C16	+550	1.083	39.0	59.0	95.0	17.0	210.1
3C20 ^b	0	0.940	24.0	31.1	114.2		231.0
3C17 ^b	+50	0.930	28.0	55.0	120.0		233.0
3C18 ^b	+100	0.925	46.3	56.1	112.2		298.0
3C19 ^b	+200	0.930	41.0	47.0	118.0		342.0

^a KD = fracture toughness at deviation – load displacement, KQ = fracture toughness at secant offset load, KU = fracture toughness at ultimate load, and KF = fracture toughness during prefatigue precracking.

^bSpecimens 3C20, 3C17, 3C18, and 3C19 were not precracked before testing.

Table 2.2. Fracture toughness results determined from testing 6T-CT and 9T-CT specimens oriented in both the RW and WR direction

Specimen designation	Orientation	Test temperature (°F)	Crack length (in.)	Some fracture toughness parameters ^a (ksi $\sqrt{\text{in.}}$)				K_{Icd} (ksi $\sqrt{\text{in.}}$)
				KD	KQ	KU	KF	
6T-CT Specimens								
3C3	RW	+100	6.516	87.3	145.5	198.4	16.0	224.1
3C4	RW	+130	6.310	105.0	160.0	238.0	19.0	363.6
3C2	RW	+200	6.316	75.1	138.0	242.0	15.0	405.4
3C1	RW	+550	6.146	115.0	153.4	223.0	24.0	345.2
3C5	WR	+25	6.273	88.0	88.0	88.0	15.0	84.0
3C7	WR	+200	6.316	58.0	128.0	225.5	20.0	299.0
3C8	WR	+550	6.366	89.0	142.2	202.1	20.3	264.7
9T-CT Specimens								
3C9	RW	+200	9.360					452.0
3C10	RW	+550	9.423	69.0	224.0	292.0	24.0	375.0

^aParameter identification given in Table 2.1.

information meeting.¹⁷ A resumé of the cooperation and communication between the two research groups is given below.

Cooperative research between the HSST program, ORNL, and Japan Atomic Energy Research Institute

The Japan Atomic Energy Research Institute (JAERI) is conducting a research program on the effect of a

high-temperature steam and water environment on the crack-growth rate in reactor pressure vessel materials. JAERI suggested a cooperative arrangement with the HSST program in which HSST would supply a nominal

17. T. Kondo et al., "Fatigue of ASTM A-302 Grade B Steel in High Temperature Simulated Nuclear Reactor Environment," paper 2, presented at the Fifth Annual Information Meeting of the HSST Program, Mar. 25–26, 1971.

quantity of "pedigreed" A533-B steel to JAERI for conducting a fairly comprehensive environmental investigation and then in return JAERI would supply the HSST program with a copy of their results.

Not only was this suggestion acted upon, but, in addition, there has been a complete exchange of information. JAERI had already generated considerable information on the pressure vessel steel presently in use in Japan, namely A302 B. Dr. T. Kondo of JAERI was preparing a paper on this work to be presented at the First International Conference on Corrosion Fatigue at the University of Connecticut, Storrs, Connecticut. A preliminary presentation of this work was reported by L. F. Kooistra at the HSST Information Meeting, March 25, 1971, with Dr. Kondo's consent.

At this time the first series of tests has been completed on the HSST material in Japan. Although in the HSST-sponsored investigation Westinghouse uses a batch system for its environmental condition, JAERI uses a through-flow water treating system continuously monitored. Westinghouse will largely test A533-B plate, various weldments, and HAZ's; JAERI will test A533 B and A302 B. Westinghouse is testing at cycling rates from 60 to 600 cpm; JAERI has explored also very low cycling rates down to 0.2 cpm. In doing so, JAERI discovered a stagnation effect in the growth rate ascribed to crack blunting by incipient corrosion at the crack tip. This effect was verified by observing that increasing the O₂ content of the water increases the stagnation phenomenon.

Westinghouse has carried on its investigation at reactor operating temperature of 550°F; the Japanese investigators have explored lower temperatures also. Westinghouse used a 2T WOL (wedge opening loading) specimen, which is largely bending; JAERI uses a tensile specimen. Westinghouse started to measure crack growth by means of ultrasonics and obtaining anomalous results and switched to the specimen compliance method. JAERI used the latter from the start, and there is now good assurance that it produces reliable data.

The Westinghouse apparatus was designed for a pressure of 2000 psi; the JAERI apparatus is good for 1500 psi (primarily BWR conditions).

Both laboratories have conducted strain-controlled tests, but JAERI is starting to conduct load-controlled tests also.

In some phases of the investigation there is a difference in the results obtained by the two investigating laboratories. The Westinghouse group has found that the environment of nuclear-reactor-grade water has no effect on the crack growth rate or at least did not increase this rate. The Japanese investigators conclude

that under certain combinations of strain range, cycling speed, and temperature, the crack growth rate in a water-steam environment can be increased by a factor of 4. This maximum is attained at a strain range of 0.70%, a cycling speed of 10 cpm, and a temperature of approximately 400°F. At a lower strain range, a lower cycling speed, and a higher temperature, the factor of increase in the crack growth rate reduces from 4 to less than 1. It was also determined that at a very low cycling speed of 5 min/cycle the crack growth manifested periods of stagnation. This phenomenon is ascribed to the effect of incipient corrosion at the bottom of the crack. It is postulated that at the very slow cycling rate this corrosion can blunt the crack tip sufficiently to stall its advance. An incubation period for reinitiation is then necessary to start it growing again. This hypothesis is supported by the fact that a higher oxygen content in the water also suppresses the crack growth rate. By equating these findings to actual operation, they, at this point, add up to a favorable prediction. To wit, on operating reactor vessels the strain range is expected to be well below 0.70%, the occurrence of major load cycles is far below the cycling speed of the experiments, and operating temperatures will be about 150°F above the point of maximum crack growth rate. All these factors point in the direction of reduced crack growth rate.

Fatigue-Crack Growth Characteristics of Nuclear Pressure Vessel Grade Materials^{1 8}

T. R. Mager

Westinghouse Electric Corporation

The fracture mechanics approach is being used to study the effect of high-temperature reactor-grade primary water on the fatigue-crack growth characteristics of materials of nuclear pressure vessel grade. The 2-in.-thick WOL (wedge opening loading) specimen is being utilized to measure the fatigue-crack growth at 550°F in an environment (excluding irradiation) typical of PWRs and BWRs. The crack growth rate da/dN of pressure vessel materials is being measured as a function of ΔK_I , the change in the stress intensity factor at the tip of the crack.

It was concluded from the data that:

1. Reactor-grade primary water environment does not accelerate crack growth rate.

18. Work sponsored by HSST program under UCCND Sub-contract No. 3290 between Union Carbide Corporation and Westinghouse Electric Corporation.

2. For the range of frequency and the materials studied, the cyclic crack growth rate da/dN as a function of ΔK was essentially the same in both PWR and BWR environments.
3. The frequency (60 and 600 cpm) did not affect the cyclic crack growth rate of the materials studied.

It was recommended that future studies include: (1) the effect of low frequency (the order of 1 to 10 cpm) and (2) the effect of load spectrum on the cyclic crack growth of reactor pressure vessel material.

3. Investigations of Irradiated Materials

One of the environmental factors that must be considered in safety evaluations of reactor pressure vessels is irradiation, because the mechanical properties of metals may be modified thereby to a degree that is of considerable engineering significance. Irradiation effects are being investigated by Hanford Engineering Development Laboratory (HEDL), Westinghouse Electric Corporation, Naval Research Laboratory (NRL), and Oak Ridge National Laboratory. The areas of primary interest to the HSST program are the temperature range 450 to 600°F and the fast-neutron ($E > 1$ MeV) fluence range 1×10^{19} to 8×10^{19} neutrons/cm².

The projected work at NRL, Westinghouse, and ORNL has essentially been completed, and final reports have been or are being prepared. Results not previously reported, in addition to those from HEDL, are given here.

IRRADIATION EFFECTS ON THE FRACTURE OF HEAVY-SECTION PRESSURE VESSEL STEELS¹

J. A. Williams C. W. Hunter
Hanford Engineering Development Laboratory

Objective

The primary objective of the Hanford Engineering Development Laboratory work in support of the HSST program is to determine the embrittling effects of irradiation on pressure vessel steel. The material of interest is from HSST plate 02 ASTM A533, grade B, class 1 steel. Characterization of embrittlement by irradiation is being evaluated by plane strain fracture toughness, K_{Ic} , measurements using 1-in.-thick compact-tension (CT) specimens; tensile behavior has also

1. Research sponsored under Purchase Order No. 11Y-50917V between Union Carbide Corporation and Hanford Engineering Development Laboratory.

been studied to establish a basic engineering understanding of the irradiation effect on mechanical properties of A533-B steel.

Irradiation of 4T Specimens – ETR Dummy Gamma-Heat Test

The ETR irradiation temperature profiles were measured in a simulated 4-in.-thick compact-tension (4T-CT) fracture specimen. Large specimen irradiations and associated problems² and the ETR dummy gamma-heat irradiation experiment³ have been discussed previously.

The thermocouple locations in the dummy specimen are shown in Fig. 3.1, in which the relationship of an actual 4T-CT specimen is outlined by the dashed lines. The full reactor power differential temperature through the thickness of the specimen is given for each location in Fig. 3.2. Curve A of Fig. 3.2 corresponds to the temperature at the specimen crack line, the point of fracture initiation during a fracture test. The point reference letters in Fig. 3.2 are the same as those given in Fig. 3.1. The maximum ΔT at the crack line is 200°F; reactor coolant water was 110°F, resulting in a maximum crack line temperature of 310°F. From these temperature measurements the crack line temperature gradient for an actual 4T specimen irradiation experiment was calculated. The temperature gradient, with a peak crack line specimen temperature of 550°F obtainable using a gas gap patch design, is shown in Fig. 3.3. The ΔT from the peak to the hot face is

2. C. W. Hunter and J. A. Williams, "Irradiation Effect on the Fracture of Heavy Section Pressure Vessel Steels," *HSST Program Semiannu. Progr. Rep. Aug. 31, 1970*, ORNL-4653, pp. 31–38.

3. C. W. Hunter and J. A. Williams, "Irradiation Effects on the Fracture of Heavy Section Pressure Vessel Steels," *HSST Program Semiannu. Progr. Rep. Feb. 28, 1971*, ORNL-4681, pp. 48–53.

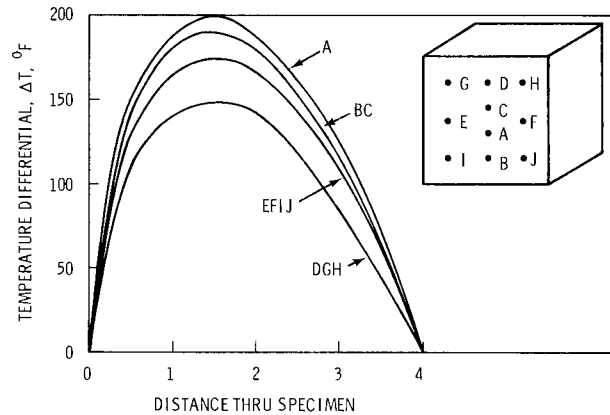


Fig. 3.2. Measured ΔT through the thickness of the 4-T dummy gamma-heat specimen at various locations.

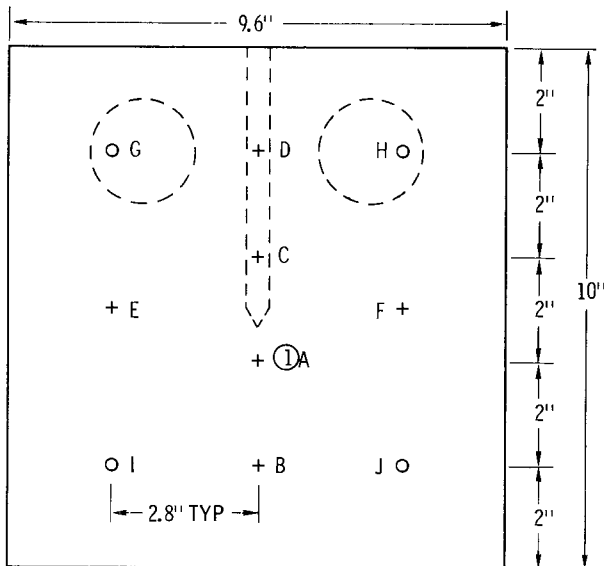


Fig. 3.1. Thermocouple locations in the ETR dummy gamma-heat test. The dashed lines relate an actual 4-T specimen to the test block. Thermocouples were located through the thickness at 0, 0.5, 1, 1.5, 2, 3, and 4 in. at the (+) locations and 1 and 3 in. at the (O) locations. A, B, ---J are location reference letters.

approximately 24°F , and that to the cold face is about 54°F . The temperatures are based on reactor coolant water of 110°F , a 5-by-5-in. gas gap patch, and a 50% He-50% Ar gas mixture. The effect of the patch design for location A, Fig. 3.2, is described above. The profiles at locations B and C would be raised in some proportion to A but with a lower peak temperature and higher ΔT . Profiles at locations E, F, I, J, G, and H

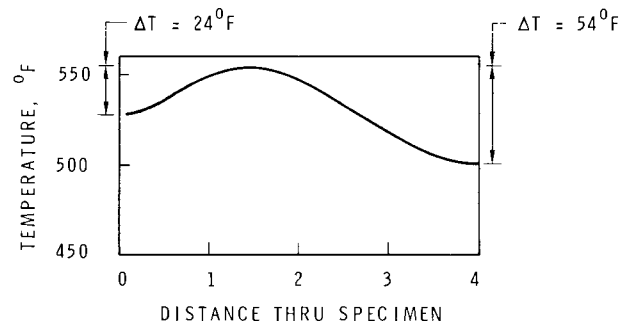


Fig. 3.3. Calculated temperature gradient through a 4T-CT specimen which would be expected during irradiation in the ETR. The temperature profile is based on that obtainable for 550°F maximum specimen temperature at the crack line, with 110°F reactor coolant, and a 5 \times 5 in. gas gap patch filled with a 50-50 He-Ar mixture.

would be affected very little since they lie outside the dimensions of the patch.

Some measure of the degree of control necessary for maintaining specimen temperatures during irradiation was obtained by measuring the specimen temperature change during reactor startup and during the reactor cycle. These data are presented in Figs. 3.4 and 3.5, respectively, for the peak crack line position. During reactor startup the peak crack line temperature is observed to be linearly proportional to reactor power: thus at full power a 10% fluctuation in reactor power would require a control variation approximately 10% of the difference between ambient water temperature and peak temperature, or 44°F . Short-term fluctuations in

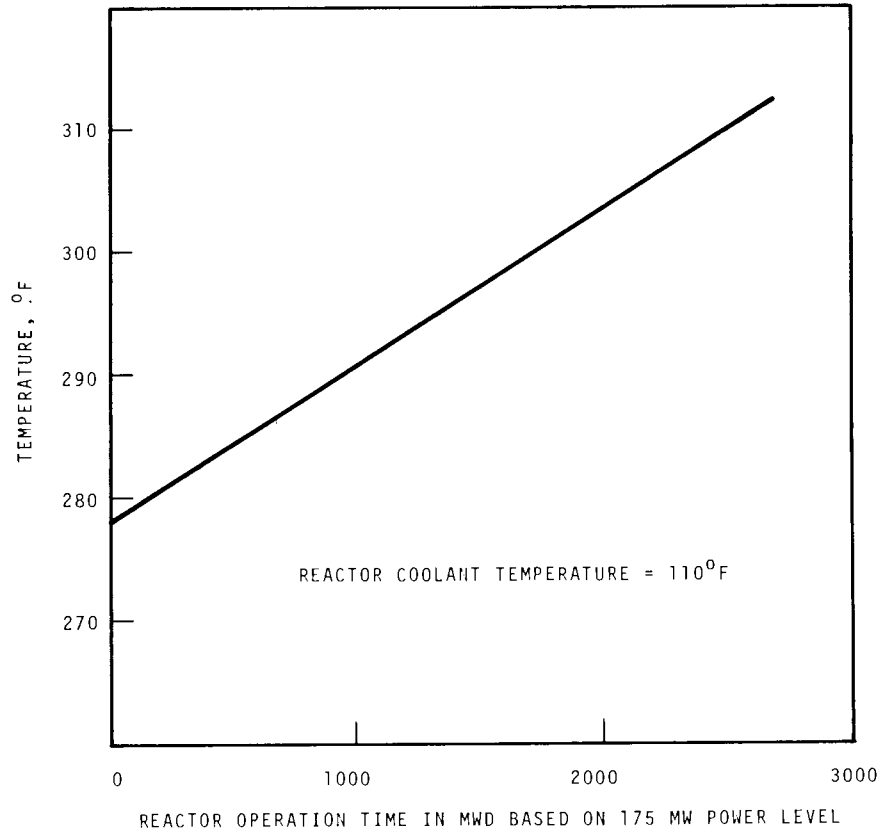


Fig. 3.4. Variation in 4-T dummy peak crack line temperature during ETR reactor cycle.

reactor power of this magnitude are not common; however, these variations may be encountered locally, and it is not uncommon for the ETR to operate in the 160- to 165-MW power region for long periods of time. A large amount of temperature control must be provided to compensate for temperature changes due to fuel burnup during the reactor cycle; this effect is shown in Fig. 3.5. The peak flux in the reactor is below reactor midplane at startup. As the reactor cycle progresses, the control rods are lifted to compensate for fuel burnup, and the peak flux is shifted toward the top of the reactor. The dummy specimen occupied the upper position and as such increased in temperature during the reactor cycle; in actual 4T-CT irradiations the specimen below midplane would receive less heat input as the reactor cycle progressed and would require a positive response from the control system. It is estimated that an additional $\pm 50^\circ\text{F}$ of control would be needed to compensate for the temperature variations due to fuel burnup during the reactor cycle.

Base Material Studies of ASTM A533 B; Correlation of Changes in Yield Strength and Fracture Toughness Produced by Irradiation

In impact energy tests linear elastic fracture mechanics K_{Ic} testing is an alternate means of evaluating the neutron irradiation embrittlement in water reactor pressure vessel materials. In addition to indicating the shift of the ductile-brittle transition temperature to higher temperatures, K_{Ic} values permit calculation of critical fracture load-flaw size relationships. The practical disadvantage is that K_{Ic} values of these materials may be easily obtained only at and below the transition temperature.

One-inch-thick compact-tension K_{Ic} specimens were irradiated at 540°F to neutron fluence levels of 2 and 8×10^{19} neutrons/cm² ($E > 1$ MeV) in the ETR; tensile specimens were irradiated at 510°F to 2, 4, 6, and 8×10^{19} neutrons/cm². All specimens were of longitudinal orientation from the quarter-thickness position of a

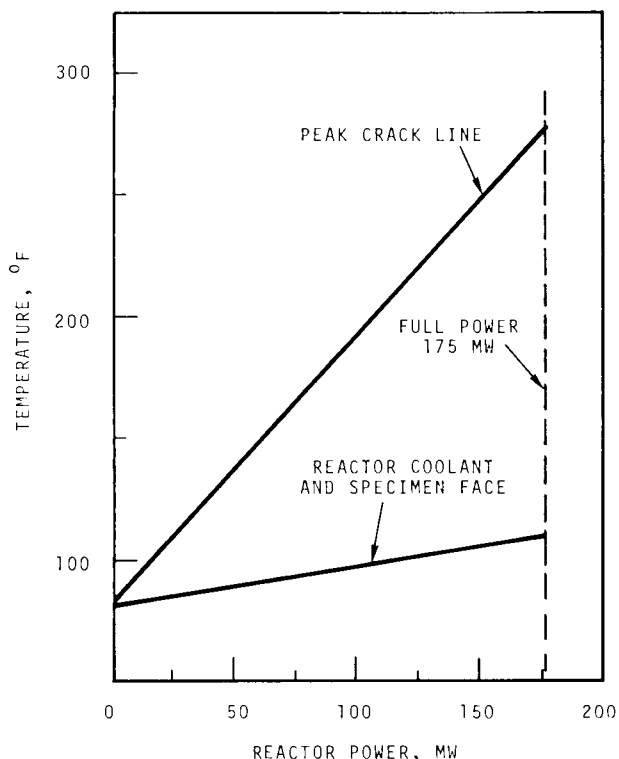


Fig. 3.5. Variation in 4-T dummy peak crack line temperature as a function of reactor power level during reactor startup.

12-in. ASTM A533, grade B, class 1 steel plate. Details of the specimen irradiation and testing have been reported.²⁻⁴

The effects of irradiation on yield strength and K_{Ic} are shown in Fig. 3.6. The yield strength increase ($\Delta\sigma_{ys}$, ksi) as a function of fluence (Φ) and temperature (T , °F) may be described by

$$\Delta\sigma_{ys} = 22[1 - \exp(-\Phi/5 \times 10^{18})] + \Phi/10^{19}(4.3 - 0.0038T). \quad (1)$$

Equation (1) was discussed in detail in the previous semiannual report.³ A fit of Eq. (1) to specific data points is shown in Fig. 3.7 for temperatures of -100, 0, 100, 300, and 500°F. Consistent with the well-established Charpy V-notch neutron embrittlement behavior^{5,6} of the 6-in. ASTM A302-B reference plate, there is a pronounced $\Delta\sigma_{ys}$ at low fluence levels followed by a reduced but linearly fluence-dependent $\Delta\sigma_{ys}$ above 2×10^{19} . The low-fluence $\Delta\sigma_{ys}$ is operative primarily on the athermal component of yield

stress, whereas the fluence dependence above 2×10^{19} is greater at lower test temperatures.

Irradiation levels of 2 and 8×10^{19} neutrons/cm² produced shifts of 185 and 275°F in the 50-ksi√in. K_{Ic} fracture toughness level. Based on the concept that brittle fracture occurs when the yield stress is greater than the cleavage microcrack growth stress, Cottrell⁷ predicts the following dependency of a shift in the ductile-brittle transition temperature (ΔTT) on $\Delta\sigma_{ys}$:

$$\frac{\Delta TT}{\Delta\sigma_{ys}} = \frac{5^\circ\text{F}}{\text{ksi}}. \quad (2)$$

At a test temperature of 0°F, fluence levels of 2 and 8×10^{19} in Eq. (1) give values of 30.6 and 56.4 ksi $\Delta\sigma_{ys}$, respectively, which upon substitution into Eq. (2) yield ΔTT values of 153 and 282°F that correspond well with the experimentally measured shifts in the K_{Ic} curves. This correlation between $\Delta\sigma_{ys}$ and shifts of the analytically rigorous toughness measurement K_{Ic} further demonstrates that irradiation embrittlement in these materials is a consequence of irradiation hardening by the mechanism of elevated yield stress forcing cleavage fracture to higher temperatures.

The correlation is significant in illustrating that the shift in fracture toughness is in agreement with correlations of shifts of other types of toughness transition tests. The correlation is limited by an as yet inadequate definition of the transition of K_{Ic} for irradiated A533 B; this can only be obtained by testing large irradiated specimens.

Base Material Studies of ASTM A533 B; Comparison of Transverse and Longitudinal Fracture and Tensile Properties

Transverse tensile properties for irradiated and unirradiated ASTM A533-B, HSST plate 02 were cursorily examined to determine if there were any significant

4. C. W. Hunter and J. A. Williams, "Fracture and Tensile Behavior of Neutron Irradiated A533-B Pressure Vessel Steel," *Nucl. Eng. Des.* **17**(1), 131-48 (August 1971).

5. R. H. Sterne, Jr., and L. E. Steele, "Steels for Commercial Nuclear Power Reactor Pressure Vessels," *Nucl. Eng. Des.* **10**, 259-307 (1969).

6. J. R. Hawthorne, *Trends in Charpy-V Shelf Energy Degradation and Yield Strength Increase of Neutron-Embrittled Pressure Vessel Steels*, NRL-7011 (Dec. 22, 1969).

7. A. H. Cottrell, "Theory of Brittle Fracture in Steel and Similar Metals," *Trans. Met. Soc. AIME* **212**, 192-203 (April 1958).

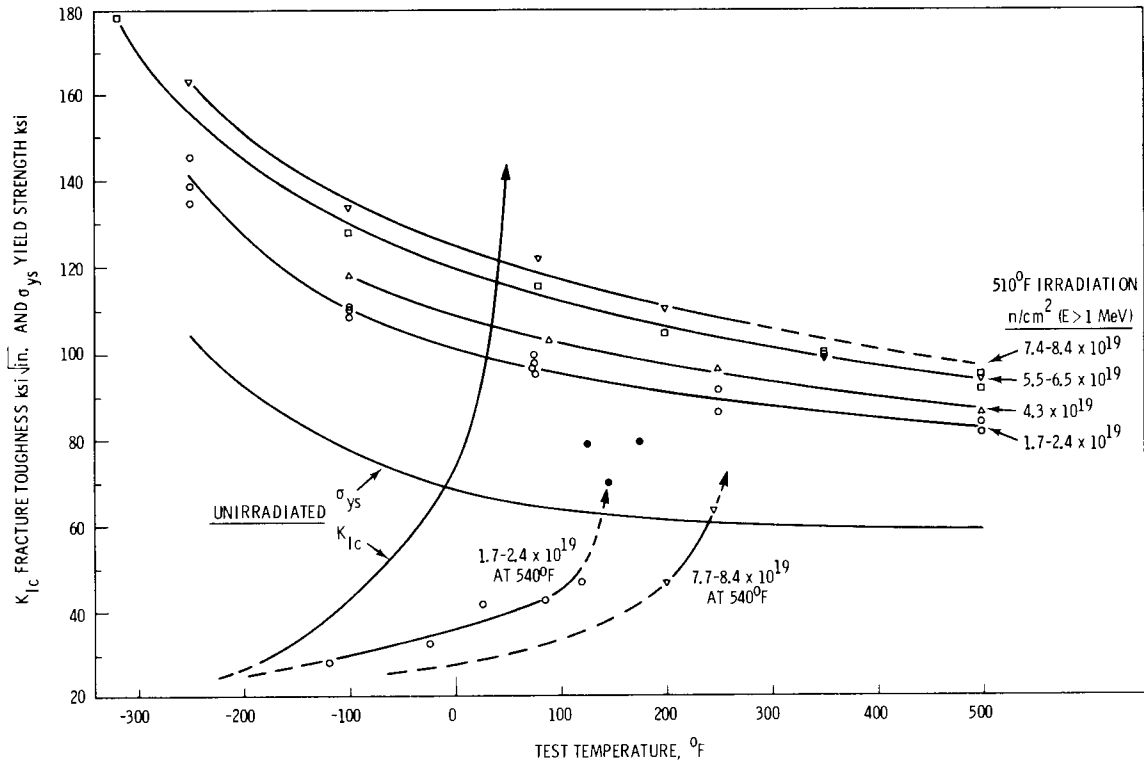


Fig. 3.6. Neutron-irradiation-produced changes in yield strength and fracture toughness of ASTM A533-B pressure vessel steel. Closed points invalid by ASTM E399.

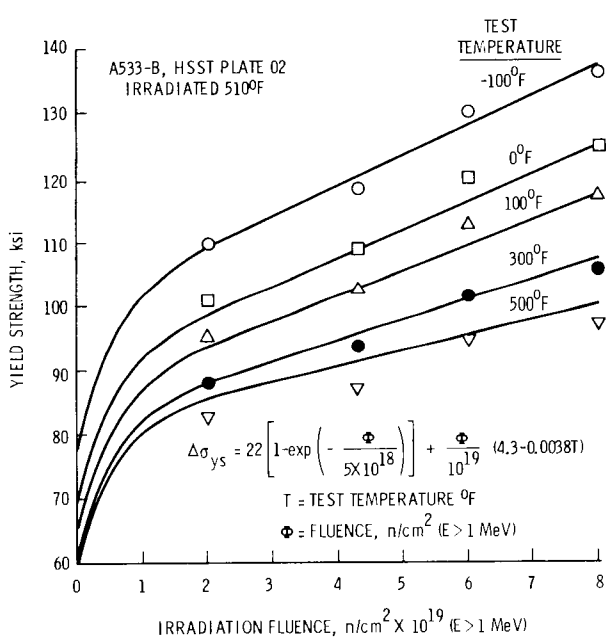


Fig. 3.7. Effect of irradiation fluence on the yield strength of A533-B is shown for different test temperatures. The curves are the fit of the $\Delta\sigma_{ys}$ equation.

orientation effects. Fracture toughness results of unirradiated transverse (WR) specimens are given in Table 3.1 and Fig. 3.8; longitudinal fracture data shown in Fig. 3.8 were previously reported.³ The plane strain fracture toughness properties of longitudinal (RW) and transverse (WR) orientation are observed to be identical within the valid measurement limits of 1T-CT specimens. It is expected that the irradiation response of WR K_{Ic} properties will be similar to RW properties on the basis of tensile properties reported in Table 3.2 and Figs. 3.9 and 3.10.

Transverse tensile tests of unirradiated specimens were conducted over a temperature range of -250 to 500°F. There were no observable effects on yield or ultimate strength attributed to orientation difference between RW and WR specimens. Similarly, WR tensile specimens irradiated to approximately 2.9 and 4.5×10^{19} neutrons/cm² and tested from room temperature to 500°F exhibited a response to irradiation comparable with that of longitudinal specimens. Figure 3.9 compares yield strength properties, and Fig. 3.10 compares ultimate strength properties of WR and RW orientations; details of RW tensile data were reported previously.³

Table 3.1. Fracture toughness of unirradiated ASTM A533, grade B, class 1 steel from HSST plate 02 steel, WR orientation

Specimen identification	Test temperature (°F)	Plate position ^a (in.)	K_f (ksi√in.)	Yield strength (× 10 ³ psi)	Crack length, a (in.)	K_Q (ksi√in.)	$2.5 \left(\frac{K_Q}{\sigma_{ys}} \right)^2$	K_{IC} (ksi√in.)
02GA581	-250	3.25	13.8	105	1.178	26.8	0.162	<i>b,c</i>
02GA586	-185	4.5	12.4	91	1.126	37.5	0.42	<i>b</i>
02GA595	-135	8.5	11.7	83	1.088	35.0	0.44	35.0
02GA591	-100	7.25	11.2	78	1.059	40.4	0.67	40.4
02GA592	-75	7.25	10.1	75	0.998	43.5	0.84	43.5
02GA579	-50	3.25	13.4	72	1.137	69.7	2.3	<i>d</i>

^aFrom plate surface to specimen center.

^bInvalid by surface trace, insufficient fatiguing.

^cInvalid by $K_f > \sigma_y F / 2\sigma_y T (K_Q)$.

^dInvalid by $B < 2.5 (K_Q / \sigma_y T)^2$.

Table 3.2. Tensile properties of irradiated and unirradiated A533, grade B, class 1 steel from HSST plate 02, transverse specimens

Specimen identification	Test temperature (°F)	Fluence ($E > 1$ MeV) (× 10 ¹⁹ neutrons/cm ²)	Plate position ^a (in.)	Yield strength, 0.2% offset (× 10 ³ psi)	Ultimate strength (× 10 ³ psi)	Total elongation (%)
02GA659	-250	Unirradiated	7.3	102.9	122.5	20.0
02GA660	-150	Unirradiated	7.3	81.5	106.3	19.2
02GA661	-50	Unirradiated	7.3	72.9	97.5	22.5
02GA662	71	Unirradiated	7.3	68.3	89.5	19.9
02GA670	199	Unirradiated	8.0	63.2	83.6	15.2
02GA671	300	Unirradiated	8.0	63.2	84.5	14.1
02GA672	400	Unirradiated	8.0	60.1	83.4	14.4
02GA673	501	Unirradiated	8.0	61.4	86.7	14.3
02GA642	74	2.7	4.7	99.6	113.9	14.4
02GA663	250	2.7	8.0	88.7	106.1	14.9
02GA639	500	2.7	4.7	77.3	98.5	12.2
02GA664	500	3.1	8.0	81.9	105.4	12.8
02GA651	77	4.6	7.3	105.9	119.7	13.0
02GA666	250	4.6	8.0	90.8	108.4	13.0
02GA652	250	4.5	7.3	97.9	113.4	13.0
02GA667	500	4.5	8.0	83.2	107.1	12.2

^aFrom top surface of plate.

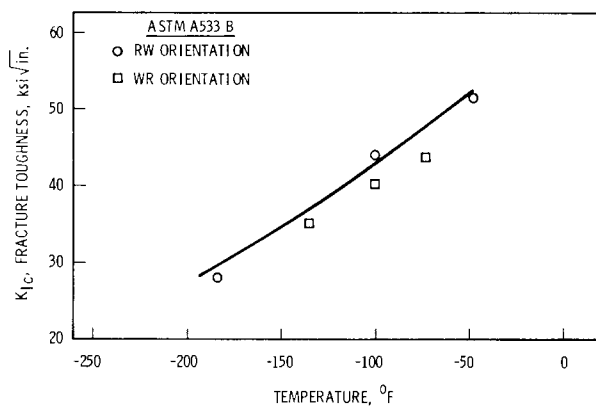


Fig. 3.8. Comparison of fracture toughness K_{IC} of longitudinal and transverse orientations for ASTM A533-B pressure vessel steel, HSST plate 02.

ASTM A533-B Submerged-Arc Weldment; Irradiation Effects on Weld Metal Fracture and Tensile Properties

The fracture toughness of ASTM A533-B submerged-arc weldment metal irradiated at 540°F to a fluence of 2.7 to 3.1 × 10¹⁹ neutrons/cm² ($E > 1$ MeV) is compared with unirradiated weld metal in Fig. 3.11 and reported in Table 3.3. The specimens were taken from the longitudinal orientation of the weld; the plane of the crack is normal to the plate surface, and the propagation direction is parallel to the weld direction. The observed shift of the 50-ksi√in. toughness level is approximately 390°F; the shift might actually be less than this with more extensive evaluation of the unirradiated fracture toughness. Though only valid unirradiated data are shown in Fig. 3.11, conservative

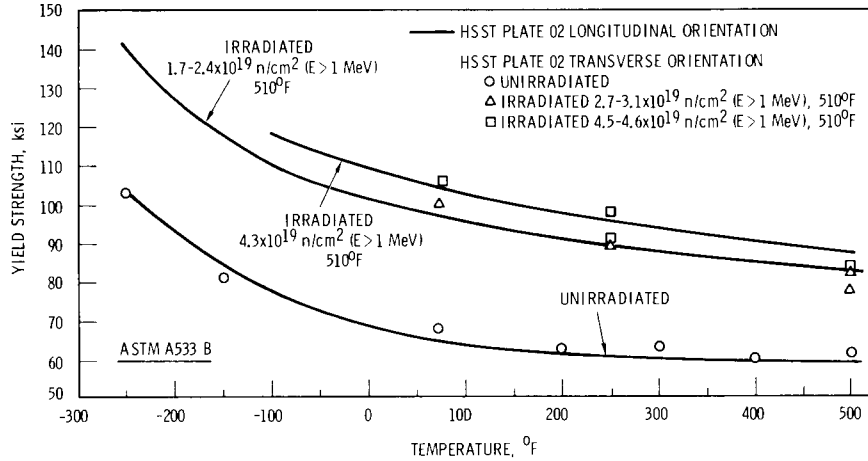


Fig. 3.9. Comparison of transverse and longitudinal yield strength for irradiated and unirradiated ASTM A533-B pressure vessel steel, HSST plate 02.

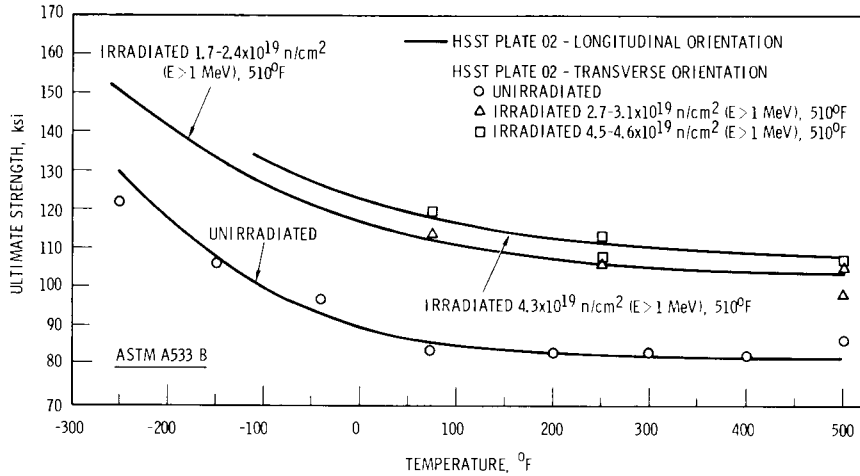


Fig. 3.10. Comparison of transverse and longitudinal ultimate strength for irradiated and unirradiated ASTM A533-B pressure vessel steel, HSST plate 02.

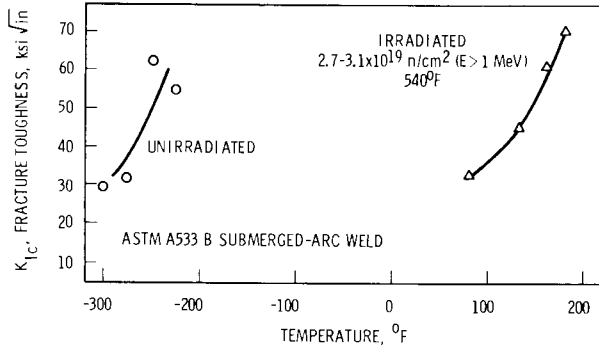


Fig. 3.11. Fracture toughness K_{IC} of unirradiated and irradiated ASTM A533-B submerged-arc weldment.

fatigue-crack preparation might have yielded lower values of K_{IC} in the lower-temperature tests; this would place the 50-ksi $\sqrt{\text{in}}$. toughness at a somewhat higher temperature, yielding a more conservative estimate of the irradiation embrittlement sensitivity of A533-B submerged-arc weld metal. Using the data of Shabbits et al.⁸ the unirradiated 50-ksi $\sqrt{\text{in}}$. toughness level occurs at -175°F, resulting in a shift of only 315°F.

8. W. O. Shabbits, W. H. Pryle, and E. T. Wessel, *Heavy Section Fracture Toughness of A533 Grade B Class I Steel Plate and Submerged Arc Weldment*, WCAP-7414 (December 1969).

Table 3.3. Fracture toughness of irradiated ASTM A533, grade B, class 1 steel, submerged-arc weld

Specimen identification	Test temperature (°F)	Fluence ($E > 1$ MeV) ($\times 10^{19}$ neutrons/cm ²)	Plate position ^a (in.)	K_{Ic} (ksi√in.)	Yield strength ($\times 10^3$ psi)	Crack length, a (in.)	K_{Ic} (ksi√in.)	$2.5 \left(\frac{K_{Ic}}{\sigma_{ys}} \right)^2$	K_{Ic} (ksi√in.)
51A5029	90	2.9	10.12	10.7	99.5	1.030	33.7	0.29	33.7
51A5030	132	2.7	10.12	10.3	97.0	1.003	45.3	0.55	45.3
51A5027	160	3.1	10.12	10.6	95.5	1.029	61.3	1.02	61.3
51A5028	180	2.9	10.12	10.8	94.5	1.035	70.9	1.41	

^aFrom plate surface to specimen center.

The effects of irradiation on the yield and ultimate tensile strengths of ASTM A533-B submerged-arc weld are shown in Figs. 3.12 and 3.13, respectively, and listed in Table 3.4. Results are of tests from room temperature to 500°F for 510°F irradiations to fluences of 0.5×10^{19} and 4.0 – 4.6×10^{19} neutrons/cm² ($E > 1$ MeV); base plate properties are also shown for comparison.

The irradiation strengthening of weld yield properties is similar to, if not slightly greater than, that of longitudinal base properties from room temperature to 500°F. An additional comparison of the similar effect of irradiation on weld and base plate yield properties is shown in Fig. 3.14. The data points are for the A533-B submerged-arc weld metal at room temperature and

500°F, while the curves are determined from the yield strength–fluence–temperature relationship for base plate material given in Eq. (1).

The ultimate strength of weld metal is less sensitive to irradiation than the yield strength. At room temperature the weld ultimate strength increased 36 ksi, while the weld yield strength increased 46 ksi after irradiation to about 4.3×10^{19} neutrons/cm² ($E > 1$ MeV); these values correspond to about a 22% increase in ultimate strength and a 75% increase in yield strength. Compared with the base plate results of Fig. 3.13, it appears that the weld ultimate strength is more sensitive to irradiation; the irradiated ultimate strength of the weld does not exceed that of the base plate since it was much lower initially.

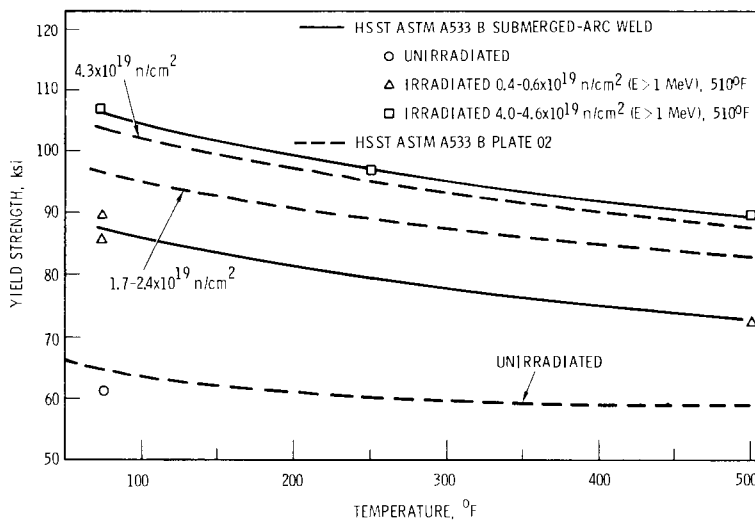


Fig. 3.12. Yield strength of irradiated ASTM A533-B submerged-arc weld. Base plate properties are shown for comparison.

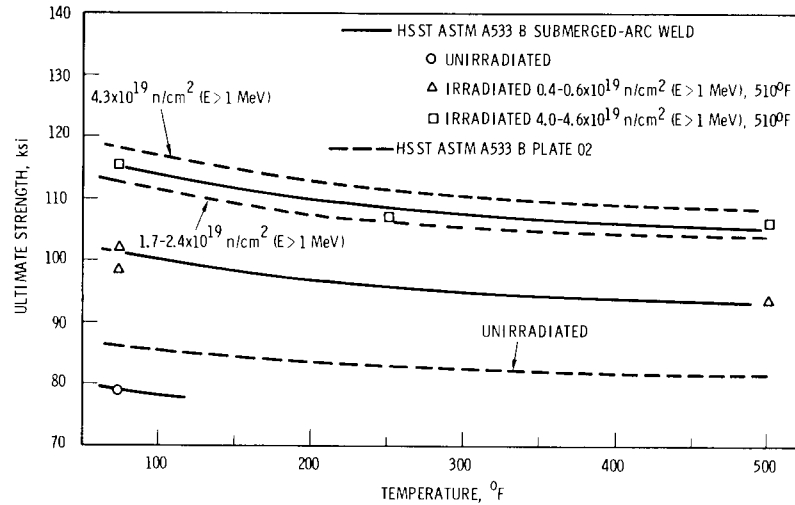


Fig. 3.13. Ultimate strength of irradiated ASTM A533-B submerged-arc weld. Base plate properties are shown for comparison.

Table 3.4. Tensile properties of irradiated A533, grade B, class 1 steel, submerged-arc weld

Specimen identification	Test temperature (°F)	Fluence ($E > 1$ MeV) ($\times 10^{19}$ neutrons/cm ²)	Plate position ^a (in.)	Yield strength, 0.2% offset ($\times 10^3$ psi)	Ultimate strength ($\times 10^3$ psi)	Total elongation (%)
51A5201	72	Unirradiated	3.5	61.3	78.9	21.9
51A5202	77	4.6	3.5	107.1	115.5	16.6
51A5204	250	4.0	3.5	96.6	107.1	12.6
51A5203	500	4.5	3.5	89.5	106.1	10.3
51A5206	73	0.43	4.2	85.3	98.7	16.0
51A5208	74	0.68	4.2	89.5	101.9	19.3
51A5207	500	0.59	4.2	72.3	94.1	12.9

^aFrom top surface of plate to specimen center.

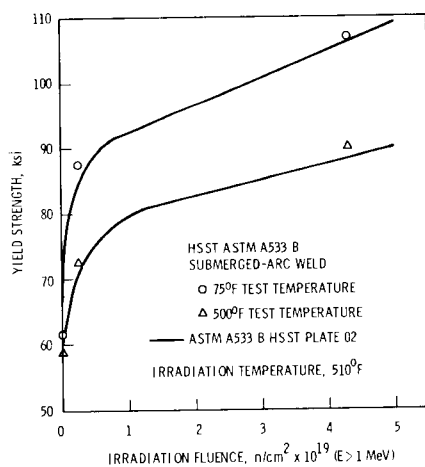


Fig. 3.14. Effect of irradiation fluence on the yield strength of ASTM A533-B submerged-arc weld. Data points are those of weld material, while the curves are of base plate material.

RADIATION HARDENING AND EMBRITTLEMENT IN ASTM A533, GRADE B, CLASS 1 STEEL

W. J. Stelzman

Additional data have been developed from the load-time records taken during the testing of submerged-arc weldment test specimens both before and after irradiation. Figure 3.15 shows the fracture energy variation with test temperature for specimens at the $1/12$ -T location. The submerged-arc weldment description and test results have been discussed previously.^{9,10} Figure

9. D. A. Canonico, "Characterization of Heavy-Section Steel Weldments," *HSST Program Semiannu. Progr. Rep. Feb. 28, 1969*, ORNL-4463, pp. 29-35.

10. R. G. Berggren, W. J. Stelzman, and T. N. Jones, "Radiation Hardening and Embrittlement in ASTM Grade B, Class 1 Steel," *HSST Program Semiannu. Progr. Rep. Aug. 31, 1970*, ORNL-4653, pp. 38-40.

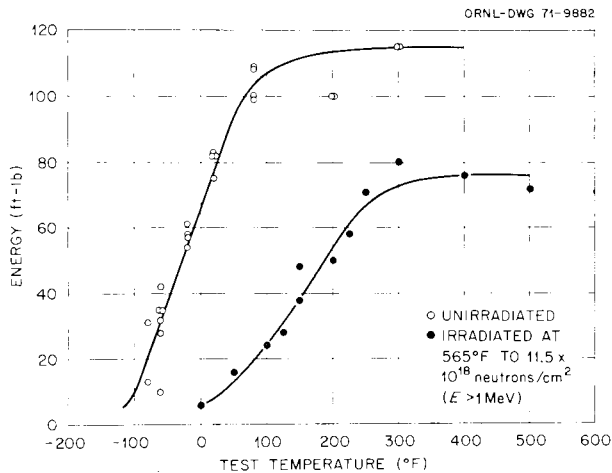


Fig. 3.15. Effect of irradiation on the variation of Charpy V-notch test results on irradiated and unirradiated specimens of HSSST submerged-arc weldment 51B at $1/12$ -T location, WL orientation.

Fig. 3.16 shows the fracture load parameters, and Fig. 3.17 shows the fracture energy parameters for the same tests. Irradiation translates the load parameters to higher test temperatures and higher loads and the energy parameters to higher test temperatures but to lower energies.

Comparison of the effects of irradiation in the temperature range 550 to 565°F on $1/12$ -T material from the submerged-arc weldment and $3/8$ -T material from plate section 02FB, a comparable base plate material previously reported,¹¹ indicates that irradiation causes the load parameters in both cases to shift to higher loads and higher test temperatures. However, the magnitude of the loads for each separate condition (irradiated or unirradiated) does not appear to differ greatly, although the shift to higher temperature due to irradiation appears to be much greater for the submerged-arc weldment. Comparison of the energy parameters indicates a fair-sized decrease in all energy parameters except the energy to maximum load, where the decrease is small. The shift of energies to higher test temperatures after irradiation is also apparent. The magnitude of the energy parameters of both materials in the unirradiated condition, although not equal, are comparable; however, after irradiation the submerged-arc material shows a much greater shift of energies to

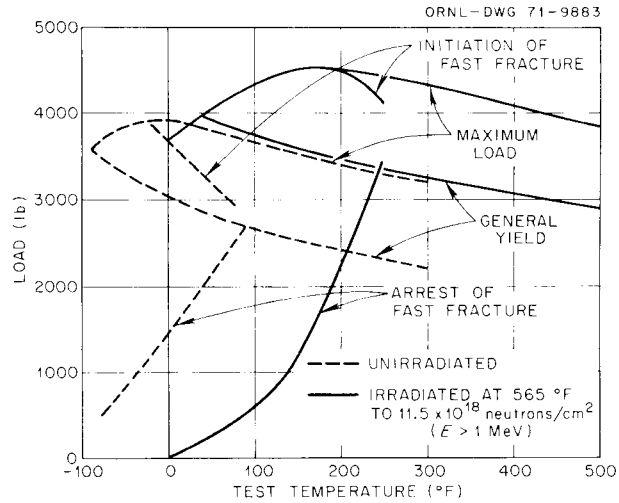


Fig. 3.16. Effect of irradiation on load parameters determined in instrumented Charpy tests on irradiated and unirradiated HSSST submerged-arc weldment 51B; WL-oriented specimens.

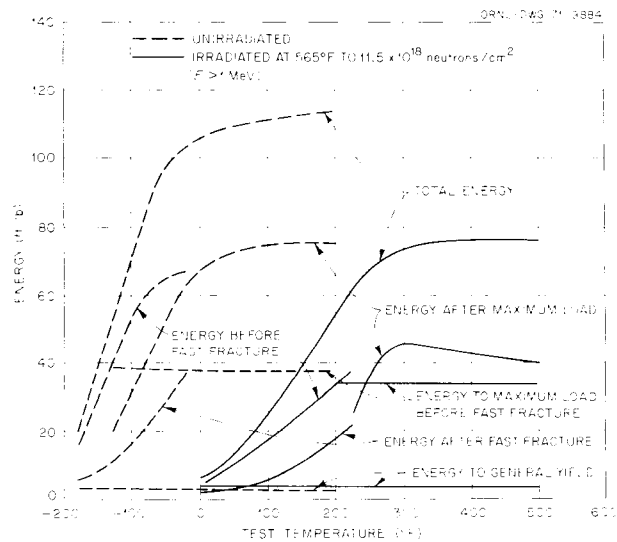


Fig. 3.17. Effect of irradiation on energy parameters determined in instrumented Charpy test on irradiated and unirradiated HSSST submerged-arc weldment 51B; WL-oriented specimens.

higher test temperatures than the 02FB material. This supports the conclusion that the submerged-arc weldment shows a greater sensitivity to radiation damage than the base plate at comparable 550 to 565°F irradiations. The preceding comparison is made more

11. R. G. Berggren, W. J. Stelzman, and T. N. Jones, "Radiation Hardening and Embrittlement in ASTM Grade B, Class 1 Steel," *HSSST Program Semiannu. Progr. Rep. Feb. 28, 1970*, pp. 127-33.

difficult due to the 2:1 difference in fluence, the difference in significance of the thickness locations in base plate and weldment, and the difference in base plate material (02 instead of the actual 01 base plate). Similar data for plate 01 irradiated at 550°F and unirradiated at surface and 1/4-T locations will be developed for better comparison; however, the same 2:1 difference in fluence will still exist. Hence, no direct comparison is possible at this time.

POSTIRRADIATION DYNAMIC-TEAR AND CHARPY-V PERFORMANCE OF 12-IN.-THICK A533-B STEEL PLATES AND WELD METAL^{1,2}

J. R. Hawthorne
U.S. Naval Research Laboratory

Introduction

Postirradiation notch ductility characteristics of two 12-in.-thick A533-B, class 1 plates and of one 12-in.-thick A533-B submerged-arc weld deposit have been determined by the dynamic-tear (DT)^{1,3,14} and Charpy-V (C_v)^{1,5} test methods. Materials for this investigation were obtained from the HSST program and are fully representative of current practices used for melting, fabricating, and welding A533-B steel for nuclear reactor pressure vessels.

The primary objective of this study was to develop exploratory information on the DT performance of steel in the irradiated condition. Together with yield strength, DT shelf level forms an engineering indication of steel resistance of fracture in the maximum toughness (shelf-level) condition. Ratio analysis diagram (RAD) procedures^{1,6} requiring only these determinations have been devised for the quantitative assessment of fracture resistance. For the frangible state, the RAD allows for the establishment of critical flaw size-stress

conditions for the alloy through fracture mechanics relationships. Of similar importance, the DT midenergy range transition temperature approximates the fracture transition elastic (FTE) temperature. The FTE is defined as that temperature above which stresses in excess of yield are required to propagate a large flaw. The DT performances of steels such as A533 and of companion weld metals thus are of direct and current interest to reactor design and operation.

As part of a larger investigation, the current study was designed to help determine the possible correlation of C_v and DT test results for irradiated structural steels. Unlike the relatively new DT test method, the C_v test method has seen extensive use in radiation effects investigations. Development of a correlation between DT and C_v shelf energy would serve to open the way for utilization of RAD procedures in the evaluation of both reactor vessel surveillance data and the large bank of C_v data generated by past accelerated irradiation studies. Trends in C_v shelf energy and yield strength behavior with irradiation at reactor vessel service temperatures have been reported^{1,7} for A533 and other pressure vessel steels. The current study also considered that a correlation of C_v and DT transition behavior with irradiation would benefit predictions of FTE performance from existing data.

Additional objectives of the study included assessment of the relative radiation embrittlement sensitivity of plate vs weld deposit and the determination of possible differences in radiation response of 12-in.-thick plate due to test orientation or through-thickness test position. Findings are compared with results for several thinner gage plates and weld metals of the same nominal composition.^{1,8}

Composition and Heat Treatment

Test plate sections were identified as portions of HSST plates 01 and 02. The submerged-arc weldment carried the HSST code number 50 and was fabricated commercially by Combustion Engineering, Inc. Chemical compositions of the individual materials are summarized in Table 3.5, and detailed descriptions of

12. This work was sponsored and performed by the U.S. Naval Research Laboratory under an informal cooperative agreement with the HSST program.

13. E. A. Lange, P. P. Puzak, and L. A. Cooley, *Standard Method for the 5/8-in. Dynamic Tear Test*, NRL-7159 (Aug. 27, 1970).

14. P. P. Puzak and E. A. Lange, *Standard Method for the 1-in. Dynamic Tear Test*, NRL-6851 (Feb. 13, 1969).

15. *Standard Methods for Notched Bar Impact Testing on Metallic Materials*, ASTM Designation E-23-66, American Society for Testing and Materials Standards, Part 31, pp. 284-300, May 1967.

16. W. S. Pellini, *Evolution of Engineering Principles for Fracture-Safe Design of Steel Structures*, NRL-6957 (Sept. 23, 1969).

17. J. R. Hawthorne, *Trends in Charpy-V Shelf Energy Degradation and Yield Strength Increase of Neutron Embrittled Pressure Vessel Steels*, NRL-7011 (Dec. 22, 1969); *Nucl. Eng. Des.* **11**(3), 427-46 (1969).

18. J. R. Hawthorne and U. Potapovs, *Initial Assessments of Notch Ductility Behavior of A533 Pressure Vessel Steel with Neutron Irradiation*, NRL-6772 (Nov. 22, 1968); American Society for Testing and Materials, STP-457, pp. 113-34, 1969.

Table 3.5. Chemical composition of plate and submerged-arc weld deposit

Material	Source of data	Chemical composition (wt %)									
		C	Mn	P	S	Si	Ni	Cr	Mo	Cu	V
Plate 01	NRL	0.22	1.37	0.008	0.008	0.22	0.66	0.15	0.54	0.18	0.02
	Ref. 19	0.22	1.48	0.012	0.018	0.25	0.68		0.52		
Plate 02	NRL	0.23	1.48	0.008	0.016	0.19	0.68	0.12	0.51	0.14	0.02
	Refs. 19, 20	0.22	1.48	0.012	0.018	0.25	0.68		0.52		
Weld deposit	NRL	0.13	1.13	0.011	0.008	0.19	0.68	0.05	0.45	0.23	0.03
Weld 50	Ref. 20	0.12	1.35	0.014	0.012	0.23	0.65		0.52		

Table 3.6. Summary of irradiation experiments

Irradiation series	Material	Thickness location	Test orientation	Fluence ($E > 1$ MeV) ($\times 10^{19}$ neutrons/cm ²)	
				Fission spectrum	Calculated spectrum
<300°F (149°C)	Plate 01	1/4 T	WR	2.7	<i>a</i>
	Plate 02	1/4 T	RW	3.1	<i>a</i>
		1/4 T	WR	2.8	<i>a</i>
		Surface	WR	3.3	<i>a</i>
550°F (288°C)	Plate 01	1/4 T	WR	2.8	2.5
	Plate 02	1/4 T	RW	2.7	2.4
		1/4 T	WR	~2.6 ^b	~2.3
	Weld 50	1/4 to 1/2 T	<i>c</i>	2.5	2.2

^aNot available.^bDT specimens irradiated at 475°F (246°C).^cSpecimen long dimension perpendicular to welding direction.

materials fabrication and heat treatment have been published.¹⁹⁻²¹

The standard C_v specimens and DT specimens 1 5/8 × 7 × 5/8 in. thick were taken from plate 01 in the transverse (WR) test orientation only; similar specimens were taken from plate 02 in both longitudinal (RW) and transverse (WR) test orientations. Specimens from weld 50 were removed from the larger of the two welded

grooves forming the 2:1 offset double-U weld joint and were oriented with the long specimen axis perpendicular to the welding direction. Specimen notches in all cases were perpendicular to the plate or weldment surface.

Irradiations

The investigation employed both <300°F (149°C) and 550°F (288°C) specimen irradiations. The low-temperature exposures (four) were conducted in the materials test reactor (MTR), and the controlled elevated-temperature exposures (four) were performed in the Union Carbide Research Reactor (UCRR). In some experiments two 0.252-in.-diam tension test specimens were included with the DT-C_v specimen array.

A summary of irradiation experiments is given in Table 3.6. Approximately the same neutron fluence level was attained in each exposure [$2.5-3.3 \times 10^{19}$ neutrons/cm² ($E > 1$ MeV)]. Both the <300°F (149°C) irradiation series and the 550°F (288°C)

19. C. E. Childress, *Fabrication History of the First Two 12-in. Thick ASTM A-533 Grade B, Class 1 Steel Plates of the Heavy Section Steel Technology Program, Documentary Report 1*, ORNL-4313 (February 1969).

20. C. E. Childress, *Fabrication Procedures and Acceptance Data for ASTM A 533 Welds and a 10-in. Thick ASTM A 543 Plate of the Heavy Section Steel Technology Program, Documentary Report 3*, ORNL-4313, Pt. 3 (January 1971).

21. F. J. Loss, J. R. Hawthorne, and C. Z. Serpan, Jr., *A Reassessment of Fracture-Safe Operating Criteria for Reactor Vessel Steels Based on Charpy-V Performance*, NRL-7152 (Sept. 8, 1970); *Trans. Amer. Soc. Mech. Eng., Winter Annual Meeting*, New York, December 1970.

irradiation series emphasized plate 02. Limited stock precluded a low-temperature radiation assessment of the weld deposit.

Results

Tables 3.7 and 3.8 summarize findings for the several reactor experiments. Examples of C_v and DT changes

typically produced by low- and elevated-temperature irradiation are given in Figs. 3.18 and 3.19. Note that the inherent fracture characteristics of the larger DT specimen places the DT transition curve to the right of the C_v curve. Figure 3.20 illustrates the special case of a properties gradient through the thickness region under test, while Fig. 3.21 compares C_v and DT data for the weld deposit. Additional graphical presentations of data

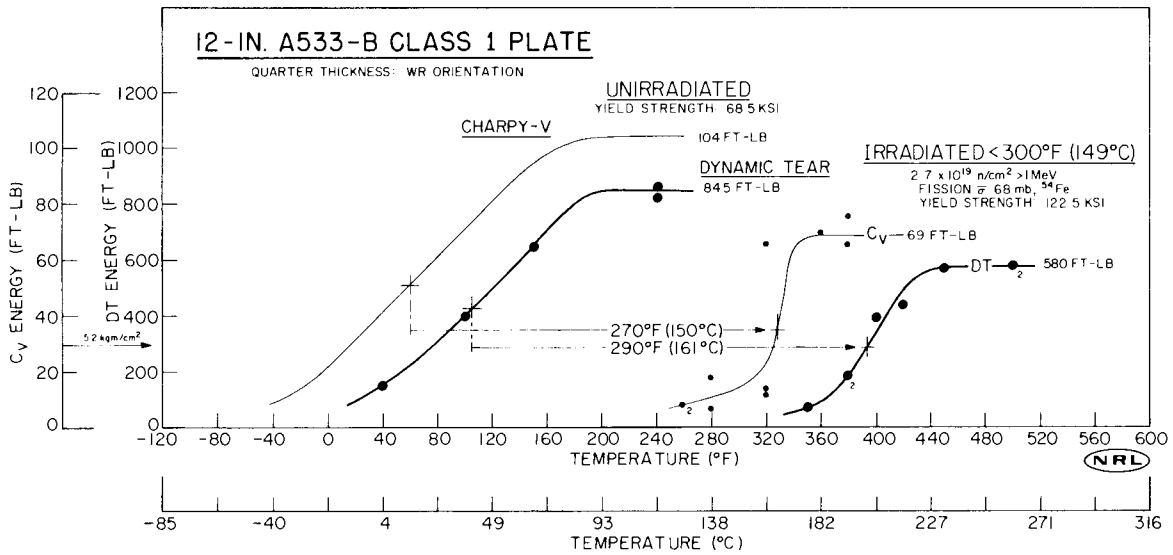


Fig. 3.18. Comparison of the Charpy-V and dynamic-tear test performance of a thick A533-B, class 1 steel plate (plate 01) before and after $<300^{\circ}\text{F}</math> ($149^{\circ}\text{C}</math>) irradiation. All specimens were taken from the quarter-thickness location and represent the transverse test orientation.$$

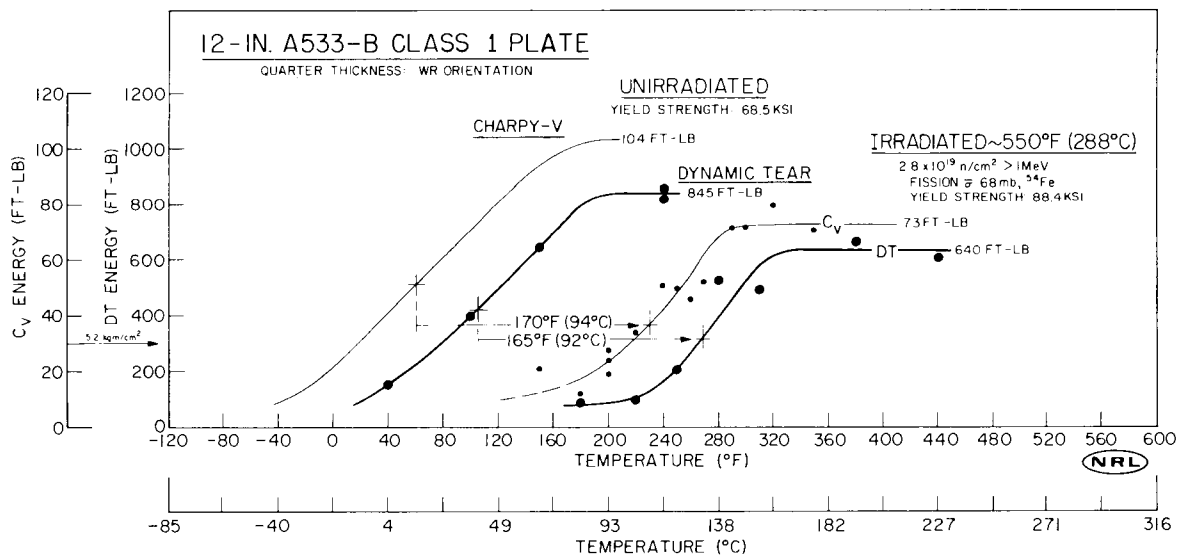


Fig. 3.19. Comparison of the Charpy-V and dynamic-tear test performance of a thick A533-B, class 1 steel plate (plate 01) before and after $550^{\circ}\text{F}</math> ($288^{\circ}\text{C}</math>) irradiation. All specimens were taken from the quarter-thickness location and represent the transverse test orientation.$$

Table 3.7. Summary of Charpy-V and dynamic-tear transition temperature determinations for plate and submerged-arc weld deposit

Material	Fluence, ^a Φ_{fs} [$\times 10^{19}$ neutrons/cm ² (>1 MeV)]	Transition temperature																	
		C _v mid-energy						DT mid-energy						C _v 30 ft-lb					
		Initial		Irradiated		Increase		Initial		Irradiated		Increase		Initial		Irradiated		Increase	
		°F	°C	°F	°C	Δ °F	Δ °C	°F	°C	°F	°C	Δ °F	Δ °C	°F	°C	°F	°C	Δ °F	Δ °C
<300°F (149°C) Irradiation																			
Plate 02 ($\frac{1}{4}$ T, WR)	2.8	85	29	360	182	275	153	115	46	380	193	265	147	45	7	360	182	315	175
Plate 02 ($\frac{1}{4}$ T, RW)	3.1	85	29	330	166	245	136	115	46	415	213	300	167	30	-1	325	163	295	164
Plate 02 (Surf., WR)	3.3	60 ^b 30 ^c	-51 1	165	74	225	125	0	-18	310	154	310	172	-105 ^b -30 ^c	-76 -34	165 ^b	74	270	150
Plate 01 ($\frac{1}{4}$ T, WR)	2.7	60	16	330	166	270	150	105	41	395	202	290	161	15	-9	325	163	310	172
550°F (288°C) Irradiation																			
Plate 02 ($\frac{1}{4}$ T, WR)	2.6	85	29	235	113	150	83	115	46	<i>d</i>				45	7	210	99	165	92
Plate 02 ($\frac{1}{4}$ T, RW)	2.7	85	29	235	113	150	83	115	46	255	124	140	78	30	-1	200	93	170	94
Plate 01 ($\frac{1}{4}$ T, WR)	2.8	60	16	230	110	170	94	105	41	270	132	165	92	15	9	215	102	200	111
Weld 50	2.5	20	-7	240	116	220	122	55 ^e	13	235	113	180	100	-45	-43	225	107	270	150

^aSee Table 3.6 for corresponding calculated spectrum fluence >1 MeV.

^bLayer 1 (surface).

^cLayer 2 ($\frac{1}{2}$ to 1 in. below surface).

^dDT specimens irradiated at $\approx 475^\circ\text{F}$ (246°C).

^eRef. 17.

Table 3.8. Summary of Charpy-V and dynamic-tear shelf energy determinations for plate and submerged-arc weld deposit

Material	Fluence, ^a Φ_{fs} [$\times 10^{19}$ fissions/cm ² (>1 MeV)]	Approx. C_v shelf energy (ft-lb)			DT shelf energy (ft-lb)			Approx. DT/ C_v shelf energy ratio	
		Initial	Irrad.	Percent reduction	Initial	Irrad.	Percent reduction	Initial	Irrad.
<300°F (149°C) Irradiation									
Plate 02 ($\frac{1}{4}$ T, WR)	2.8	99	64	35	830	490	41	8.4:1	7.7:1
Plate 02 ($\frac{1}{4}$ T, RW)	3.1	122	83	32	890	660	26	7.3:1	7.9:1
Plate 02 (Surf., WR)	3.3	98 ^b 109 ^c	64 ^b	~35	750	455	39	7.7:1	~7.1:1
Plate 01 ($\frac{1}{4}$ T, WR)	2.7	104	69	34	845	580	34	8.1:1	8.4:1
550°F (288°C) Irradiation									
Plate 02 ($\frac{1}{4}$ T, WR)	2.6	99	≈85	14	830	490 ^d	41	8.4:1	5.8:1 ^d
Plate 02 ($\frac{1}{4}$ T, RW)	2.7	122	≈102	14	890	≈805	10	7.3:1	7.9:1
Plate 01 ($\frac{1}{4}$ T, WR)	2.8	104	73	23	845	640	27	8.1:1	8.8:1
Weld 50	2.5	125	70	44	≈1350 ^e	≈570	58	10.8:1	8.2:1

^aSee Table 3.6 for corresponding calculated spectrum fluence >1 MeV.

^bLayer 1 (surface).

^cLayer 2 ($\frac{1}{2}$ to 1 in. below surface).

^dDT specimens irradiated at $\approx 475^\circ\text{F}$ (246°C).

^eRef. 17.

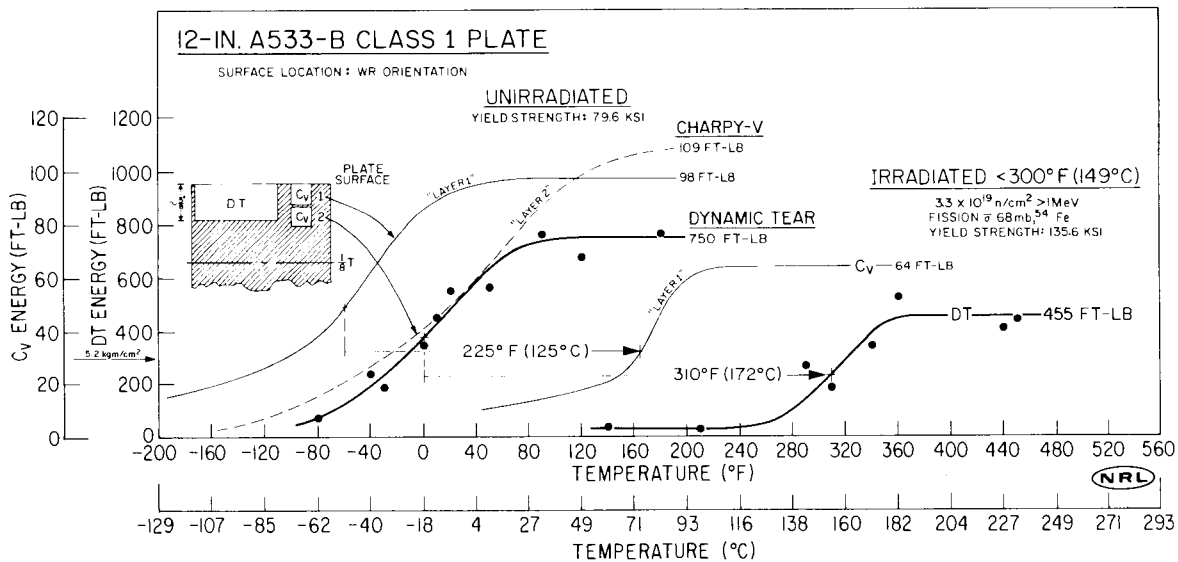


Fig. 3.20. Relative Charpy-V and dynamic-tear test performance of a thick A533-B, class 1 steel plate (plate 02) before and after $<300^\circ\text{F}$ (149°C) irradiation. Specimens were taken from the plate surface location as indicated by the insert diagram (transverse test orientation).

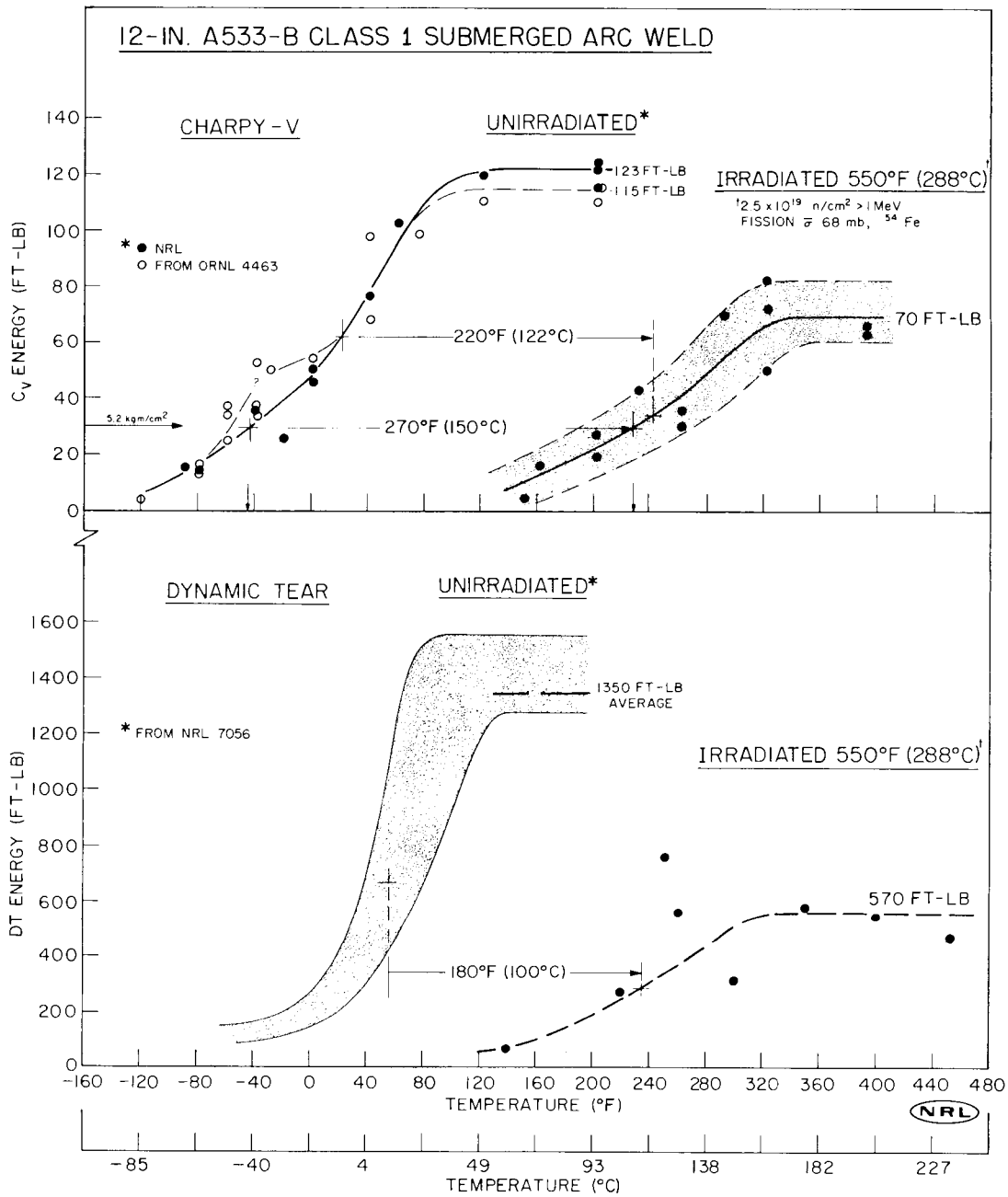


Fig. 3.21. Comparison of the Charpy-V and dynamic-tear test performance of a thick A533-B, class 1 submerged-arc weld deposit before and after 550°F (288°C) irradiation. Specimens were taken between the quarter- and half-thickness locations with their long dimension perpendicular to the welding direction.

are given in Figs. 3.22 to 3.24. In all cases it should be noted that the C_v and DT energy scales are given in a ratio of 1:10.

A common but arbitrary measure of irradiation response is the C_v 30 ft-lb transition temperature increase; however, the mod-energy range transition temperature increase was applied in this case as a more appropriate measure for C_v vs DT performance comparisons. In Table 3.7 it is seen that C_v and DT transition increases for individual plate quarter-thickness locations compare well on the basis of this index. It is reemphasized that data for the surface layer (Fig. 3.20) require special consideration. Results for the weld deposit also show reasonable agreement between C_v and DT mid-energy transition increases. The above-average data scatter noted in Fig. 3.21 for both pre- and postirradiation weld conditions denote a need for more research on the fracture characteristics of submerged-arc welds. For example, irradiated DT specimens exhibited pronounced shear lip development, which, on close examination, suggested that the fracture occurred along preferred paths within the multilayered weld deposit; that is, the fracture path tended to follow certain layers within the duplex weld microstructure (fine plus coarse grain regions). Observations concerning such tendencies account for the apparent data scatter more readily than recorded differences in specimen-to-specimen exposure conditions.

The compilation of DT and C_v shelf energy values (Table 3.8) for the several reactor experiments show that percent reductions in shelf level determined independently by the two test methods are in relatively good agreement. In Fig. 3.18, a 34% decrease in both C_v and DT shelf energy is indicated. In Fig. 3.19 the C_v and DT shelf energy reductions are 23 and 27% respectively. A more important observation from Table 3.8 is that the ratio of DT shelf energy to C_v shelf energy before and after irradiation is a fairly constant value in each case except for the submerged-arc weld deposit. Pre- and postirradiation ratios for the data in Figs. 3.18 and 3.19 are, respectively, 8.1:1 and 8.4:1, and 8.1:1 and 8.8:1. As discussed below, data for other A533 materials and for A543, class 1 plates support this finding.²¹

Referring to Fig. 3.20, the indicated properties gradient has been associated with a local gradation in microstructure resulting from the water-quench heat treatment. As a measure of the gradient, C_v specimens taken in two adjacent layers next to the plate surface indicated a 75°F (42°C) difference in preirradiation transition temperatures. Obviously, an attempt to relate either of the C_v brittle-ductile transition indications

with the DT transition performance would be misleading. Since the C_v shelf level appears relatively insensitive to test depth, however, comparisons between the "average" C_v shelf value and the DT shelf value were felt reasonable. Good correspondence in percentage shelf reductions and in shelf energy ratio relationships were again observed.

An in-depth analysis of the characteristics and significance of radiation-induced DT toughness gradients in a pressure vessel wall has been presented elsewhere.²²

Discussion

The observed comparability of radiation-induced DT and C_v transition temperature increases in all plate and weld assessments and in the concomitant DT and C_v shelf energy reductions is most revealing. For A533-B plate, it would appear that, knowing the preirradiation correspondence of C_v and DT performance, postirradiation DT features such as transition temperature and shelf level could be calculated with reasonable accuracy from postirradiation C_v results. A DT mid-energy range transition temperature so derived would approximate the postirradiation FTE temperature to guide reactor startup and shutdown pressure-temperature applications. From calculated DT shelf values and yield strength information, RAD procedures could also be applied to ascertain the general level of fracture resistance for the fluence level in question. Figure 3.25, from a report by Loss, Hawthorne, and Serpan,²¹ shows the highly consistent correspondence of C_v to DT shelf energy found among many A533 plates (including those of this study), an A302-B plate, and two A543, class 1 plates. The data for both unirradiated and irradiated conditions describe an 8.0:1 ratio of DT to C_v shelf energy. Note that all data fall within the limits of a 10% deviation from the 8.0:1 correspondence line. The data encompass a C_v shelf energy range of 40 to 140 ft-lb and a DT shelf energy range of 300 to 1200 ft-lb.

It is interesting to note that for the submerged-arc weld, the postirradiation condition but not the preirradiation condition conforms to the 8.0:1 ratio relation. Whether or not similar correspondence would be observed with other exposure temperature-influence conditions has yet to be determined. Unlike the submerged-arc weld, data for an A533-B electroslag

22. F. J. Loss, J. R. Hawthorne, and C. Z. Serpan, Jr., *Analysis of Radiation Induced Embrittlement Gradients on Fracture-Characteristics of Thick-Walled Pressure Vessel Steels*, NRL-7209 (pending publication).

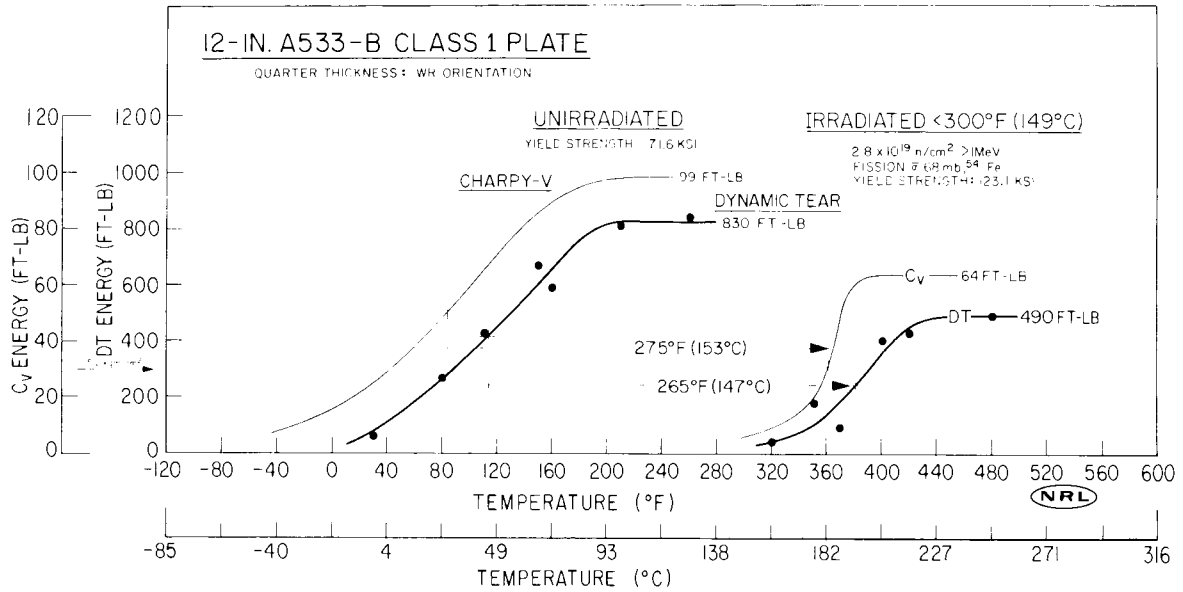


Fig. 3.22. Comparison of the Charpy-V and dynamic-tear test performance of a thick A533-B, class 1 steel plate (plate 02) before and after <math>< 300^{\circ}\text{F}</math> (149°C) irradiation. All specimens were taken from the quarter-thickness location and represent the transverse test orientation.

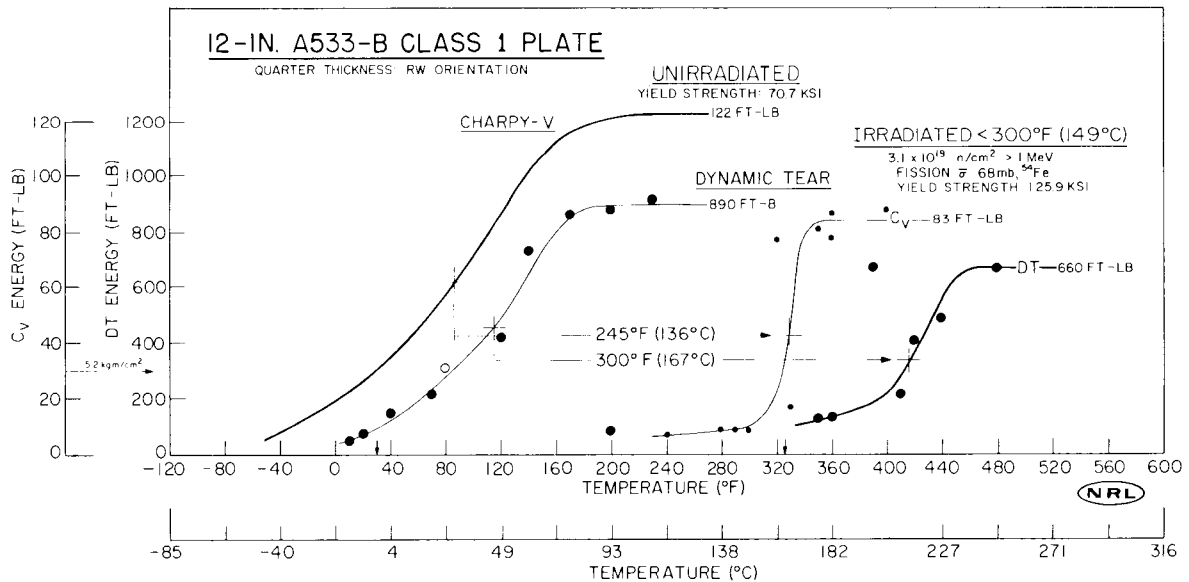


Fig. 3.23. Comparison of the Charpy-V and dynamic-tear test performance of a thick A533-B, class 1 steel plate (plate 02) before and after <math>< 300^{\circ}\text{F}</math> (149°C) irradiation. All specimens were taken from the quarter-thickness location and represent the longitudinal orientation.

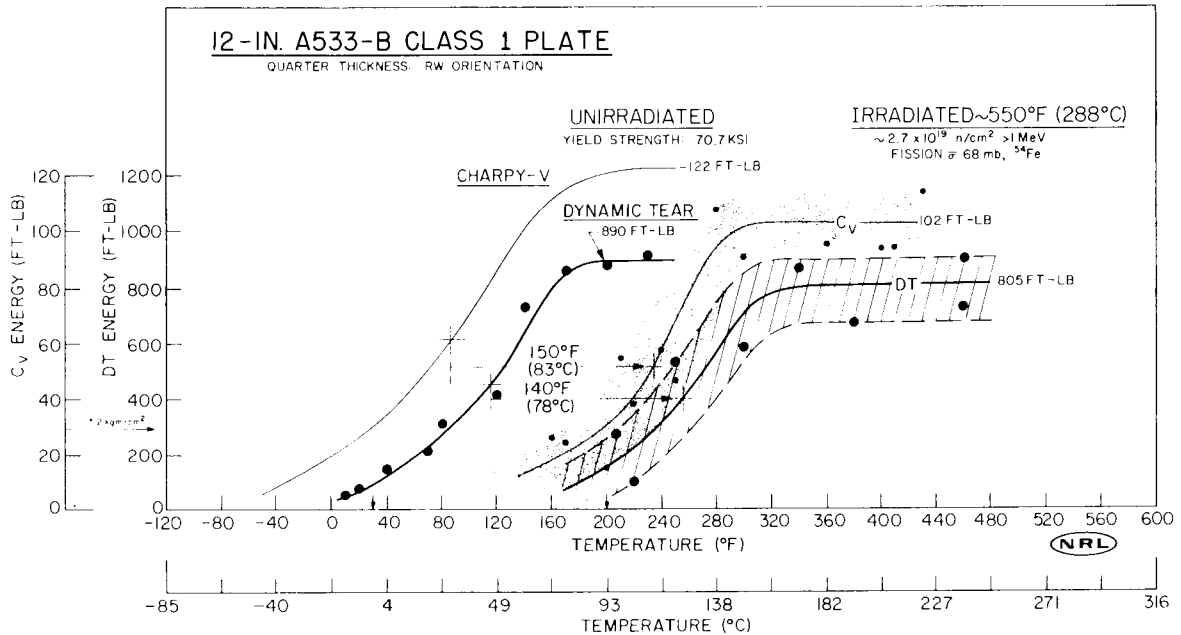


Fig. 3.24. Comparison of the Charpy-V and dynamic-tear test performance of a thick A533-B, class 1 steel plate (plate 02) before and after 550°F (288°C) irradiation. All specimens were taken from the quarter-thickness location and represent the longitudinal orientation.

weld in the preirradiation condition do conform to the ratio relationship (see datum 16 in Fig. 3.25). Therefore the high preirradiation ratio behavior of the submerged-arc weld may be characteristic of submerged-arc or other similar multipass welds. The need for additional assessments of such welds is suggested.

In Fig. 3.26, changes in the shelf level performance of plates 01 and 02 with neutron exposure are shown on the RAD. Preirradiation performance is indicated by the cross-hatched symbols. Open symbols represent the 550°F (288°C) irradiation condition; closed symbols depict the <300°F (149°C) irradiation condition. The measured yield strength elevation of plate 01 with 550°F exposure (Table 3.9) was taken as an approximation of postirradiation yield strength increase for plate 02. Significant reductions in notch toughness are indicated for both RW and WR test orientations. However, data for the 550°F exposure condition remain to the left (i.e., "above") the ratio infinity (∞) line. In this zone plane strain fracture is remote even with thick-section components. A similar unsusceptibility to plane strain fracture is suggested by results for the weld metal (not shown). Notably, the performance of plates 01 and 02 of the weld with 550°F irradiation compares favorably with the performance of several other A533 plates and weld deposits indicated by the

data envelope¹⁷ (hatched region) of Fig. 3.26. More severe reductions in toughness accomplished by <300°F (149°C) exposures of plates 01 and 02 succeeded in shifting the WR orientation performance indications to the region described by 15- ∞ ratios. Here, plane strain fracture is considered a faint possibility in very thick-section components (>6 to 7 in.) according to fracture mechanics interpretations of behavior under mechanical constraint behavior.

Shelf data for both plates when compared with the data trend (RW orientation) for the ASTM A302-B reference plate (Fig. 3.26) are indicative of superior toughness in pre- and postirradiation conditions. The trend in toughness degradation described for the A302-B plate was established from <300°F exposure data; however, 550°F exposure data appeared to follow the same trend path.¹⁷ Trend lines drawn through the data for plates 01 and 02 are seen to exhibit the same initial shape as that for the A302-B plate. Thus it can be speculated that the three stages of change in shelf level vs yield strength revealed for the A302-B steel are a characteristic of A533-B steel as well. Similar trend features have been observed for A543 steel.¹⁷

Radiation embrittlement sensitivities of the plate and weld deposit relative to the performance of the ASTM reference plate are indicated in Fig. 3.27. Note that the

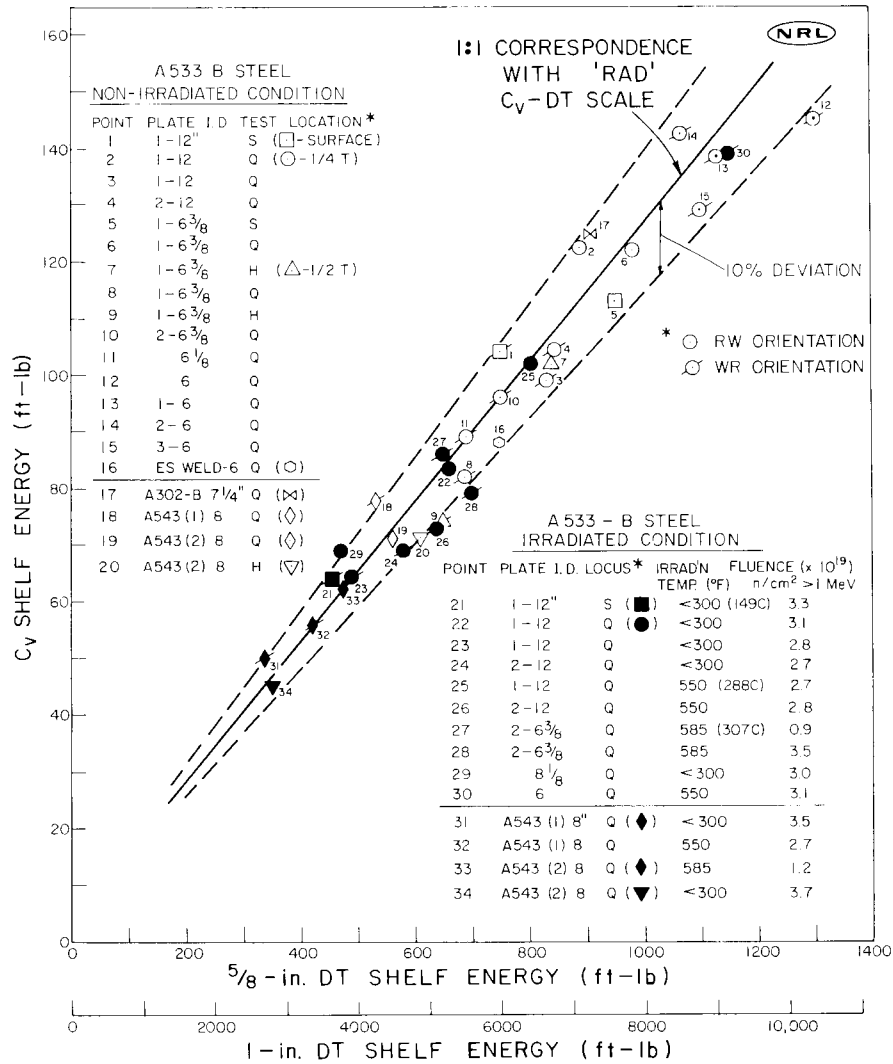


Fig. 3.25. Pre- and postirradiation comparisons of Charpy-V and dynamic-tear shelf energies from numerous plates of A533 steel. Comparisons are also illustrated from two plates of A543 steel, the A302-B ASTM reference plate, and an A533 electrosag weld (Ref. 21).

ordinate of this figure is given as "Increase in C_v 30 ft-lb Transition Temperature." The range of sensitivity variations observed with several other A533 plates and weld deposits in 550°F (288°C) exposures is also indicated.^{17,18} In terms of apparent sensitivity to <300°F radiation embrittlement, plates 02 and 01 (quarter-thickness locations) are comparable to the reference plate. A lower radiation embrittlement susceptibility is described for the surface layer of plate 02. This is believed to be primarily a reflection of the different microstructure at the plate surface location.²³ In another study, Berggren found the surface of plate 01 to be less sensitive to radiation at 150°F than the plate interior.²⁴ Referring next to the 550°F (288°C)

exposure condition, plate 02 and the A302-B reference plate again show similar irradiation responses. On the other hand, plate 01 and weld 50 show greater susceptibilities to embrittlement at this temperature. The higher copper contents of plate 01 (0.18%) and weld 50 (0.23%) relative to plate 02 (0.14%) help

23. D. A. Canonico, "Microstructure Studies of HSST Plate 01," *HSST Program Semiannu. Progr. Rep. Aug. 31, 1968*, ORNL-4377, pp. 29-32.

24. R. G. Berggren et al., "Radiation Hardening and Embrittlement in ASTM A533, Grade B, Class 1 Steel," *HSST Program Semiannu. Progr. Rep. Feb. 28, 1969*, ORNL-4463, pp. 117-20.

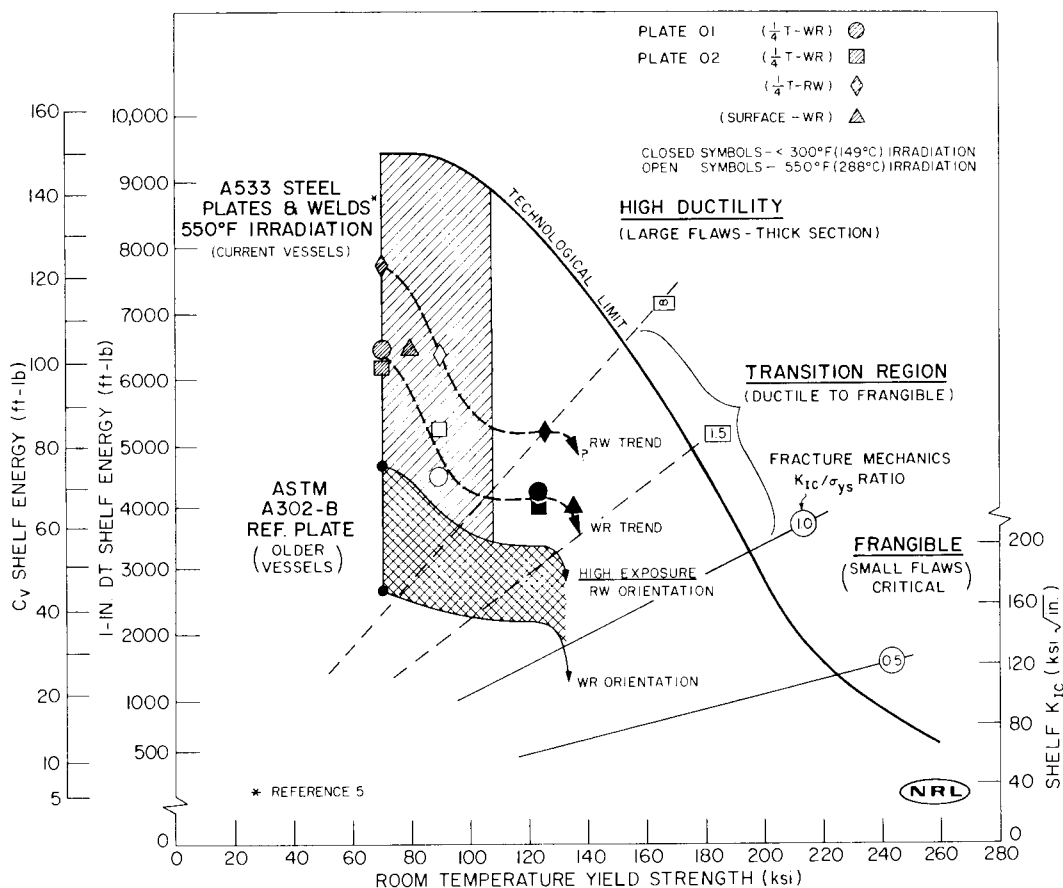


Fig. 3.26. Ratio analysis diagram (RAD) for assessment of fracture resistance in the shelf level condition. Trends in shelf energy degradation with irradiation for the A533-B, class 1 plates (01 and 02) appear to follow established trends for the A302-B ASTM reference plate (Ref. 17).

account for the differences in sensitivity among these materials.²⁵ To further explain weld deposit performance, it has been suspected²⁶ that a cast structure is more sensitive to radiation embrittlement than a wrought structure. Surprisingly, the radiation embrittlement tendencies of plates 01 and 02 and of the weld at 550°F (288°C) are greater than that which would be projected from relative copper content and the trend for the A302-B reference plate (0.21% Cu). It is

proposed that the higher nickel content of the A533-B materials, or other small composition differences, may be contributing directly or indirectly to their greater radiation sensitivity at this representative service temperature.²⁷

Conclusions

Charpy-V (C_v) and $\frac{5}{8}$ -in. dynamic-tear (DT) specimens taken from 12-in.-thick A533-B, class 1 plates and from a 12-in.-thick submerged-arc weld deposit have been irradiated at <300°F (149°C) and at 550°F (288°C). The materials, identified as plates 01 and 02 and weld 50 from the HSST program, are representative

25. U. Potapovs and J. R. Hawthorne, *The Effect of Residual Elements on 550°F Irradiation Response of Selected Pressure Vessel Steels and Weldments*, NRL-6803 (Nov. 22, 1968); also *Nucl. Appl.* 6(1), 27-46 (January 1969).

26. J. R. Hawthorne and U. Potapovs, *Through-Thickness 550°F Irradiation Response of 8-in. A533-B, Class 1 Production Weldment*, NRL Report of Progress, pp. 26-28 (February 1969).

27. J. R. Hawthorne, E. Fortner, and S. P. Grant, "Radiation Resistant Experimental Weld Metals for Advanced Reactor Vessel Steels," *Welding J., Res. Suppl.* 35(10), 453s-460s (October 1970).

Table 3.9. Summary of ambient temperature yield strength determinations for plate and submerged-arc weld deposit

Material	Fluence, ^a Φ_{fs} [$\times 10^{19}$ neutrons/cm ² (>1 MeV)]	Yield strength (ksi)		
		Initial	Irrad.	Increase
<300°F (149°C) Irradiation				
Plate 02 ($\frac{1}{4}$ T, WR)	2.8	71.6	123.1	51.5
Plate 02 ($\frac{1}{4}$ T, RW)	3.1	70.7	125.9	55.2
Plate 02 (Surf., WR)	3.3	79.6	135.6	56.0
Plate 01 ($\frac{1}{4}$ T, WR)	2.7	68.5	122.5	54.0
550°F (288°C) Irradiation				
Plate 02 ($\frac{1}{4}$ T, WR)	2.6	71.6	91.6 ^b	20
Plate 02 ($\frac{1}{4}$ T, RW)	2.7	70.7	90.7 ^b	20
Plate 01 ($\frac{1}{4}$ T, WR)	2.8	68.5	88.4	19.9
Weld 50	2.5	63.7	88.7 ^b	25

^aSee Table 3.6 for corresponding calculated spectrum fluence >1 MeV.

^bEstimated.

of current steelmaking and welding practices. Primary observations and conclusions drawn from the investigation are as follows.

1. Postirradiation mid-energy transition temperature increases determined independently by C_v and DT test methods were comparable in both plate and weld assessments (quarter-thickness locations). The effect of a plate surface layer was not qualified in view of the C_v properties gradient with thickness at this location.

2. Postirradiation shelf energy reductions determined by C_v and DT test methods were comparable in plate assessments.

3. Postirradiation shelf energy reductions determined by C_v and DT test methods were not comparable in the submerged-arc weld assessment. Fracture appearances of irradiated weld DT specimens suggest preferred paths for fracture consistent with the duplex-layered microstructure of submerged-arc welds. A need for additional research on the fracture characteristics of multipass weld deposits is evidenced by pre- and postirradiation results.

4. Ratios of DT to C_v shelf energy for pre- and postirradiation conditions of plate (quarter-thickness

and surface layers) and for the postirradiation conditions of the weld conform well to the general 8.0:1 DT-to- C_v ratio relationship observed in a broader study of A533, A302-B, and A543 steels.

5. Observations for mid-energy transition increase and shelf energy reduction suggest that postirradiation DT properties of A533-B plate can be predicted with reasonable accuracy from postirradiation C_v results if preirradiation C_v vs DT characteristics are known.

6. Postirradiation shelf level performance assessments by ratio analysis diagram (RAD) procedures indicate relatively good toughness retention by both plate and weld deposit with 550°F (288°C) exposures. For the $<300^\circ\text{F}$ (149°C) exposure condition, RAD analyses indicate that plane strain fracture would be possible but would require very thick components and very large flaws.

7. Comparisons of C_v 30 ft-lb transition temperature increases show that plates 01 and 02 and the ASTM A302-B reference plate have similar irradiation responses at $<300^\circ\text{F}$ (149°C). At 550°F, plate 02 and the reference plate have comparable irradiation responses; however, plate 01 and the weld deposit show higher embrittlement tendencies at this temperature.

8. Radiation embrittlement sensitivity at 550°F (288°C) was found to increase with increasing copper content as expected; however, embrittlement sensitivities of all three A533 materials exceeded expectations. An influence of nickel content on radiation sensitivity development is proposed.

Acknowledgments

This investigation was sponsored by the U.S. Atomic Energy Commission, Division of Reactor Development and Technology, Fuels and Materials Branch. The continuing support of this agency is acknowledged with gratitude. The author expresses particular appreciation to Mr. A. VanEcho of the Fuels and Materials Branch for his personal efforts and guidance in the acquisition of the test materials.

The sections of plate and submerged-arc weld employed in this study were donated by the Heavy-Section Steel Technology (HSST) Program, F. J. Witt, Director.

The author thanks F. J. Loss and L. E. Steele for their consultation in the development of the materials irradiation plan. The author also thanks C. Z. Serpan, Jr., for the neutron exposure data given in this report. Appreciation is further expressed to H. E. Watson and his staff for their many efforts and contributions during the period of experiment irradiation and postirradiation operations.

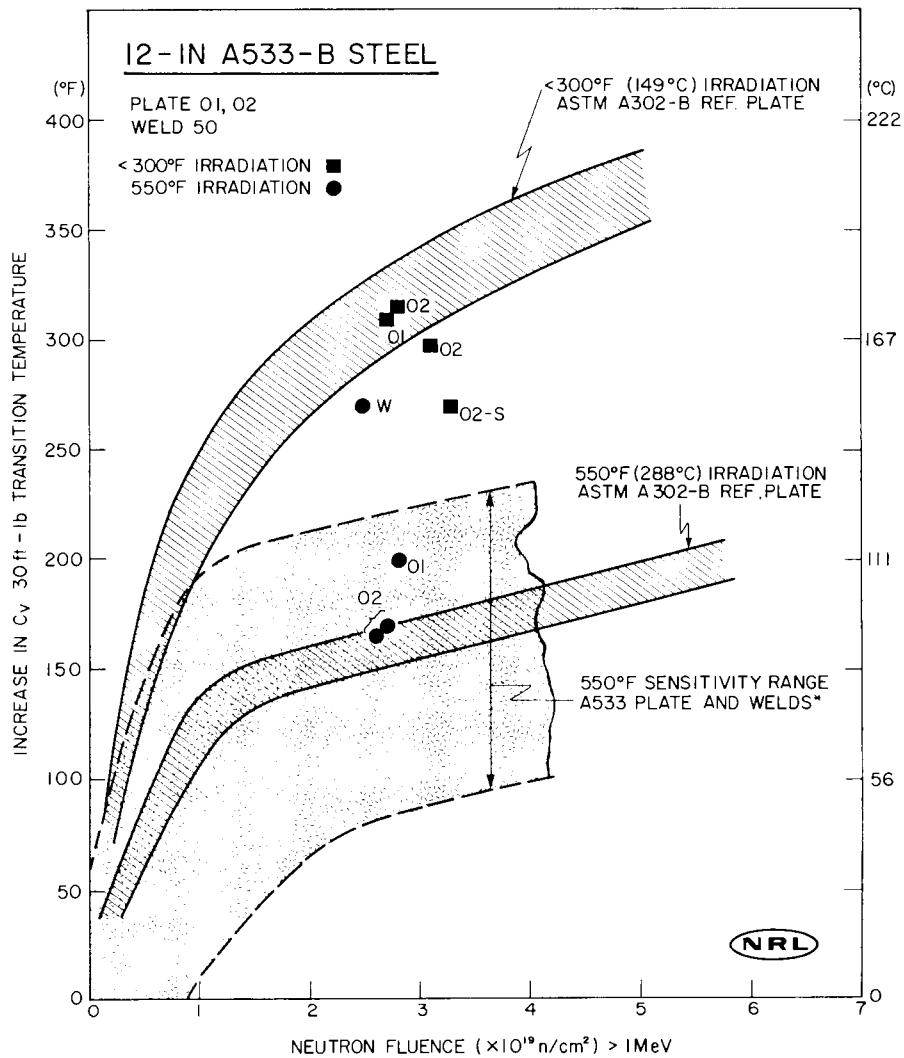


Fig. 3.27. Increase in Charpy-V 30 ft-lb (5.2 kg/cm²) transition temperature with increasing fluence at <300°F (149°C) and at 550°F (288°C). Data for the thick section A533-B, class 1 plates (01 and 02) and the weld deposit are shown relative to trends for the A302-B ASTM reference plate and for other A533 plates and welds. Note that at 550°F irradiation embrittlement sensitivities of plate 01 and weld 50 significantly exceed that of the reference plate (Ref. 17).

4. Pressure Vessel Investigations

The testing of large flawed tensile specimens and complementary smaller specimens continues to be a major area of work. In addition, a series of small nozzled epoxy vessels have been tested, data from which have been used to obtain shape factors applicable to brittle fracture calculations using linear elastic fracture mechanics. Preparation of the facility for testing the intermediate test vessels has been accelerated, and the fabrication of the pressure vessels themselves continues to be actively followed.

TESTING OF 6-in.-THICK FLAWED TENSILE SPECIMENS¹

S. C. Grigory
S. P. Ying

Southwest Research Institute

Thirteen 6-in.-thick tensile specimens have been tested to date. The results of ten of these tests were reported previously. The last three specimens tested were 6-in.-thick quenched and tempered plate with weldments normal to the longitudinal axis of the specimen. The machined flaws were sharpened by fatigue cracking placed in the weld metal.

A series of six 1-in.-thick tensile specimens, exact $\frac{1}{6}$ -scale replicas of the 6-in.-thick specimens, were broken over a temperature range of 50 to 200°F. These specimens contained machined flaws sharpened by a process utilizing electron-beam welding and hydrogen charging.

The acoustic emissions of both the 6- and 1-in. specimens were monitored during the tests.

Six-in.-thick Flawed Tensile Specimens with Weldments

Specimen description

The basic dimensions of the welded tensile specimens and the machined notch are given in Fig. 4.1. It may be seen that the three welded specimens are slightly smaller than the previous ten specimens tested; instead of the usual 6- by 18-in. cross section, the cross section is 5.6 by 16.75 in. Also, the welded plates are quenched and tempered 6-in.-thick plate, whereas the previous ten specimens were center material from the 12-in.-thick HSST plates.

The flaws were machined semicircular notches sharpened by fatigue cracks. The notch-sharpening procedures were previously described.² The notch dimensions before and after sharpening are given in Table 4.1, and the three welded specimens after failure are shown in Fig. 4.2. The flaws were placed in the center of the welds, so that the test was essentially a test of weld metal in the presence of a flaw in a heavy section.

Test results

The three welded specimens were tested at temperatures of 0, 75, and 160°F. Pertinent test parameters are given in Table 4.2, and the load-strain curves are given in Fig. 4.3. The actual loads achieved on these tests were somewhat lower than previous tests because of the reduced cross-sectional area.

A very definite pop-in occurred during the test of specimen 13, tested at 75°F. The crack had been visually inspected at the 5.9×10^6 lb load increment

1. Research sponsored under UCCND Subcontract No. 3202 between Union Carbide Corporation and Southwest Research Institute.

2. F. J. Witt, *HSST Program Semiannu. Progr. Rep. Feb. 28, 1971*, ORNL-4681.

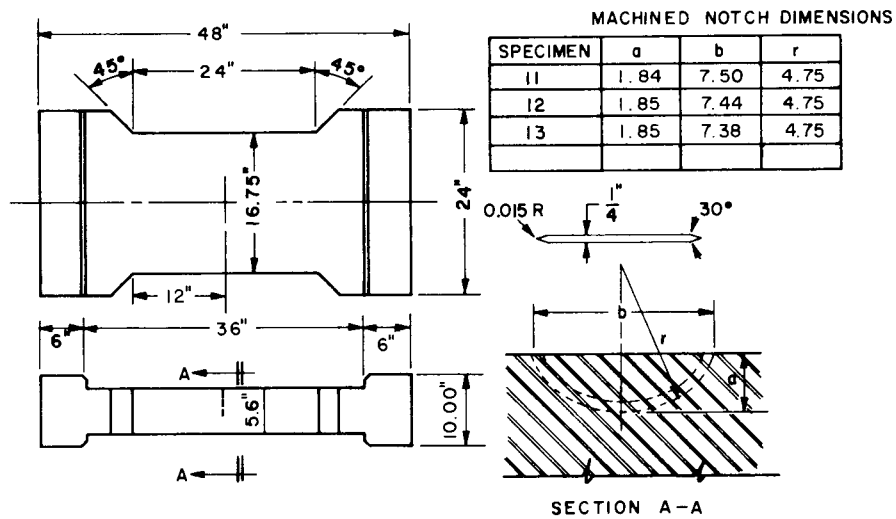


Fig. 4.1. Specimen and notch geometries of the welded tensile specimens.

Table 4.1. Notch dimensions before and after notch sharpening

Specimen No.	Machined notch dimensions (in.)			Notch dimensions after sharpening (in.)		Notch dimensions ^a at ultimate load (in.)	
	Depth	Length	Radius	Depth	Length	Depth	Length
11	1.84	7.50	4.75	2.45	7.75	2.58	7.75
12	1.85	7.44	4.75	2.75	8.00		
13	1.85	7.38	4.75	2.25	7.50	2.44	7.50

^aMeasurement made after fracture.

and was observed to be very tight. While data were being obtained at the 5.95×10^6 lb load increment (gross section stress of 63.5 ksi), a loud report was heard, and the load on the specimen dropped. The crack was inspected a second time and was observed to have opened a noticeable amount.

The elastic limit load given in Table 4.2 is the load at which the sharp break occurs in the stress-strain curves shown in Fig. 4.3. Actually, the specimens showed signs of yielding between 3 and 4×10^6 lb.

One-in.-thick Flawed Tensile Specimens

Specimen description

The 1-in.-thick tensile specimens are $1/6$ -scale models of the 6-in.-thick specimens. They are tested in an exact scale replica of the grip plates used on the Southwest

Research Institute 15×10^6 lb tensile test machine for testing the 6-in.-thick specimens, so that the load distribution on the test section is duplicated in the 1-in.-thick specimens.

All 1-in. specimens tested to date have been longitudinal specimens. The first two tested were center material from HSST plate 03; all subsequent specimens have been center material from HSST plate 01. Also, the flaws in the first two specimens were sharpened by a fatigue crack induced by bending the specimen; the flaws in all subsequent specimens were sharpened by charging a brittle zone at the root of a machined notch with hydrogen.² The notches were placed in the specimens using electrical discharge machining. The brittle zone at the root of the notch was created by concentrated heating with an electron-beam welder. A 10% solution of H_2SO_4 was used as an electrolyte for



Fig. 4.2. Fracture surfaces of welded 6-in.-thick flawed tensile specimens.

Table 4.2. Tensile test data for 6-in.-thick welded specimens

Test parameter	Specimen 11	Specimen 12	Specimen 13
Test temperature, °F	0	160	75
Gage length, in.	24	24	24
Width, in.	16.75	16.75	16.75
Thickness, in.	5.6	5.6	5.6
Gross area, in. ²	93.8	93.8	93.8
Net area, in. ²	78.9	76.6	81.1
Elastic limit load, kips	5.6	5.0	5.6
Elastic limit stress, ksi			
Gross section	59.7	53.3	59.7
Net section	71.0	65.3	69.0
Ultimate load, kips	6.25	6.19	6.15
Ultimate stress, ksi			
Gross section	66.6	65.9	65.5
Net section	79.2	80.8	75.8
Average strain, %			
At ultimate ^a	1.02	3.70	1.32
At fracture ^a	1.02	3.80	1.32

^aBased on deflection of gage length (24 in.).

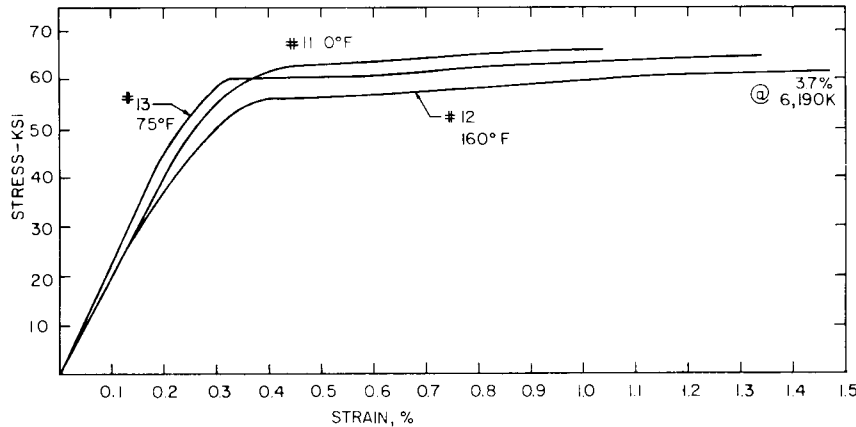


Fig. 4.3. Load-strain curves for the three welded tensile specimens.

hydrogen charging. All machining and precracking, except for the fatigue work, has been performed at ORNL. The precracks formed using the electron-beam welder will hereafter be referred to as EB cracks.

Three specimens with EB cracks were tested as received. Since it was suspected that either residual hydrogen or residual stress remaining in the specimen as a result of the precracking technique could affect the test results, one specimen was stress relieved and a second was baked at 400°F for 2 hr to drive off residual hydrogen. There was no appreciable difference in the test results of these specimens, tested at 200°F, but all subsequent specimens have been baked at 400°F as a precautionary measure.

Test results

Figure 4.4 shows a 1-in. test specimen in the test fixture with clip gages attached. Six clip gages were used on the first specimens tested; however, the number was reduced to four after it was decided that the hole drilled in the side of the specimen affected the strain distribution at the adjacent strain gages and that the strain gage information was more desirable than the data from the clip gages. Sixteen strain gages were placed on each specimen.

Some of the pertinent test parameters are given in Table 4.3. A complete review of the strain data will be presented in a technical summary report that is being prepared.

Acoustic Emissions Monitoring

The reactor industry is actively engaged in developing acoustic emission monitoring equipment for in-service

reactors, but the information available on the characteristics of the emissions in heavy-section structures is scant. However, much work is being performed on small cracked specimens, with certain trends and relationships being noted. It is important that these relationships be confirmed for heavy-section plates and that the possibility be investigated that other phenomena, not detectable in small specimens, occur in heavy sections. Two areas of particular interest in this endeavor are (1) the variation of rate of emissions with strain or stress level and (2) the variation of total counts (frequency cycles of a given transducer) with stress intensity factor.

Acoustic emissions from 6-in.-thick flawed weld metal specimens and 1-in.-thick tensile specimens of base metal were monitored during the tensile tests in the temperature range 0 to 200°F. The rates of emissions and their accumulations were studied as functions of the applied stresses and the stress intensity factors respectively. The acoustic emission due to plastic deformation was also observed from a large specimen tested at 150°F. It was found that variation of acoustic emission with stress level or stress intensity factor for the large specimens is similar compared with that of small-crack specimens, but the emission from 6-in. specimens is higher than that from the 1-in. specimens.

Experiments

Acoustic emission monitoring of 1-in.-thick flawed specimens. Acoustic emissions from six 1-in.-thick flawed base-metal specimens tested at 50, 75, 100, and 200°F have been monitored. Each specimen had an electron-beam weld crack with a circular segment surface, as described above, and direction of the tension

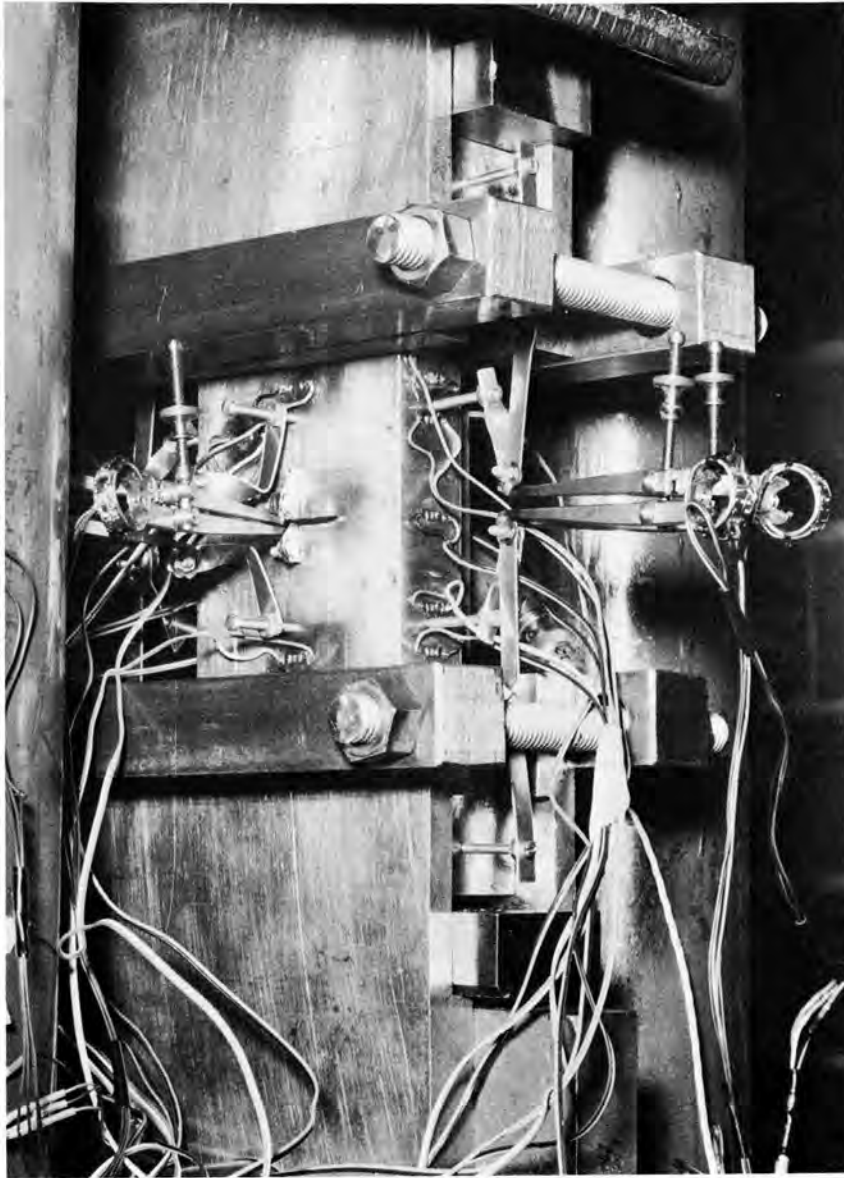


Fig. 4.4. Test setup for the 1-in.-thick flawed tensile specimens.

was perpendicular to the plane of the major and the minor axes of this surface. Figure 4.5 shows the transducer mounted on the specimen on the unflawed surface. During each test, two acoustic transducers were monitored: the one directly attached to the back side of the specimen and another mounted at the lower part of the tensile machine, where any possible hydraulic noise may be detected.

Since the signals obtained from both transducers were recorded on magnetic tapes, the signals from the

transducer monitoring the hydraulic noise provided the necessary information to distinguish the acoustic emission of the specimen from hydraulic noise. It was found that the hydraulic noise was quite low except at the very beginning of the tests. Most of the noises could not transmit to the transducer on the specimen because the high-frequency hydraulic noise was damped by several mechanical joints between the two transducers.

The details of the transducers and the electronic equipment were previously described.²

Table 4.3. Tensile test data for 1-in.-thick specimens

Specimen No.	Test temperature (°F)	HSST plate No.	Gage length (in.)	Width (in.)	Thickness (in.)	Gross area (in. ²)	Net area (in. ²)	Elastic limit load (kips)	Elastic limit stress (ksi)		Ultimate load (kips)	Ultimate stress (ksi)		Average strain at ultimate ^a (%)
									Gross section	Net section		Gross section	Net section	
2	210	03	4	3	1	3	2.66	175	58.4	65.7	230.6	78.6	88.9	5.61
3	50	03	4	3	1	3	2.42	176	58.6	72.7	223.0	74.3	92.2	5.75
4	50	01	4	3	1	3	2.60	145	48.2	55.7	195.0	65.0	75.0	1.21
5	75	01	4	3	1	3	2.61	160	53.3	61.4	235.0	78.4	90.0	4.98
6	200	01	4	3	1	3	2.60	160	53.3	61.6	224.0	74.6	86.1	4.30
7 ^b	200	01	4	3	1	3	2.60	165	55.0	63.4	220.0	73.3	84.6	5.77
8	200	01	4	3	1	3	2.58	155	51.6	60.1	215.0	71.6	83.3	5.32
9	75	01	4	3	1	3	2.59	160	53.3	61.8	225.0	75.0	86.8	4.62

^aBased on deflection of specimen gage length (4 in.)

^bStress relieved.

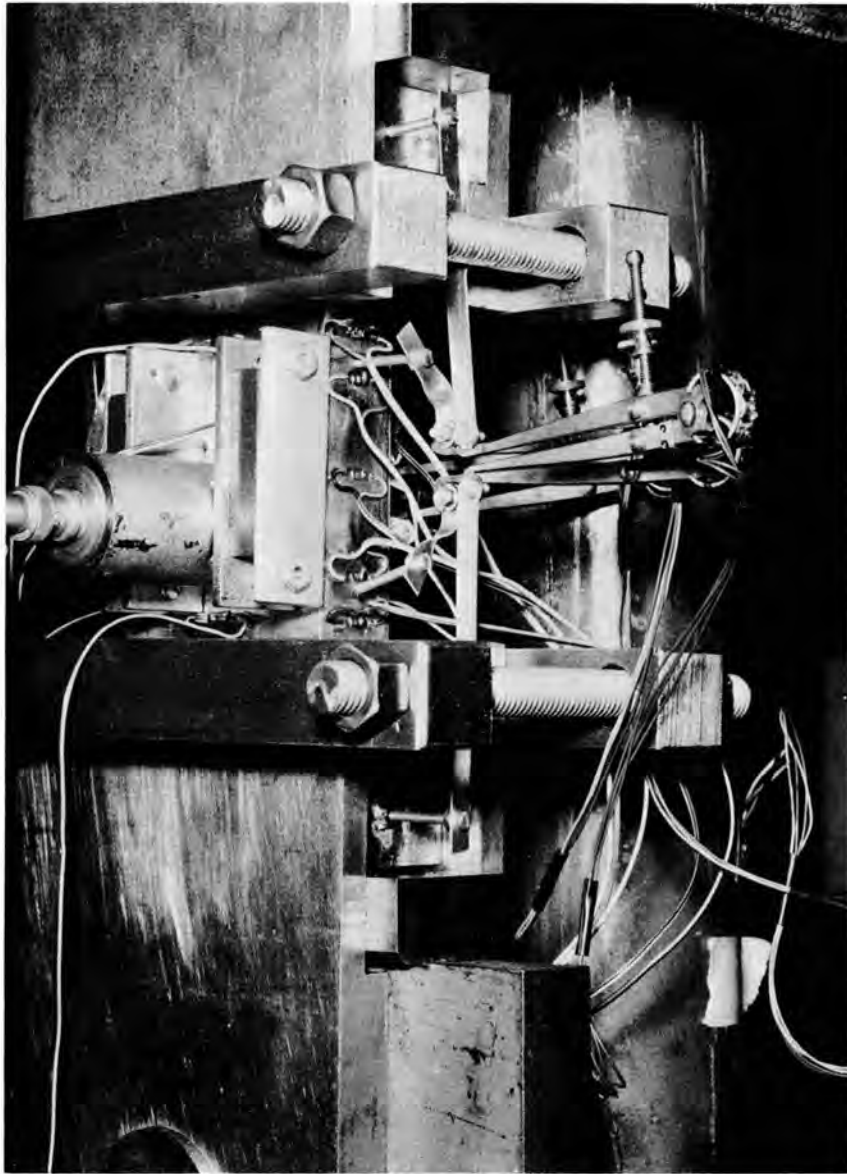


Fig. 4.5. Monitoring transducer on the back of the specimen.

Acoustic emission monitoring of 6-in.-thick flawed specimens. Three 6-in.-thick flawed weld-metal specimens were tested at 0°F, room temperature, and 160°F. Three transducers were monitoring simultaneously during each tensile test. One was attached near the notch and served as the pickup sensor of the data channel; the other two were mounted at the side of the specimen with equal distance from the notch. Only the acoustic emission signals that were generated in the notch area were transmitted to these two transducers at the same time. All other mechanical noises from other

regions arrived at different times. By utilization of this principle, the acoustic emission signals can be distinguished from all other kinds of noises.

Results

Acoustic emission from 1-in.-thick tensile specimens. Preliminary reduction data of 1-in. specimens for the tests at 50, 100, and 200°F are presented in Fig. 4.6, in which the accumulation of acoustic emissions is plotted as the function of the stress intensity factor K_I . These

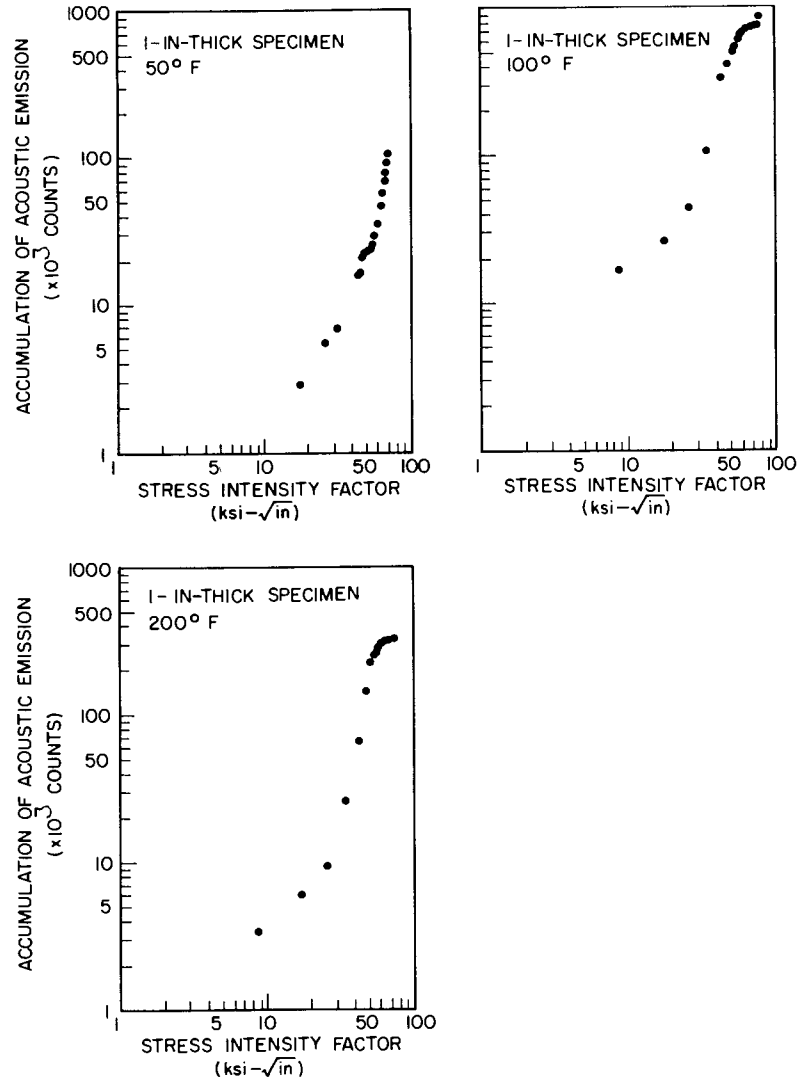


Fig. 4.6. Acoustic emission from 1-in.-thick tensile specimen.

are typical acoustic emission curves, similar to those obtained from the 6-in.-thick specimens reported previously. The acoustic emission increases rapidly before the yield, and the curve has a small plateau near the yield point. The emission increases again until the specimen breaks.

Data were obtained in 25-kip increments below 125 kips and in 5-kip increments when the approximate failure load was approached. It was noticed that during the few steps at the beginning of the tests, the acoustic emission stopped when loading was stopped for strain data recording; however, when the stresses were near and beyond the yield points, there were emissions when

a constant load was held on the specimen. This occurred because of the different behaviors of elastic and plastic emissions.

As shown in Fig. 4.6, the curves plotted on logarithmic coordinates are almost linear prior to the yield points. This portion of the curves fits the equation for the accumulation counts of emissions $N = AK_I^n$, where A is a constant and n is the slope of the curve on a logarithmic coordinate. The slopes n are plotted vs the test temperatures in Fig. 4.7.

Two 1-in.-thick specimens received special treatment before they were tested at 200°F. One was given a postweld heat treat for stress relief and another was

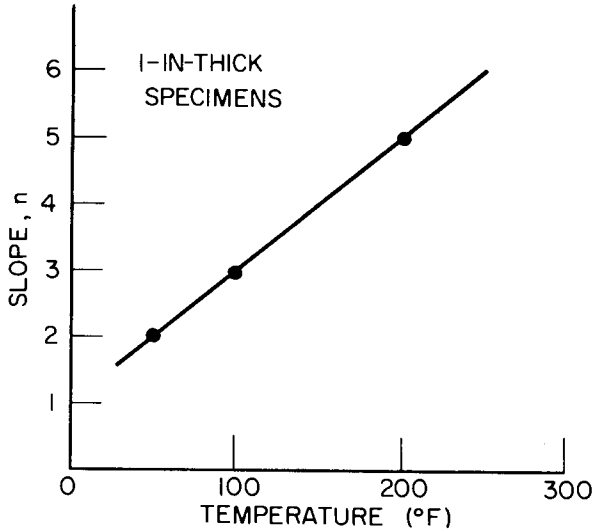


Fig. 4.7. Temperature-dependent effect of acoustic emission.

heated at 400°F for 2 hr to bake the hydrogen out. For comparison, the acoustic emission counts obtained from these two specimens are presented in Fig. 4.8. The heat-treated specimen had a lower emission rate.

Acoustic emission from 6-in.-thick welded tensile specimens. Figure 4.9 shows the acoustic emission data obtained from the tensile tests of three 6-in.-thick flawed weld-metal specimens. The accumulation counts were also plotted vs the stress intensity factors on logarithmic coordinates. The slopes of the linear parts of the curves before the yield points are nearly the same for three different test temperatures. The values of the slopes are about 3 ± 0.5 . These variations of the slopes are comparable with possible experimental errors.

The tensile tests were also conducted at small increments of the applied stresses. It was of interest to observe the acoustic emission when a constant load was held on the specimen until no increase in strain occurred. The emissions were particularly interesting after the applied stresses passed the yield point during the test at 160°F. The stresses were held constant at 57.6, 59.8, 63.2, and 65.9 ksi once, twice, or three times at each step. The specimen failed during the third period of holding the load at the constant stress of 65.9 ksi. The accumulation of acoustic emission and the rate of acoustic emission during the constant-stress periods are plotted as a function of the applied stress on linear coordinates in Fig. 4.10.

Since the sensitivities of the acoustic emission monitoring system were set at slightly different levels for the tests in this report, in comparison with the tests

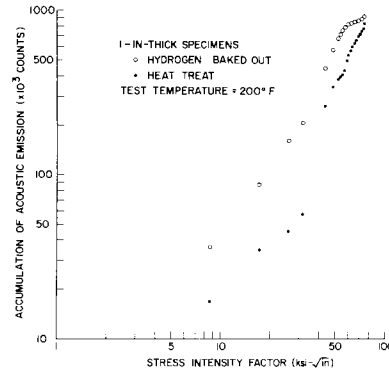


Fig. 4.8. Acoustic emission from 1-in.-thick tensile specimens tested at 200°F.

previously reported, the counts of emission should be adjusted for the different sensitivity levels. From the calibrated counts of acoustic emissions obtained in these two series of tests, it was found that the emission from 6-in.-thick specimens is higher than that from the 1-in.-thick specimens.

SHAPE FACTORS FOR NOZZLE CORNER CRACKS

R. W. Derby

Shape factors for nozzle corner cracks in two types of epoxy model pressure vessels were determined experimentally. The vessels are shown in Fig. 4.11, and the important dimensions are given in Table 4.4. Experimental elastic stress analyses for the nozzle for both vessels are presented.

Shape factors are defined implicitly by the fundamental equation of fracture mechanics:

$$K_I = C\sigma_n \sqrt{\pi a}, \quad (1)$$

where K_I is the stress intensity factor, σ_n is the nominal stress, a is crack depth, and C is the shape factor.

Since

$$K_I = K_{Ic} \quad (2)$$

Table 4.4. Data on epoxy models

	Inside radius (in.)	Wall thickness (in.)	Nominal nozzle radius (in.)	Nozzle wall thickness (in.)
Small, thick walled	1.70	0.71	0.507	0.48
Large, thinner wall	2.69	0.59	0.93	0.56

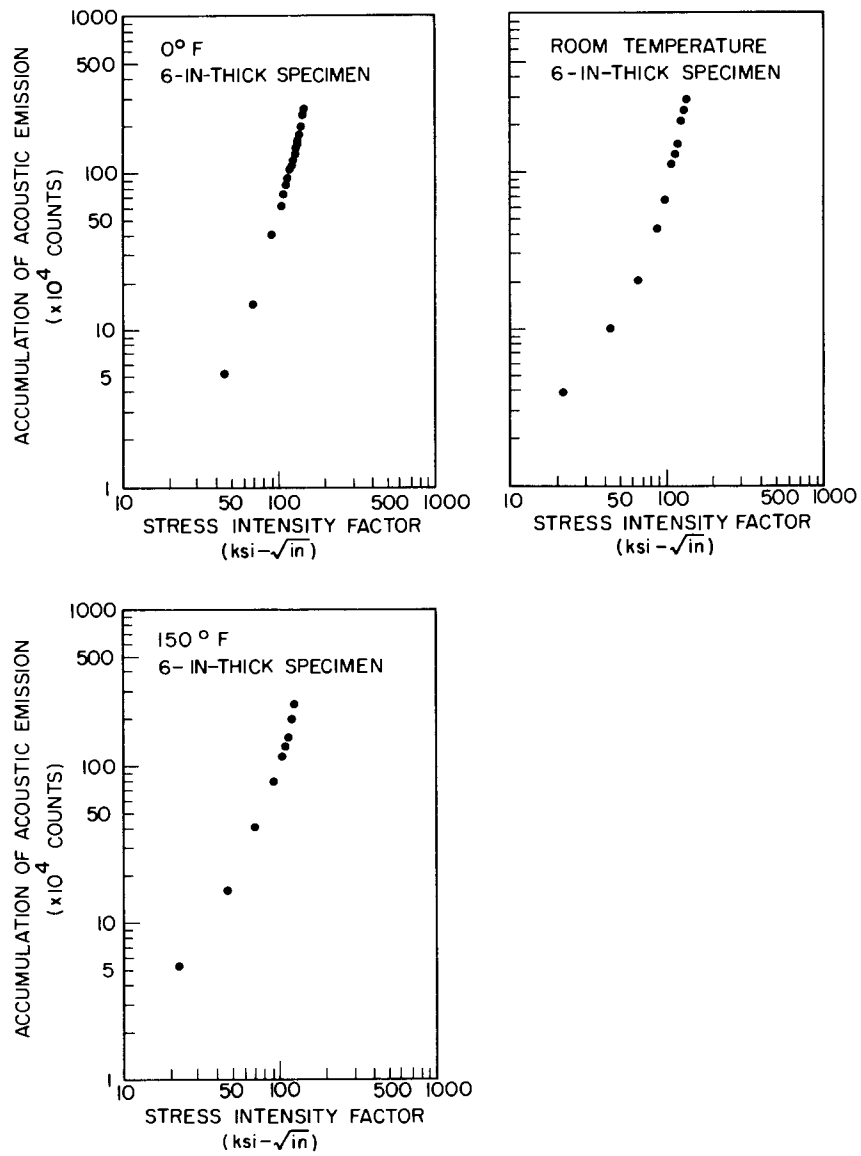


Fig. 4.9. Acoustic emission from 6-in.-thick welded tensile specimens.

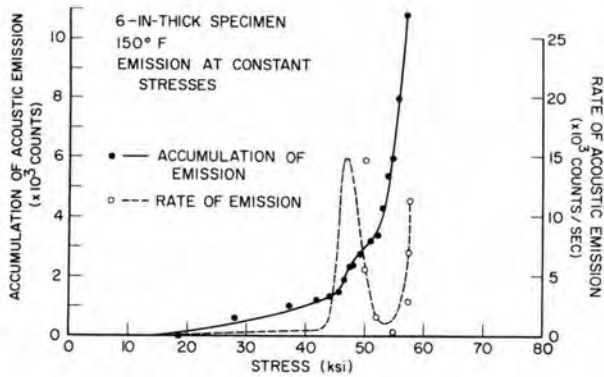


Fig. 4.10. Acoustic emission at constant stress.

at fracture, we can evaluate the shape by substituting a known value of K_{Ic} , crack depth, and nominal stress at failure into Eq. (1). The potential difficulties of this procedure are numerous. The most serious is the

control of material properties so that scatter in K_{Ic} will not obscure the result for which one is looking. A second and related difficulty is the production of a large number of uniform, flaw-free vessels.³ Another, less obvious, difficulty is producing K_{Ic} specimens with acceptable fatigue cracks.

Definitions

The following rigorous definitions have been adopted in this discussion.

Nominal stress

The nominal stress used in Eq. (1) is simply the average hoop stress of the pressure vessel, given by Pr/t , where P is internal pressure, r is the inside radius, and t is the section thickness.

3. A. A. Abbatiello, R. W. Derby, and T. A. King, "Producing Epoxy-Model Pressure Vessels for Fracture Tests," *Exp. Mech.* 7(1), 46 (1971).



Fig. 4.11. Two types of pressure vessels used in the study.

Crack depth

Crack depth is measured in the direction of the 45° diagonal of the nozzle corner from the intersection of the diagonal with the nozzle corner to the intersection of the diagonal with uncracked material. This definition is illustrated in Fig. 4.12.

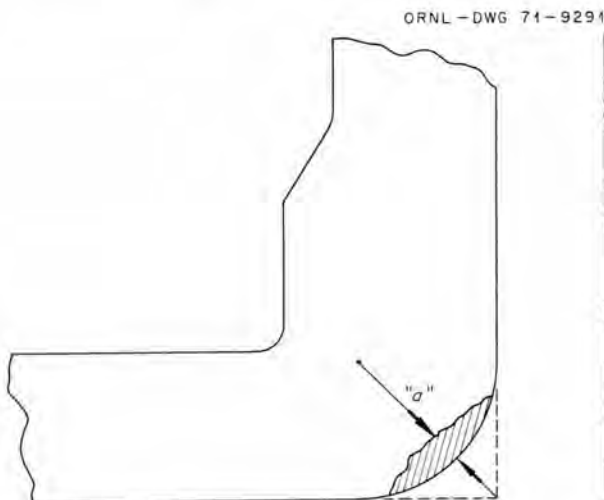


Fig. 4.12. Definition of size for a nozzle corner crack.

Nozzle radius

The radius r_z of the nozzle is taken to be the distance between the center line of the nozzle and the point formed by the intersection of the nozzle diagonal with the corner radius (see Fig. 4.13). This definition was suggested by Yukawa.⁴

Results

K_{Ic} measurements

To ascertain that the value of K_{Ic} substituted for K_I in Eq. (1) was indeed representative of the vessel material, we adopted the procedure of cutting the remainder of each vessel up into rectangular beams immediately after each burst test. These beams, which were used to measure K_{Ic} , were approximately $\frac{1}{2}$ in. square and 6 in. long. Such a specimen mounted in a bending fixture is shown in Fig. 4.14. A fatigue crack was grown in each specimen from a small slot. Significant experimental details are given below.

4. S. Yukawa, personal communication, 1971.

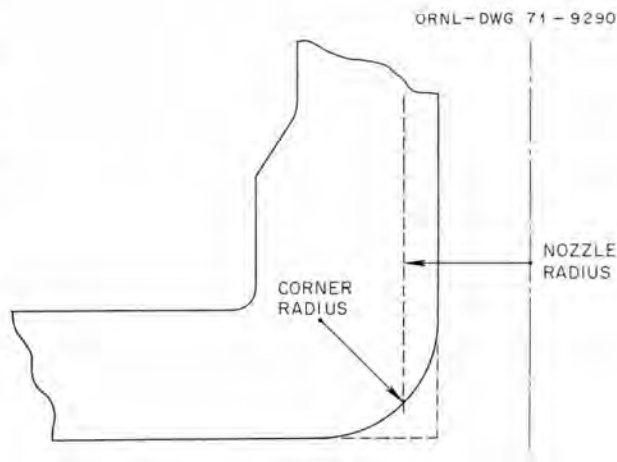


Fig. 4.13. Definition of nozzle radius r_z .



Fig. 4.14. Half-in.-square K_{Ic} specimen mounted in bending fixture.

1. To minimize the difference in environment between the vessel and the beams, the cracks in the latter were grown under the same oil as used in the vessels.
2. Because of frequency effects, both vessels and beams were loaded at 3 cpm. (Increasing the rate lowers the crack growth rate and may even reduce it to the vanishing point.)
3. The straightness of the fatigue crack is extremely sensitive to the squareness of the specimen;

a perpendicularity tolerance of 0.001 in. is required. Furthermore, a starter notch introduced with a tiny cutting wheel mounted on a milling machine works much better than a carefully guided jeweler's saw.

4. We found that both beams and vessels were most fragile when the fatigue machine was started up after a shutdown of several hours. Many beams would break on the first cycle. Because this difficulty was attributed to some kind of temperature effect at the crack tip, we warmed the oil in the beam cycling machine to 120°F before resuming cycling. The temperature was then allowed to return gradually to a normal 70°F. This procedure saved many beams. A similar effect was achieved for the vessels by operating at reduced pressure during the first 30 min of cycling.

5. To insure that both vessels and beams were at the same state of toughness, we allowed an interval of many hours (usually overnight) to elapse between the completion of the fatigue cycling and the destructive test.

6. The toughness was found to be age dependent. Thus all the vessels were seasoned over a year before being subjected to cyclic loading. This precaution allowed aging effects to become negligible.

The actual values of K_{Ic} were calculated from an equation presented by Brown and Srawley.⁵ The parameters involved are moment at failure, beam geometry, and crack depth. Scatter in the K_{Ic} values is shown by the histogram in Fig. 4.15. The skewed distribution is noteworthy and indicates that environmental variables were adequately controlled; otherwise, a few very weak specimens would have been found. The higher values were probably due to friction. The K_{Ic} was taken to be the class mark of the modal class, 900 psi $\sqrt{\text{in.}}$.

Shape factor determination

The actual measurements on the vessels were simple. The pressure at burst was measured with a sensitive pressure gage, and the size of the fatigue crack was measured with a comparator after burst. The pressure was used to calculate nominal stress at failure. This value, along with crack size and K_{Ic} , were substituted into Eq. (1) to calculate the shape factor. The results are presented in nondimensional terms in Fig. 4.16. Also shown for comparison on the same coordinates is Yukawa's flat plate model.⁶

5. W. F. Brown, Jr., and J. E. Srawley, *Plane Strain Crack Toughness Testing of High Strength Metallic Materials*, ASTM STP No. 410, p. 13 (1966).

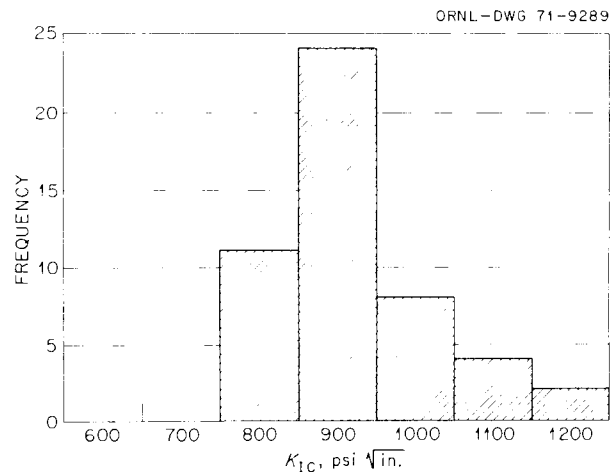


Fig. 4.15. Histogram showing distribution of 49 K_{Ic} specimens cut from the remains of 18 vessels made from 13 different batches of epoxy.

Sample Calculation for a Reactor Vessel

The relevant dimensions of a pressurized-water-reactor pressure vessel are given in Fig. 4.17. Suppose that an acceptance test is scheduled for this vessel. The problem is to calculate the combinations of flaw size and pressure that would cause failure in the nozzle corner. The vessel and nozzle are made of A533, grade B, class 1 steel. Since the highest temperature at which K_{Ic} has been obtained for this steel is 50°F, we shall use K_{Ic} at that temperature in the calculations.⁷ This value is 140 ksi $\sqrt{\text{in.}}$.

The curve based on the experimental data for the large epoxy vessels was used to estimate shape factors for the reactor vessel. Although these vessels are relatively thicker than reactor vessels, the shape factors are expected to be about the same. Various crack sizes were assumed, and K_{Ic} , as mentioned above, was taken to be 140 ksi $\sqrt{\text{in.}}$. Hence, Eq. (1) gives the nominal stress at failure. Burst pressures were then calculated from Pr/t . Results of the calculations are shown in Fig. 4.18. A small extrapolation of the curve in Fig. 4.16 allows one to plot the dashed part of the curve in Fig. 4.18. Two primary conclusions that can be drawn are:

6. S. Yukawa, *Evaluation of Periodic Proof Testing and Warm Prestressing Procedures for Nuclear Reactor Vessels*, HSSTP-TR-1, General Electric Company (July 1, 1969).

7. W. O. Shabbits, W. H. Pryle, and E. T. Wessel, *Heavy Section Fracture Toughness Properties of A533 Grade B, class I Steel Plate and Submerged Arc Weldment*, WCAP-7414 (December 1969).

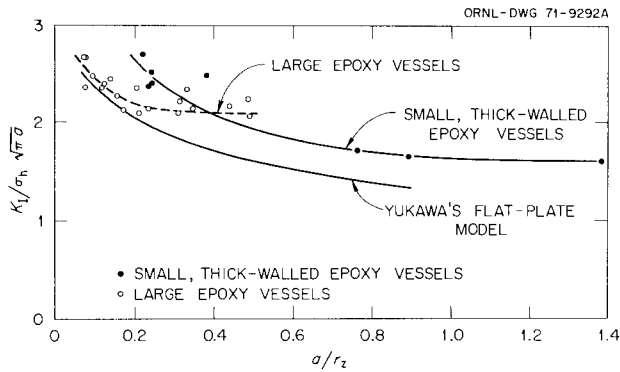


Fig. 4.16. Summary of results. Shape factor is shown as a function of the nondimensional term, crack size divided by nozzle radius.

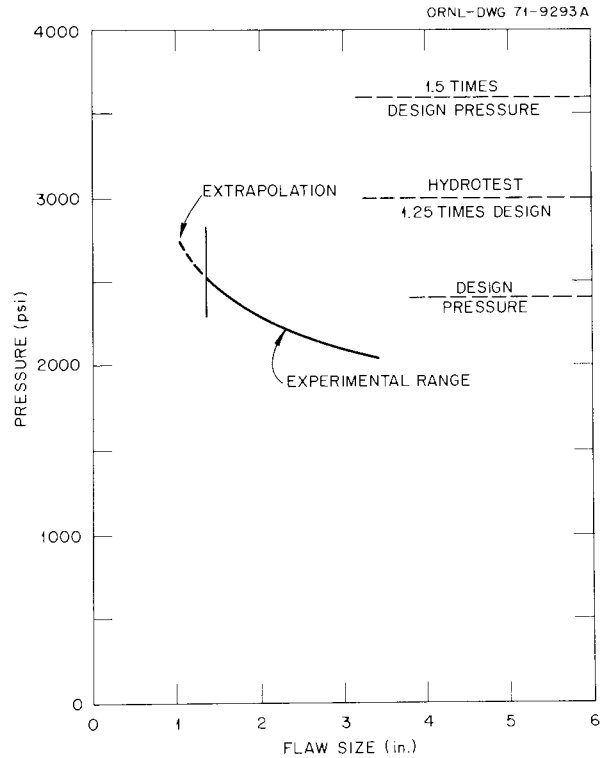


Fig. 4.18. Burst pressure as a function of nozzle-corner crack size for a 50° F test of the vessel shown in Fig. 4.17.

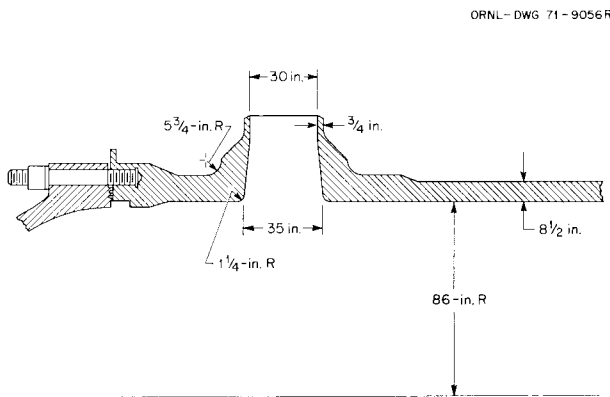


Fig. 4.17. Typical PWR inlet nozzle. Cladding and support structure are not shown.

(1) the tolerable flaw size at hydrotest pressure (1.25 times design pressure) and 50°F is surprisingly small and (2) near design pressures relatively large changes (50%) in flaw size are required to bring about small changes in burst pressure.

Nozzle experimental stress analyses

To determine the severity of the stresses in the nozzle corner region, an experimental stress analysis was performed on both vessels. The results are discussed below.

Procedure. The strain gages were applied to the inside of the vessel before assembly of the components. Next, a number of small holes were tapped in the hemispherical end caps. Brass bolts were dipped in epoxy and screwed into these holes. When the epoxy had set,

each bolt made an excellent "lead-through." Wires from the strain gages were soldered to the bolts on the inside (see Fig. 4.19). Finally, the vessel was glued together, and lead wires were soldered onto the exterior end of the brass bolts.

The first observation of strain gage readings revealed a difficulty that has been reported by other investigators, namely, that epoxy dissipates the heat generated in the strain gages so slowly that temperature effects seriously distort the indicated strain. The situation was further complicated by the original test plan to place the vessel in a blast pit and pressurize with bottle gas. This procedure resulted in oscillating zero values. A partial solution was to submerge the complete vessel in a bath of mineral oil and to pressurize with mineral oil. The presence of the oil next to the gages vastly improved the heat dissipation. It was, however, necessary to pause for about 15 sec between switching in a channel and taking a reading.

Small thick-vessel results. Some of the results of the analyses of the small thick vessel are shown in Fig. 4.20. The dashed lines indicate extrapolations to the stresses



Fig. 4.19. Small epoxy vessel with strain gages in place ready for assembly.

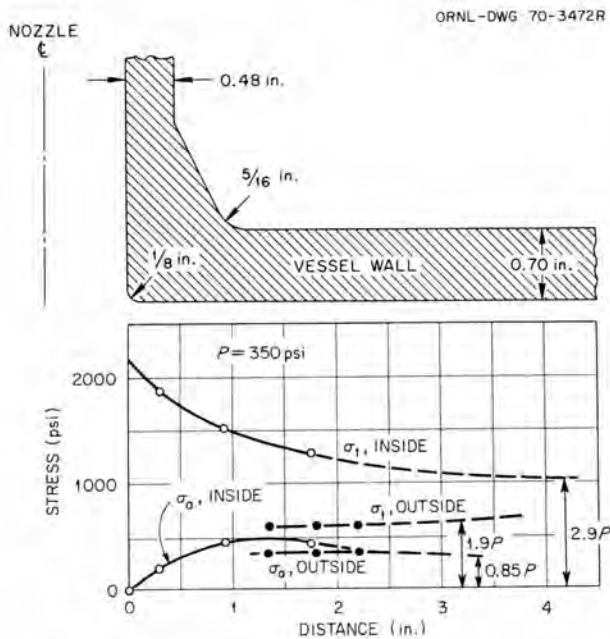


Fig. 4.20. Axial and tangential stresses on the inside and outside of the wall of the small, thick-walled, epoxy vessel.

given by Lamé's equation for tangential stress and by "force over area" for the axial stress.

A finite-element analysis of a similar vessel assumed to be made of steel was performed by Krishnamurthy.^{8,9} This vessel is geometrically similar to the epoxy model except that the nozzle wall of the steel vessel is relatively thicker but unreinforced. The

most relevant results of Krishnamurthy's analysis, adjusted to a pressure of 350 psi, are shown in Fig. 4.21. The agreement is excellent. For example, at the inside nozzle corner the experimental analysis gives 2200 psi, while the finite-element analysis gives 2280 psi. The outside σ_t was measured as 600 psi, whereas the computer shows 610 psi.

Large-vessel results. The experimental analysis of the larger epoxy model is shown in Fig. 4.22. The results are for an internal pressure of 60 psi.

PROCUREMENT OF INTERMEDIATE TEST VESSELS

C. E. Childress

A contract has been negotiated with Taylor Forge Company for six 6-in.-thick intermediate test vessels, essentially as shown in Fig. 4.23. The vessel consists of four major forged components of A508, class 2 materials. The mechanical properties for the transition section and the flat and hemispherical heads were fairly typical, that is, the average ultimate tensile strength (UTS) was between 85 and 90 ksi and the yield strength (YS) averaged 65 to 70 ksi. However, the mechanical

8. N. Krishnamurthy, "Three-Dimensional Finite Element Analysis of Thick-Walled Pipe-Nozzle Junctions with Curved Transitions," paper presented at 1st Int. Conf. Structural Mechanics in Reactor Technology, Berlin, 1971.

9. N. Krishnamurthy, *Three-Dimensional Finite Element Analysis of Thick-Walled Vessel-Nozzle Junctions with Curved Transitions*, ORNL-TM-3315 (Mar. 24, 1971).

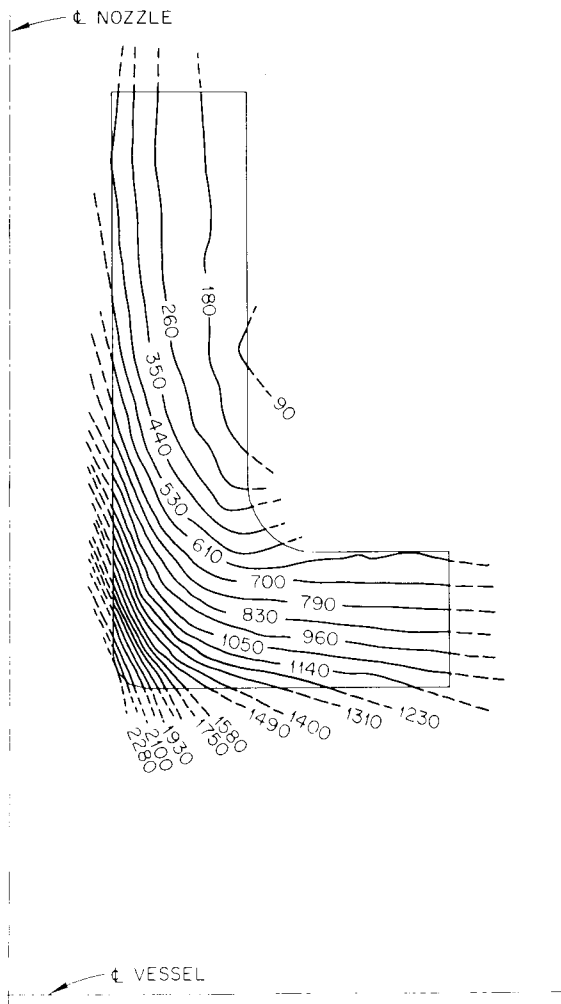


Fig. 4.21. Tangential stresses in the nozzle region of a thick-walled steel vessel which is geometrically similar to the vessel of Fig. 4.19 except the steel vessel has a thicker, but unreinforced nozzle.

properties reported for the shell courses were on the order of 103 to 109 ksi UTS and 83 to 88 ksi YS, with a nil-ductility transition temperature of -20°F as determined by drop-weight tests. The yield strength reported for the shells (83 to 88 ksi) was about the expected ultimate tensile strength of the weld material to be used in fabricating the vessels.

The shell courses were originally tempered at 1280°F maximum. Canonico and Berggren¹⁰ developed in-

10. HSST Program Semiannu. Progr. Rep. Feb. 28, 1971, ORNL-4681.

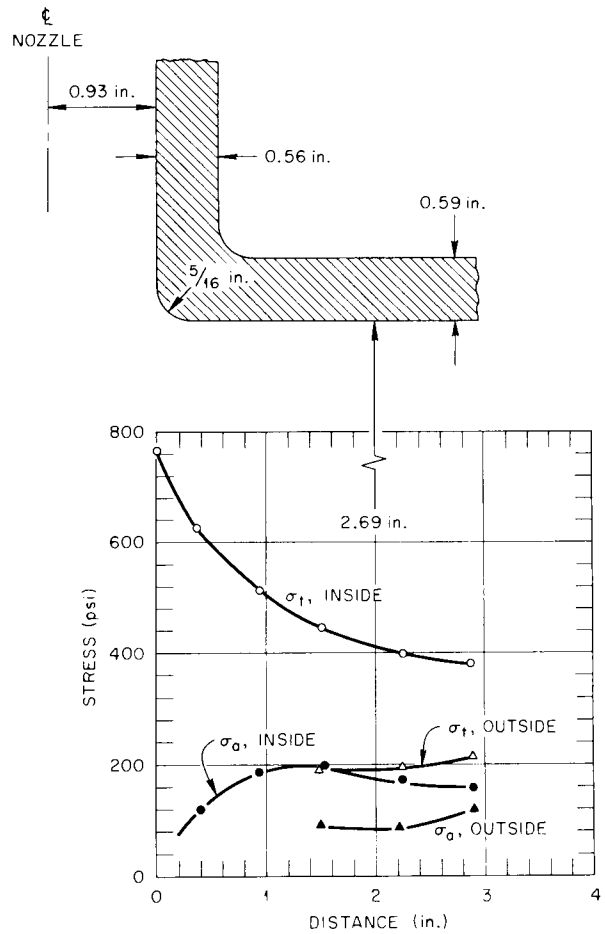


Fig. 4.22. Axial and tangential stresses on the inside and outside of the wall of the larger epoxy vessel.

formation at ORNL which indicated that the strength properties of the shells could be lowered without a significant sacrifice in toughness by retempering at a higher temperature. Using material from shell prolongations and Data-trak testing procedures, they showed that the strength properties could be lowered to about 92 to 95 ksi UTS and 69 to 72 ksi YS by retempering at 1320°F maximum.

The first shell (National Forge shell 9) was instrumented with seven thermocouples strategically located throughout the OD and ID as shown in Fig. 4.24. The heatup period comprised some 14 hr. At the end of the 6-hr hold period each thermocouple was recording a temperature of 1320°F except the ID thermocouple, which recorded 1310°F . The shell was then furnace cooled at about 200°F/hr to 600°F . Test material was

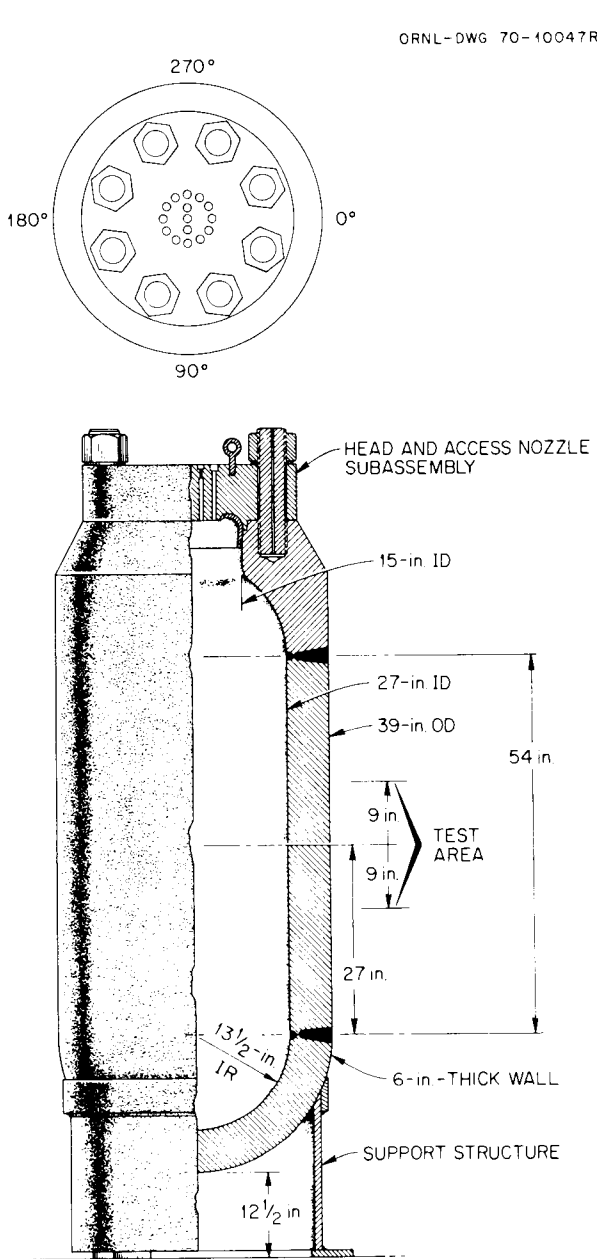


Fig. 4.23. HSST intermediate test vessel.

removed from the prolongation and stress relieved at $1125 \pm 25^\circ\text{F}$ for 24 hr. The test results for retempered shell 9 are given below.

Ultimate tensile strength (psi)	Yield strength (psi)	C_y values at $+10^\circ\text{F}$ (ft-lb)
91,500	72,000	66-40-33
92,250	71,500	62.5-79-55.5

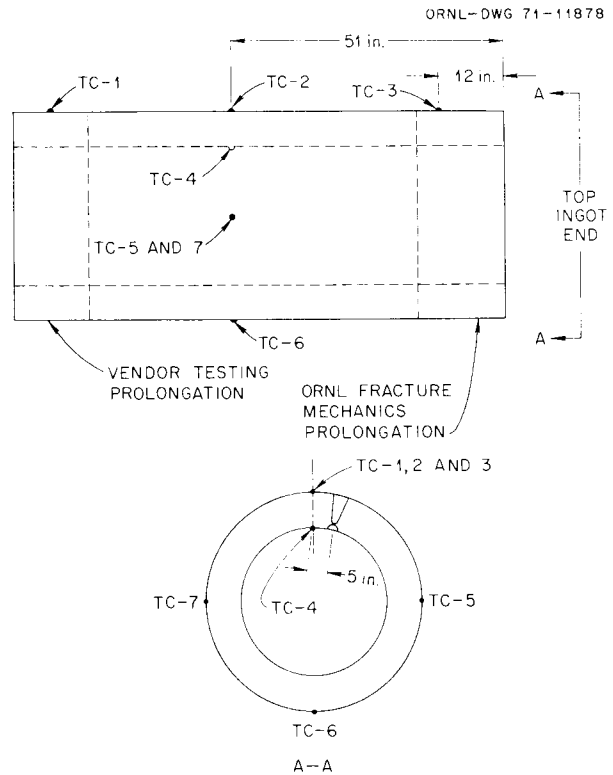


Fig. 4.24. Location of thermocouples for monitoring post-weld heat treatment of shell 9.

Canonico performed metallographic studies comparing the materials originally tempered at 1280°F with the retempered material. Results of his studies show that there is no apparent difference in the metallographic structure of the original material and the retempered material.

Based on the obvious success in the retempering of shell 9, it was decided to proceed with retempering the remaining shells in a like manner. (Note that the shell courses have been numbered 4 through 9, although it was originally intended that they be numbered 1 through 6. When it became necessary to remake one of the ingots, National Forge decided to drop the originally assigned first three numbers and continue consecutively from 4 through 9.) The mechanical properties for the retempered shells are listed in Table 4.5.

On completion of final inspection the parts were shipped to the Taylor Forge (TF) plant in Paola, Kansas, for assembly. Taylor Forge qualified three welding procedures: two submerged-arc (WP-380) and a shielded-metal-arc procedure (WP-381). All tests were qualified in the flat position; the joint configuration for each is shown in Fig. 4.25.

Table 4.5. Test results after retempering at 1320° F

Shell	Ultimate tensile strength (ksi)	Yield strength (ksi)	Reduction of area (%)	Elongation (%)	C _v at +10° F (ft-lb)	Percent shear	Lateral expansion
4	93.75	72	71	27	48	41	0.046
					50.5	37	0.044
					52	40	0.043
	91.5	69.5	67	26	53.5	40	0.046
61.5					37	0.057	
61					40	0.050	
65					47	0.059	
5	94.75	72.5	68.4	25.5	60	43	0.060
					77.5	40	0.061
					66	43	0.060
	93.75	72.5	69.7	25.5	59	45	0.059
					77	46	0.062
6	94	72	71.8	27	60.5	41	0.048
					65.5	40	0.055
					70.4	40	0.059
	94.5	74	70.4	27	53.5	39	0.045
					60	40	0.052
					61	37	0.050
7	92	71.5	71.2	27	71	45	0.060
					53.5	34	0.047
					72	40	0.064
	91.25	67.5	68.8	25	51	40	0.044
					55.5	31	0.046
57	34	0.049					
8	91.25	71.5	68.4	26	86.5	45	0.073
					61.5	43	0.052
					70.5	41	0.060
	91.75	71.5	70.4	26.5	66.5	41	0.059
					69.5	34	0.054
58.5	32	0.050					
9	91.5	72	69.9	27	66	43	0.060
					40	35	0.039
					33	33	0.031
	92.25	71.5	71	27	62.5	42	0.055
					79	47	0.061
55.5	37	0.049					

The joint configuration for procedure WP-379, used in making the longitudinal seams, is shown in Fig. 4.25a. The OD groove is prepared by machining and inspected with magnetic particles prior to welding. Essentially the conditions of the procedure are as follows:

1. preheat 300 to 500°F and maintain until postweld heat treatment (PWHT);
2. filler wire: RACO-127, $\frac{3}{16}$ in. in diameter, single wire feed;
3. interpass temperature: 500°F maximum;
4. flux: Linde type 0091, size 65 X 200;
5. travel speed: approximately 12 in./min.;
6. current: ac, 750 A, 30 to 32 V;
7. on completion of the OD side, the ID is ground to solid metal and welded in much the same manner as the OD.

The basic parameters noted for procedure WP-379 (for longitudinal seams) are also applicable to procedure WP-380 (circumferential seams), except that the ID portion of the weld is applied with shielded-metal-arc electrodes.

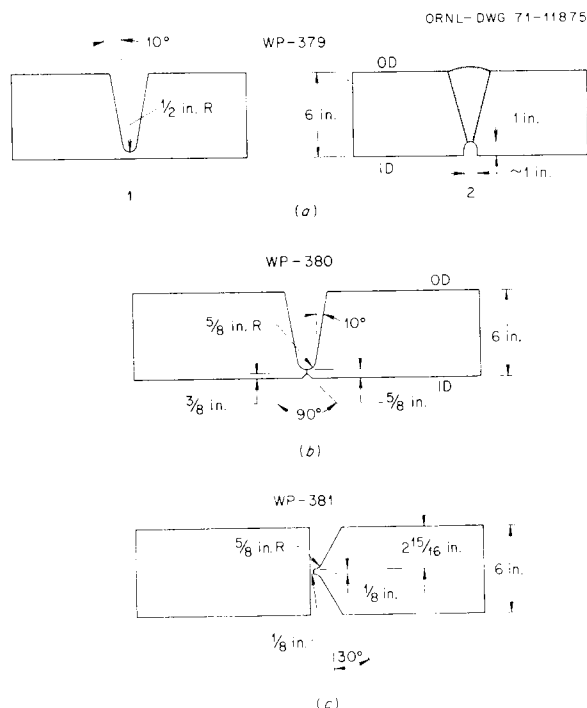


Fig. 4.25. Joint preparations for Taylor Forge welding procedures.

The joint configuration for the shielded-metal-arc procedure is shown in Fig. 4.25c. This procedure is used for all repair welding and for attachment of a nozzle to vessel V-5. Each half is prepared by machining and is inspected with magnetic particles prior to fit-up. The first three passes are applied with $\frac{3}{32}$ -in.-diam electrodes using 140 to 180 A and 24 to 26 V. Subsequent passes are applied with $\frac{3}{16}$ -in.-diam electrodes with amperage and voltage ranges of 190 to 240 and 24 to 26 respectively. The nature of the welding current for all passes is direct-current reverse polarity (DCRP). All welding is performed with Alloy Rods type 8018NM electrodes.

All test plates were subjected to a final PWHT at 1125°F for 28 hr.

A weld deposit chemistry analysis from procedure WP-379 (RACO heat 34445, flux lot 3977) showed:

C	Mn	P	S	Si	Cr	Mo	Ni	V
0.10	0.86	0.016	0.021	0.19	0.06	0.49	0.06	Trace

Mechanical properties from an all-weld tensile specimen from the $\frac{1}{4}$ -T location are:

UTS (ksi)	YS (ksi)	Elongation (%)	Reduction of area (%)
85	71.5	28	62.5

The results of Charpy V-notch tests made on full-size specimens tested at +10°F are:

Location	C_v (ft-lb)	Mils lateral expansion	Percent ductile fracture
Parent metal $\frac{1}{4}$ T	36-40-45	25-28-34	30-40-40
HAZ $\frac{1}{4}$ T	43-47-49	34-41-38	50-50-50
Weld $\frac{1}{4}$ T, top	90-96-97	66-57-70	80-80-80
Weld $\frac{1}{16}$ in., bottom surface	77-84-74	53-53-52	80-95-80

A deposit analysis from procedure WP-380 (RACO heat 34445, flux lot 3977) gave:

C	Mn	P	S	Si	Cr	Mo	Ni	V
0.13	0.77	0.015	0.020	0.19	0.07	0.50	0.08	Trace

Mechanical properties from an all-weld tensile specimen from the $\frac{1}{4}$ -T location are:

UTS (ksi)	YS (ksi)	Elongation (%)	Reduction of area (%)
81.5	69.4	28	64.9

The results of Charpy V-notch tests made on full-size specimens tested at +10°F are:

Location	C_v (ft-lb)	Mils lateral expansion	Percent ductile fracture
Parent metal $\frac{1}{4}$ T	37-55-60	29-41-46	20-25-25
HAZ $\frac{1}{4}$ T	48-57-62	40-45-49	40-40-50
Weld $\frac{1}{4}$ T, bottom	87-92-92	66-63-68	90-80-80
Weld $\frac{1}{16}$ in., top surface	84-91-95	66-73-74	80-80-80

A deposit analysis from procedure WP-381 (Alloy Rods heat 01L3333, lot F25827A, and heat CTY538, lot B012A27A) showed:

C	Mn	P	S	Si	Cr	Mo	Ni	V
0.09	1.33	0.012	0.012	0.52	0.05	0.52	0.99	0.02

Mechanical properties from an all-weld tensile specimen from the $\frac{1}{4}$ -T location showed:

UT (ksi)	YS (ksi)	Elongation (%)	Reduction of area (%)
95.3	84.8	29	70.8

The results of Charpy V-notch tests made on full-size specimens tested at $+10^{\circ}\text{F}$ are:

Location	C_v (ft-lb)	Mils lateral expansion	Percent ductile fracture
Parent metal $\frac{1}{4}$ T	78-78-68	56-56-51	40-40-40
HAZ $\frac{1}{4}$ T	86-96-128	62-75-64	60-60-90
Weld $\frac{1}{4}$ T, top	75-73-85	60-57-65	70-70-80
Weld $\frac{1}{16}$ in., bottom surface	76-72-70	65-62-61	80-80-80

The completed vessels will be identified by the designations V-1 through V-6. Vessels V-1 and V-2 will be fabricated as shown in Fig. 4.23. In addition to the two circumferential seams shown in Fig. 4.23, vessels V-3, V-4, and V-6 will contain a longitudinal seam; V-6 will also contain a second girth seam situated midway between the two shown in Fig. 4.23, with the two longitudinal seams located 180° apart. Vessel V-5 will be fabricated as shown in Fig. 4.23 with a nozzle attached near the vicinity of the test area.

One of the main purposes of the HSST program is to determine the effects of flaws, material inhomogeneities, and discontinuities on the behavior of vessels under normal operating and accident conditions. For this, and other reasons, the fabrication is required to maintain identification, orientation, etc., of each component in each vessel. In addition, each vessel must pass a rigid nondestructive inspection test and a leak-tightness test prior to delivery.